UNIVERSITY OF CALIFORNIA, SAN DIEGO
MARINE PHYSICAL LABORATORY OF THE
SCRIPPS INSTITUTION OF OCEANOGRAPHY
SAN DIEGO, CALIFORNIA 92152

STUDIES OF DEEP SEA EROSION
USING DEEP-TOWED INSTRUMENTATION

David A. Johnson

SIO REFERENCE 71-24

1 September 1971

F.N. SPIESS, DIRECTOR
MARINE PHYSICAL LABORATORY

MPL-U-65/71

ii

DOCUMENT CONTROL DATA - R & D

(Security classification of title, body of abstract and indexing annotation must be entered when the overall report is classified)

1 ORIGINATING ACTIVITY *(Corporate author)*	2a. REPORT SECURITY CLASSIFICATION
University of California, San Diego, Marine Physical Laboratory of the Scripps Institution of Oceanography San Diego, California 92152	Unclassified
	2b. GROUP

3. REPORT TITLE

STUDIES OF DEEP SEA EROSION USING DEEP-TOWED INSTRUMENTATION

4. DESCRIPTIVE NOTES *(Type of report and inclusive dates)*

Summary

5. AUTHOR(S) *(First name, middle initial, last name)*

David A. Johnson

6. REPORT DATE	7a. TOTAL NO. OF PAGES	7b. NO. OF REFS
1 September 1971	155	126

8a. CONTRACT OR GRANT NO.	9a. ORIGINATOR'S REPORT NUMBER(S)
NSF Grant GA 20014, ONR N00014-69-A-0200-6002 NR 260-103, and The International Nickel Company	SIO Reference 71-24
	9b. OTHER REPORT NO(S) *(Any other numbers that may be assigned this report)*
	MPL-U-65/71

10. DISTRIBUTION STATEMENT

Document cleared for public release and sale; its distribution is unlimited.

11. SUPPLEMENTARY NOTES	12. SPONSORING MILITARY ACTIVITY
	Office of Naval Research

13. ABSTRACT

Detailed geological and geophysical studies were conducted in a region of the equatorial Pacific (near $9^{\circ}40'$ N, $134^{\circ}00'$ W), using the deep-towed instrumentation of the Marine Physical Laboratory. Sediment cores and near-bottom reflection profiles show a sharp angular unconformity a few cm beneath the sea floor, which separates a thin upper layer of Holocene sediment from a chalk of Tertiary age. This unconformity is interpreted as a Pleistocene erosion surface which truncates sediments ranging in age from Upper Eocene to Middle Miocene. Bottom currents have evidently caused the erosion and redistribution of sediment tens to hundreds of meters in thickness. Much of the eroded material has been redeposited into a large (15 km x 25 km) topographic basin containing sediments which are considerably thicker than those in the surrounding region. Prominent channels feed into the basin from the areas where erosion has taken place. Significant ocean floor erosion in the central Pacific did not begin until the late Tertiary, and was perhaps restricted to the glacial stages of the Pleistocene when bottom currents may have been considerably stronger than those present today. During successive episodes of high current speeds the erosion surface deepened and became increasingly irregular. The prominent unconformity which is observed today represents only the shape of the erosion surface when current speeds most recently decreased to the point where erosion could no longer take place. The results of this study are comparable with observations in other widely separated regions in the central Pacific, suggesting that some of the processes responsible for erosion in the deep-tow survey area may have affected a substantial portion of the Pacific Ocean floor. Various climatic and oceanographic processes are modified in response to glaciation, and these processes may interact to create conditions on the deep sea floor which favor increased sediment erosion and redistribution. These processes include the intensity of the atmospheric and surface water circulation, the rate of production of deep water in high latitudes, the rate of dissipation of tidal energy on the deep sea floor, and the intensity of chemical dissolution and biological activity at the sea floor. The conditions which apparently led to active sediment erosion in the central Pacific probably developed gradually during a time span of 10,000 to 100,000 years, in contrast to the episodic events of relatively short duration which are commonly characteristic of subaerial erosion processes.

TABLE OF CONTENTS

Page

LIST OF FIGURES

LIST OF TABLES

LIST OF PLATES

ACKNOWLEDGEMENTS

for his early encouragement in applying the deep-tow instrumentation to the study of deep ocean sedimentation processes.

The sediment cores were analyzed with the help of several individuals. T. J. Walsh provided assistance in splitting and sampling the cores, and in photographing the cores and radiolarian specimens. W. R. Riedel, A. Sanfilippo, and T. C. Moore, Jr. assisted in the identification of several radiolarian specimens. Foraminifera were identified by F. L. Parker. E. L. Hamilton provided data on the physical properties of several of the cores.

Many of my colleagues at Scripps and at other institutions have provided helpful discussion during the course of this study. These individuals include G. Arrhenius, W. H. Berger, M. Hendershott, C. D. Hollister, H. W. Menard, W. Munk, J. L. Reid, Jr., W. B. F. Ryan, M. Wimbush, and E. L. Winterer. Students in the deep-tow group, including J. A. Grow, R. L. Larson, P. F. Lonsdale, B. P. Luyendyk, and W. R. Normark have provided continuing encouragement. Special thanks go to members of my doctoral committee for their continuing assistance, and for their patience in reviewing the manuscript.

Finally, I should like to thank Annette Pickens, Elaine Dunn, and my wife Diann for their assistance in typing and proofreading the manuscript.

STUDIES OF DEEP SEA EROSION
USING DEEP-TOWED INSTRUMENTATION

David A. Johnson

University of California, San Diego
Marine Physical Laboratory of the
Scripps Institution of Oceanography
San Diego, California 92152

ABSTRACT

Detailed geological and geophysical studies were conducted in
a region of the equatorial Pacific (near 07°40'N, 134°00'W), using the
deep-towed instrumentation of the Marine Physical Laboratory. Sedi-
ment cores and near-bottom reflection profiles show a sharp angular
unconformity a few cm beneath the sea floor, which separates a thin
upper layer of Holocene sediment from a chalk of Tertiary age. This
unconformity is interpreted as a Pleistocene erosion surface which
truncates sediments ranging in age from Upper Eocene to Middle Miocene.
Bottom currents have evidently caused the erosion and redistribution
of sediment tens to hundreds of meters in thickness. Much of the
eroded material has been redeposited into a large (15 km x 25 km)
topographic basin containing sediments which are considerably thicker
than those in the surrounding region. Prominent channels feed into
the basin from the areas where erosion has taken place. Significant

ocean floor erosion in the central Pacific did not begin until the late Tertiary, and was perhaps restricted to the glacial stages of the Pleistocene when bottom currents may have been considerably stronger than those present today. During successive episodes of high current speeds the erosion surface deepened and became increasingly irregular. The prominent unconformity which is observed today represents only the shape of the erosion surface when current speeds most recently decreased to the point where erosion could no longer take place. The results of this study are comparable with observations in other widely separated regions in the central Pacific, suggesting that some of the processes responsible for erosion in the deep-tow survey area may have affected a substantial portion of the Pacific Ocean floor.

Various climatic and oceanographic processes are modified in response to glaciation, and these processes may interact to create conditions on the deep sea floor which favor increased sediment erosion and redistribution. These processes include the intensity of the atmospheric and surface water circulation, the rate of production of deep water in high latitudes, the rate of dissipation of tidal energy on the deep sea floor, and the intensity of chemical dissolution and biological activity at the sea floor. The conditions which apparently led to active sediment erosion in the central Pacific probably developed gradually during a time span of 10,000 to 100,000 years, in contrast to the episodic events of relatively short duration which are commonly characteristic of subaerial erosion processes.

INTRODUCTION

The deep ocean is today the most remote and least understood environment on the surface of the earth. During recent years it has become increasingly evident that conditions on the deep sea floor are far from quiescent, and that sites of uniform, uninterrupted deposition may be rare. The utilization of techniques such as deep sea photography, continuous seismic reflection profiling, current meters, sediment coring, and deep drilling has identified features indicative of sediment redistribution in virtually every region where the sea floor has been examined in detail.

Early investigations of sediment transport in the deep ocean were undertaken along the continental margins and abyssal plains of the western North Atlantic (Ericson et al, 1952; 1961). The sediments in this region commonly contain graded bedding (Heezen et al, 1954) and displaced microfaunas (Phleger, 1951), features which indicate sediment redeposition. Apparently much of the sediment in this part of the deep ocean has been derived from shallower environments and transported hundreds of kilometers across the sea floor (Heezen, 1959). Wherever terrigenous sediment is in abundant supply, large-scale processes of erosion and redeposition such as turbidity currents (Heezen, 1963) and geostrophic contour currents (Heezen et al, 1966; Jones et al, 1970) have been suggested as the critical mechanisms controlling sedimentation.

In other areas of the sea floor, far removed from sources of large quantities of terrigenous material, the depositional record also

contains abundant evidence for reworking, but here the features indica-
tive of redeposition are observed on a relatively small scale. The
biogenous pelagic sediments of the equatorial Pacific, for example,
have been studied extensively by sediment coring (Riedel, 1971; Hays
et al, 1969) and most recently by deep drilling (Tracey et al, 1971;
Hays et al, 1971). In this region the sedimentary record commonly
contains hiatuses representing the nondeposition or erosion of tens
of millions of years of material (Bramlette and Riedel, 1971). Faunal
assemblages are often contaminated with microfossils of much greater
age which have been reworked into younger material (Riedel and Funnell,
1964). Another characteristic aspect of the sedimentation pattern
is its small-scale variability. Early investigations of closely
spaced sediment cores revealed that there is significant variability
over distances of kilometers or less (Arrhenius, 1963). Subsequent
studies suggest that such small-scale irregularities are common, and
may be characteristic of pelagic sedimentation throughout the central
Pacific (Moore, 1970; Johnson and Johnson, 1970). This variability
is puzzling, since the supply of pelagic material to the sea floor is
probably uniform over relatively large distances. It appears that
various processes are acting at or near the sea floor to create the
irregular sediment distribution patterns which are observed.

This study was undertaken in order to gain a better under-
standing of the conditions which control sediment accumulation on the
deep sea floor. During October of 1969 and February of 1970, a
detailed investigation of the sea floor was carried out on board the

R/V THOMAS WASHINGTON, operating within a small region of the equatorial Pacific near 07°40'N, 134°00'W. The specific objectives of this study were: (a) to examine in detail a small portion of the ocean floor where substantial erosion and redeposition of sediment has taken place; (b) to establish the sediment distribution pattern on a small scale; (c) to determine the processes which were responsible for producing the depositional features observed; (d) to evaluate the extent in time and in space over which these processes have been influential; and (e) to attempt to predict the effects upon the depositional record in other regions if these processes prove to be of broad general applicability.

METHODS OF STUDY

Limitations of Previous Methods

Severe limitations have been encountered in attempting to study small-scale features and processes on the deep sea floor. One of these is the limited resolution of conventional shipboard echo sounders. During ordinary echo-sounding operations in deep water, a large area of the sea floor (several km^2) is insonified, and it is necessary to make significant corrections to the echo-sounding profiles in order to reconstruct the true sea floor topography (Krause, 1962). Features with dimensions of tens of meters or less may remain completely undetected by this method.

A second limitation is navigational precision. In order to survey and sample sea floor features with dimensions of a few kilometers, such as abyssal hills, one would need to know his relative position in the area of interest to an accuracy of perhaps several tens of meters or less. Satellite navigational techniques are adequate for obtaining an "absolute" position on the earth with an accuracy of tens to hundreds of meters, but the positions are not obtained with sufficient frequency or sufficient accuracy to detect small changes in one's position within a small area. Anchored radar buoys have been employed as navigational reference points (Moore and Heath, 1967; Emery and Ross, 1968; Johnson and Johnson, 1970), but this technique is not entirely satisfactory since changing wind and current conditions cause the buoys to wander considerably relative to the sea floor.

A third limitation is the restricted period of time during
which observations of the sea floor can ordinarily be made. Manned
submersibles are limited to a period of a few hours or a few days
of continuous operation (Ballard and Emery, 1970), and surveys from
surface ships are similarly restricted because of high operating costs.
The use of free vehicles (Schick et al., 1968; Snodgrass, 1968) has
extended the period of continuous operation to several weeks, but
even this period of time may be insufficient for detecting the pro-
cesses which are geologically significant. Geologic processes in-
volving erosion are especially likely to be episodic in nature, and
consequently the measurement of a set of parameters over a limited
period of time may yield only a representation of "average" con-
ditions. This limitation is difficult to overcome, and must be
considered when interpreting short term observations.

Deep-towed Instrumentation

The limitations of resolution and navigational precision in
deep ocean surveys have been largely overcome through the recent
development (by the Marine Physical Laboratory of the Scripps Insti-
tution of Oceanography) of a deep-towed instrument package (Spiess
and Mudie, 1970). The instrument is towed at a height of 50-100 m
above the sea floor (Fig. 1), and is capable of resolving sea floor
features with relatively small dimensions which have been difficult
to observe by other methods. Navigation of both the instrument
and the towing ship is accomplished using an array of anchored
acoustic transponders (Spiess et al., 1966; Lowenstein, 1968). Each

KEY

1. DOWNWARD LOOKING ECHO SOUNDER 5. STROBE LIGHT
2. 3.5 kHz "P" BOTTOM PENETRATION 6. CAMERA
3. UPWARD LOOKING ECHO SOUNDER 7. MAGNETOMETER
4. ACOUSTIC TRANSPONDER 8. SOUND VELOCIMETER
9. SIDE LOOKING SONAR
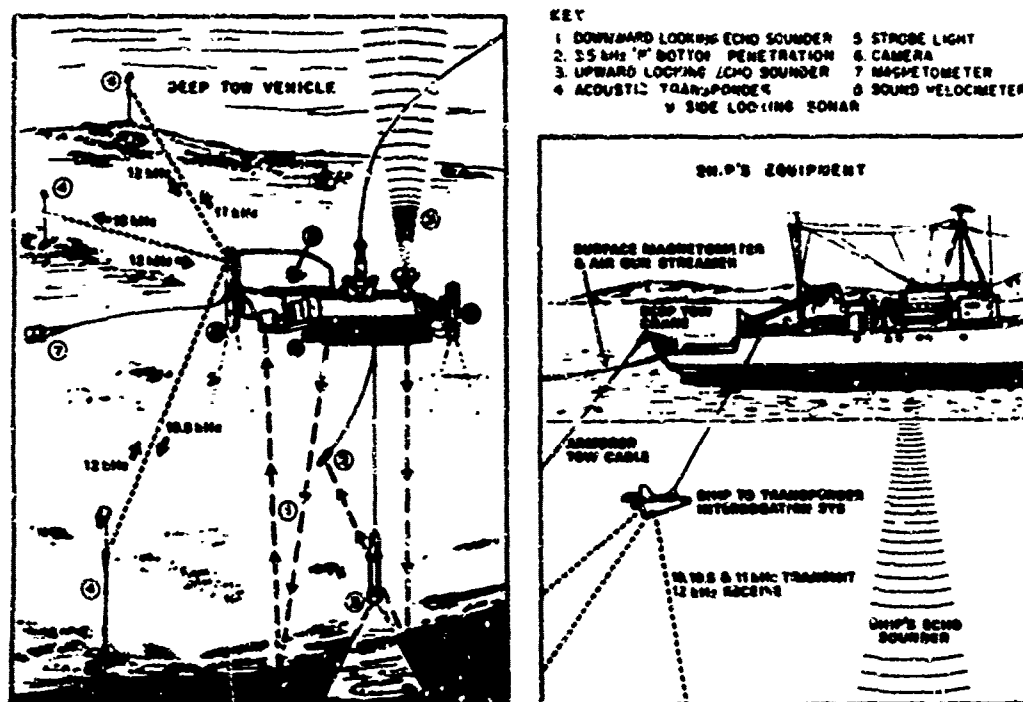
FIGURE 1   The deep-towed instrumentation of the Marine Physical
Laboratory. A detailed discussion of the various
systems is presented by Spiess and Mudie (1970).

transponder assembly contains a hydrophone positioned at a height of
100 m above the sea floor, which can be interrogated by the towed
instrument at a distance of several kilometers. By selectively
interrogating the transponders from the towed instrument and from the
ship, a range (round trip travel time) to each transponder is deter-
mined. When two or more transponders "respond", a position is
obtained; the position of the towed instrument relative to the trans-
ponder array can be determined to within several meters. The precise
geographical coordinates and orientation of the transponder array
are then determined by using an independent method of navigating the
ship, such as satellite navigation.

Approximately 130 hours of towing within the study area
yielded data along 200 km of survey track (Fig. 6). Instrumentation
of particular importance during this survey included:

  a. Narrow-beam, 40 kHz down-looking echo sounder. This system,
   in conjunction with an up-looking echo sounder, provided
   detailed topographic profiles of the sea floor.

  b. Side-scanning sonar for observing sea floor roughness.

  c. Stereo cameras for photographing the sea floor from a
   height of about ten meters.

  d. Low frequency (3.5 kHz) sub-bottom penetration system for
   detecting shallow acoustic reflectors.

Echo soundings were corrected for the velocity of sound in
sea water, using a calculated sound velocity profile for the survey
area. Bathythermograph (XBT) data were used for the temperature

structure of the upper 500 m; the temperature and salinity of in-
termediate and deep water were estimated on the basis of recent
hydrographic data (Reid, 1960).

Sediment Coring

Sediment samples were obtained using free-fall coring (Moore,
1961; Sachs and Raymond, 1965) and piston coring techniques. During
all coring operations the ship was navigated relative to the anchored
transponder array. The 42 free-fall cores were dropped in sequences,
with five to ten cores along individual profiles. Four of the five
profiles correspond to tracks along which deep-tow observations
were previously obtained. The position of each free-fall core is
known to within 50-100 m the uncertainty is due to small errors in
determining the ship's position, and a possible horizontal drift of
the cores while descending to the sea floor. During piston coring
operations (Cores E-27 and E-28) a relay transponder (Boegeman
et al, 1971) was attached to the wire above the tripping arm in order
to navigate the core itself relative to the anchored transponder
array.

The cores were split longitudinally, described and photo-
graphed, and sediment samples were taken for sedimentological and
biostratigraphic studies (Plates 4-9). Because of the short length
(<30 cm) of most of the cores, only a few samples from each core were
required. The following physical properties of the sediment were
determined: (a) median and mean grain diameters; (b) percent sand,
silt and clay; (c) saturated bulk density; (d) grain density; (e)

porosity; and (f) compressional wave velocity.

The coarse fraction ($>62\ \mu$) was separated from each sediment sample, and the radiolarian and foraminiferal assemblages were examined to determine the ages of the cores. Radiolaria of all ages were well preserved, whereas the foraminiferal assemblages showed considerable effects of dissolution, with only the more resistant species remaining. Therefore, the foraminifera were used principally to confirm the ages assigned on the basis of the radiolarian occurrences. Fifty-one Cenozoic radiolarian species (Table 1), all of which have been described previously, were used for assigning ages to the sediment. The ranges of these species are shown in Table 2, using as a basis the radiolarian zonation of Riedel and Sanfilippo (1971).

Bottom Current Measurement

Bottom currents were measured at four locations in the study area, using free-vehicle current meters (Fig. 2) developed by the Marine Life Research Group of the Scripps Institution of Oceanography (Isaacs et al, 1966; Schick et al, 1968). Each instrument was positioned several meters above the sea floor (Table 4), and recorded currents over a period of approximately four days. The direction and speed of the currents are recorded internally on a strip-chart recorder (Fig. 22). Current direction is monitored continuously, whereas the speed is commonly averaged over time increments of one hour. Current speed is designated by a sequence of tic marks along the record. The recorder is calibrated to produce a mark for a given
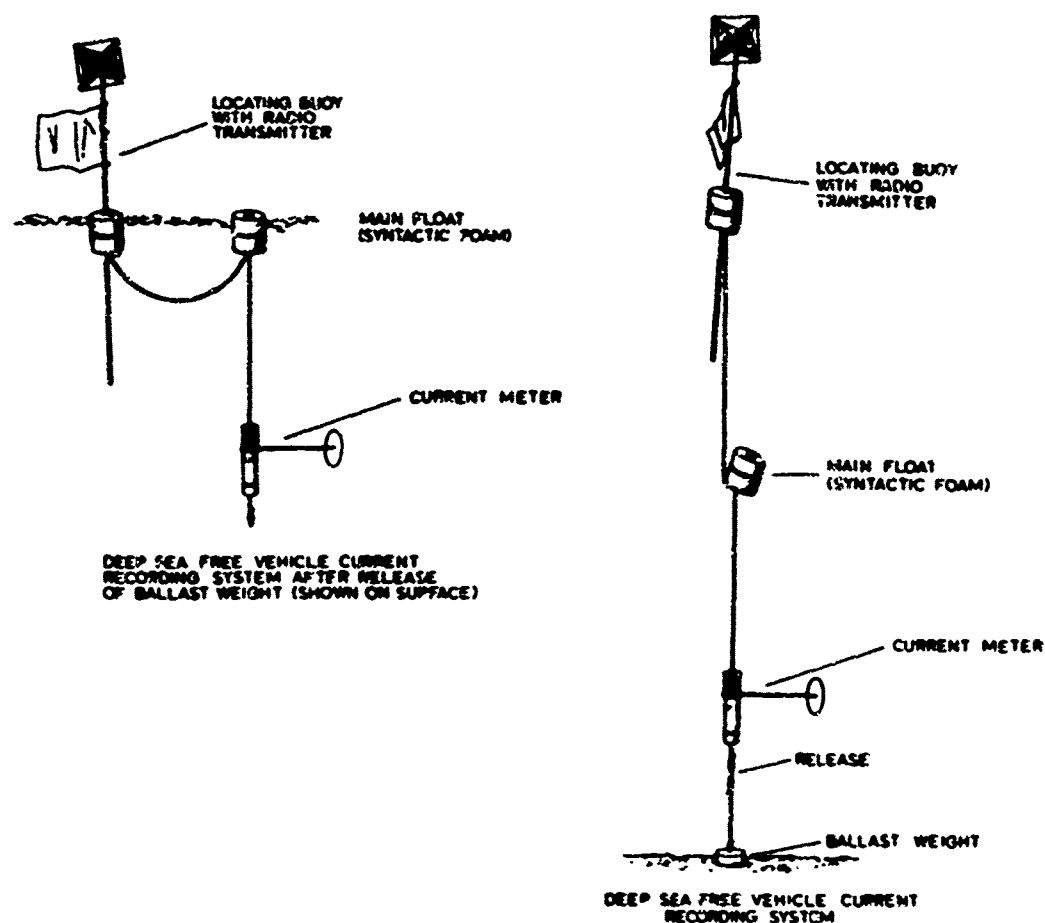
FIGURE 2   Schematic illustration of the free vehicle current meter
            assembly on the sea floor, and on the sea surface after
            release of the anchor. The instrumentation is described
            in detail by Schick et al. (1968).

TABLE 1a List of radiolarian species used for age determinations

Species	Illustrations
<u>Thyrsocyrtis triacantha</u> (Ehrenberg)	Plate 1, Fig. 1
<u>Thyrsocyrtis rhizodon</u> Ehrenberg	Plate 7, Fig. 7 in Riedel and Sanfilippo (1970)
<u>Cycladophora hispida</u> (Ehrenberg)	Plate 10, Fig. 7 in Riedel and Sanfilippo (1970)
<u>Theocampe mongolfieri</u> Ehrenberg	Plate 1, Fig. 8
<u>Sethochytris babylonis</u> (Clark and Campbell)	Plate 1, Fig. 3
<u>Lithocyclia ocellus</u> Ehrenberg group	Plate 5, Fig. 1 in Riedel and Sanfilippo (1970)
<u>Cycladophora turris</u> Ehrenberg	Plate 1, Fig. 4
<u>Thyrsocyrtis tetracantha</u> (Ehrenberg)	Plate 1, Fig. 2
<u>Lithocyclia aristotelis</u> (Ehrenberg) group	Plate 1, Figs. 13,15
<u>Artophormis barbadensis</u> (Ehrenberg)	Plate 1, Fig. 9
<u>Dorcadospyris triceros</u> (Ehrenberg)	Plate 1, Fig. 16
<u>Thyrsocyrtis bromia</u> Ehrenberg	Plate 1, Figs. 5,6
<u>Cyclampterium milowi</u> Riedel and Sanfilippo	Plate 2, Fig. 7
<u>Theocyrtis tuberosa</u> Riedel	Plate 3, Fig. 1
<u>Artophormis gracilis</u> Riedel	Plate 1, Fig. 10
<u>Lithocyclia angustum</u> (Riedel)	Plate 1, Fig. 14
<u>Theocorys spongoconum</u> Kling	Plate 3C, Fig. 3 in Riedel and Sanfilippo (1971)
<u>Dorcadospyris quadripes</u> Moore	Plate 1, Fig. 11
<u>Theocyrtis annosa</u> (Riedel)	Plate 3, Fig. 2
<u>Dorcadospyris circulus</u> Moore	Plate 8, Figs. 4,5 in Moore (1971)
<u>Dorcadospyris ateuchus</u> (Ehrenberg)	Plate 2, Fig. 11
<u>Cannartus prismaticus</u> (Haeckel)	Plate 2, Fig. 1
<u>Dorcadospyris papilio</u> (Riedel)	Plate 2, Fig. 14
<u>Cyclampterium pegetrum</u> Sanfilippo and Riedel	Plate 2, Fig. 8
<u>Dorcadospyris praeforcipata</u> Moore	Plate 9, Figs. 4,5 in Moore (1971)
<u>Calocycletta robusta</u> Moore	Plate 3, Fig. 3
<u>Lychnocanium bipes</u> Riedel	Plate 3, Fig. 5

TABLE 1b List of radiolarian species used for age determinations

Species	Illustrations
Cyrtocapsella tetrapera Haeckel	Plate 3, Fig. 11
Calocycletta virginis Haeckel	Plate 3, Figs. 6,7
Cyrtocapsella cornuta Haeckel	Plate 3, Fig. 10
Dorcadospyris simp'ex (Riedel)	Plate 2, Fig. 12
Stichocorys delmontensis (Campbell and Clark)	Plate 3, Fig. 8
Cannartus tubarius (Haeckel)	Plate 2, Fig. 2
Dorcadospyris forcipata (Haeckel)	Plate 10, Figs. 1,2 in Moore (1971)
Cyclampterium leptetrum Sanfilippo and Riedel	Plate 2, Fig. 9
Stichocorys wolffii Haeckel	Plate 3, Fig. 9
Cannartus violina Haeckel	Plate 2, Fig. 3
Dorcadospyris dentata Haeckel	Plate 2, Fig. 15
Calocycletta costata (Riedel)	Plate 3, Fig. 4
Lithopera renzae Sanfilippo and Riedel	Plate 3, Fig. 14
Dorcadospyris alata (Ri.del)	Plate 2, Fig. 13
Cyclampterium tanythorax Sanfilippo and Riedel	Plate 2, Fig. 10
Lithopera baueri Sanfilippo and Riedel	Plate 2, Fig. 2 in Sanfilippo and Riedel (1970)
Lithopera thornburgi Sanfilippo and Riedel	Plate 2, Fig. 4 in Sanfilippo and Riedel (1970)
Cannartus laticonus Riedel	Plate 2, Fig. 4
Cannartus petterssoni Riedel and Sanfilippo	Plate 1C, Fig. 19 in Riedel and Sanfilippo (1971)
Cyclampterium brachythorax Sanfilippo and Riedel	Plate 2, Fig. 15 in Sanfilippo and Riedel (1970)
Lithopera neotera Sanfilippo and Riedel	Plate 3, Fig. 15
Lithopera bacca Ehrenberg	Plate 1, Fig. 29 in Sanfilippo and Riedel (1970)
Ommatartus antepenultimus Riedel and Sanfilippo	Plate 2, Fig. 5
Ommatartus hughesi (Campbell and Clark)	Plate 2, Fig. 6
Cyclampterium neatum Sanfilippo and Riedel	Plate 2, Fig. 17 in Sanfilippo and Riedel (1970)

TABLE 2a

Stratigraphic ranges of Cenozoic radiolarian species. Radiolarian zonation is from Riedel and Sanfilippo (1971). Ranges of Eocene species are based on Figure 2 of Riedel and Sanfillippo (1970). Ranges of Oligocene and Miocene species are based on Figure 2 of Riedel and Sanfillippo (1971) and Table 1 of Moore (1971).

SPECIES / ZONES	THYRSOCYRTIS TRIACANTHA	THYRSOCYRTIS RHIZODON	CYCLADOPHORA HISPIDA	THEOCAMPE MONGOLFIERI	SETHOCYRTIS BABYLONIS	LITHOCYCLIA OCELLUS	CYCLADOPHORA TURRIS	THYRSOCYRTIS TETRACANTHA	LITHOCYCLIA ARISTOTELIS	ARTOPHORMIS BARBADENSIS	DORCADOSPYRIS TRICEROS	THEOCYRTIS DIGITA	CYCLAMPTERIUM MILOWI	THEOCYRTIS TUBEROSA	ARTOPHORMIS GRACILIS	LITHOCYCLIA ANGUSTUM	THEOCYRTIS SPONGOCONUM	DORCADOSPYRIS QUADRIPES	THEOCYRTIS ANNOSA	DORCADOSPYRIO CIRCULUS	DORCADOSPYRIS ATEUCHUS	CANNARTUS PRISMATICUS	DORCADOSPYRIS PAPILIO	CYCLAMPTERIUM PEGETRUM	DORCADOSPYRIS FORCIPATA	CALOCYCLETTA ROBUSTA
CALOCYCLETTA COSTATA																										
CALOCYCLETTA VIRGINIS																										
LYCHNOCANIUM BIPES																										
DORCADOSPYRIS ATEUCHUS																										
THEOCYRTIS TUBEROSA																										
THYRSOCYRTIS BROMIA																										

TABLE 2b

Stratigraphic ranges of Cenozoic radiolarian species. Radiolarian zonation is from Riedel and Sanfilippo (1971). Ranges of Eocene species are based on Figure 2 of Riedel and Sanfilippo (1970). Ranges of Oligocene and Miocene species are based on Figure 2 of Riedel and Sanfilippo (1971) and Table 1 of Moore (1971).

number of revolutions of the Savonius rotor, and the spacing between these marks is inversely proportional to the current speed.

Seismic Reflection Profiling

An air gun reflection profiling system on board the survey ship was used to identify the acoustic basement and to determine the sediment thickness and sediment distribution pattern. Profiles were obtained within the deep-tow survey area, and in an extensive area (measuring approximately 50 km by 50 km) surrounding the site of detailed investigation. Approximately 700 km of continuous profiles were obtained.

DESCRIPTION OF DEEP-TOW SURVEY AREA

Regional Setting

The site chosen for detailed study (near 07°40'N, 134°00'W; Fig.3) lies within the equatorial zone of high primary productivity, and consequently the principal component of the sediment is biogenous (Arrhenius, 1963). Cores from previous expeditions (Riedel, 1971) recovered outcropping Oligocene sediment at the survey site, suggesting that considerable sediment erosion may have taken place.

The surface sediment distribution pattern in this region of the Pacific has been described by numerous investigators, including Arrhenius (1952), Hays et al (1969), and Riedel (1971). Carbonate sediment is confined to the relatively shallow regions to the south of the Clipperton Fracture Zone, and to depths less than about 4500 m on the East Pacific Rise (Parker and Berger, 1971). Apart from these shallow regions, sediment types are generally siliceous in low latitudes and increasingly nonbiogenous in higher latitudes. Quaternary sediment appears to be thickest at the equator (Tracey et al, 1971), although fossiliferous Quaternary ooze extends over a wide zone between latutudes 14°N and 7°S (Hays et al, 1969). The width of this zone can be attributed to seasonal fluctuations in the circulation pattern (Knauss, 1963), and the corresponding seasonal, latitudinal, and longitudinal variations in primary productivity (Owen and Zeitzschel, 1970). Reflection profiling (Ewing et al, 1968) and deep drilling (Tracey et al, 1971) have shown that the sediment pattern
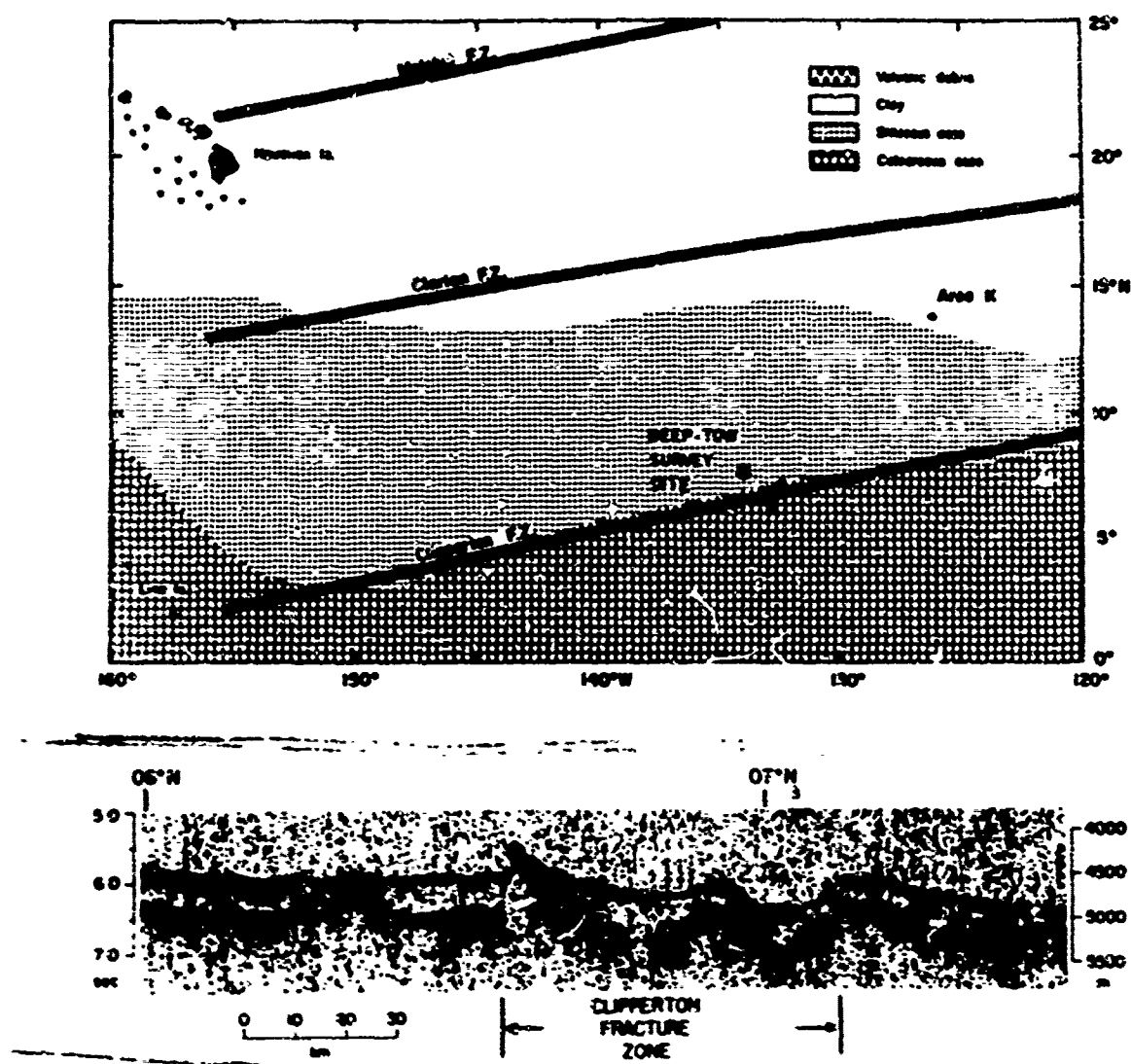
Figure 3 (top) Location of the deep-tow survey site in the equatorial Pacific.
Distribution of sediment types is modified after data of Arrhenius
(1963), Hays et al. (1969), and Riedel (1971). The solid line to the
southeast of the deep-tow area shows the location of the seismic reflec-
tion profile across the Clipperton Fracture Zone, shown below. The
location marked "Area K" was also surveyed using the deep-towed in-
strumentation. Some of the results from that survey are included in
this report.
(bottom) Continuous seismic reflection profile across the Clipperton
Fracture Zone. The relief of the acoustic basement within the fracture
zone is quite irregular, and contrasts noticeably with the relatively
smooth basement to the north and to the south. The sea floor to the
south of the fracture zone is somewhat shallower than to the north, and
the average sediment thickness increases from approximately 0.3–0.4
sec north of the fracture zone to 0.5 sec south of the zone.

has a pronounced north-south asymmetry, and that the sediment is
thickest a few degrees north of the equator. This effect can be
attributed, in part at least, to a northward component in the motion
of the Pacific plate during the Tertiary relative to the biological
equator.

The general features of the circulation of bottom water in
the central Pacific are fairly well established as a result of hydro-
graphic studies (Wooster and Volkmann, 1960; Reid et al, 1968; Edmond
et al, 1971; Gordon and Gerard, 1971) and direct current measurements
(Reid, 1969). Antarctic Bottom Water enters the Pacific Ocean south
of New Zealand and flows northward along the western wall of the Tonga-
Kermadec trench as an intensifiied western boundary current. The
current enters the North Pacific through a narrow passage northeast
of Samoa (Fig.4) and then apparently diverges. Major topographic
features including the Hawaiian Ridge, Line Islands Ridge, and
Mid-Pacific Mountains serve as barriers to bottom water flow within
the North Pacific (Edmond et al, 1971). Bottom currents are apparently
restricted to northwestward flow along the western side of the Line
Islands Ridge (C of Fig. 4), and turn eastward across the ridge
barrier at only two locations: Horizon passage (E of Fig. 4) and
Clarion Passage (F of Fig. 4). To the east of the Line Islands
Ridge and north of the Clipperton Fracture Zone the bottom water
flow appears to be eastward to northeastward (G of Fig. 4; also
Evans and White, 1971), but there are few direct current measurements
in this region.
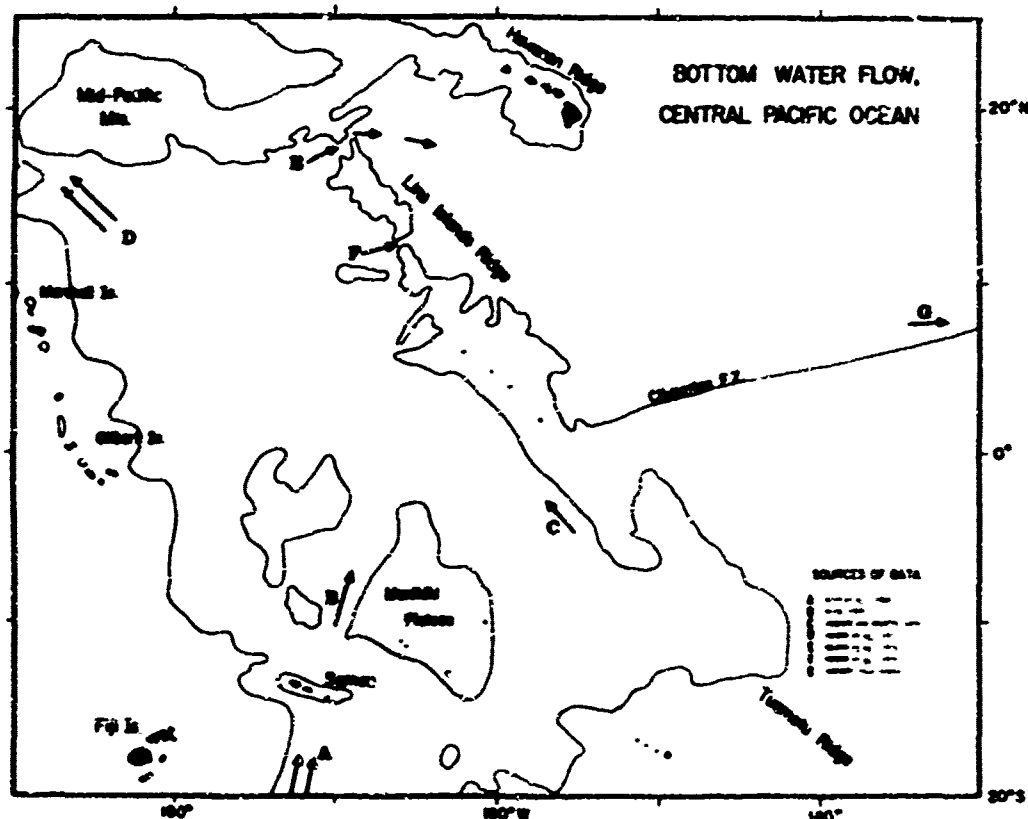
FIGURE 4   Direction of flow of bottom water in the central Pacific
            Ocean. The contour shown represents a depth of approx-
            imately 2500 fathoms (4700 meters). Arrows show the
            direction of flow of bottom water on the basis of hydro-
            graphic data and direct current measurements.

The Clipperton Fracture Zone (Menard and Fisher, 1958) is among the most prominent bathymetric and structural features in the eastern equatorial Pacific. The fracture zone is commonly a well defined north-facing escarpment (Heath and Moore, 1965; Ewing et al, 1968) with up to several hundred meters of relief. In the region nearest the study area the fracture zone is not an obvious topographic feature, but it can be identified by seismic reflection profiling (Fig.3).

Between the fracture zones of the northeast Pacific the principal topographic features are low abyssal hills up to several hundred meters in height (Chase et al, 1970). The hills are commonly elongated in a direction parallel to the trend of the magnetic anomalies, and appear to be both volcanic and tectonic in origin (Luy-endyk, 1970). In low latitudes the magnetic lineations are difficult to identify (Atwater and Menard, 1970), and topographic lineations are obscured by the thick cover of pelagic sediment (Ewing et al, 1968).

The age of the oceanic crust at the deep-tow survey site can be estimated from the recent results of deep drilling. The Deep Sea Drilling Project Sites 159, 160, and 161, together with the deep-tow survey site, lie between the Clarion and Clipperton Fracture Zones (Fig. 5). Basalt was penetrated at each of these three DSDP sites (van Andel et al, 1971). If one assumes that (1) the age of the oldest sediment cored at these drilling sites is approximately the same as the crustal age, and (2) the rate of crustal formation was nearly uniform during the time interval
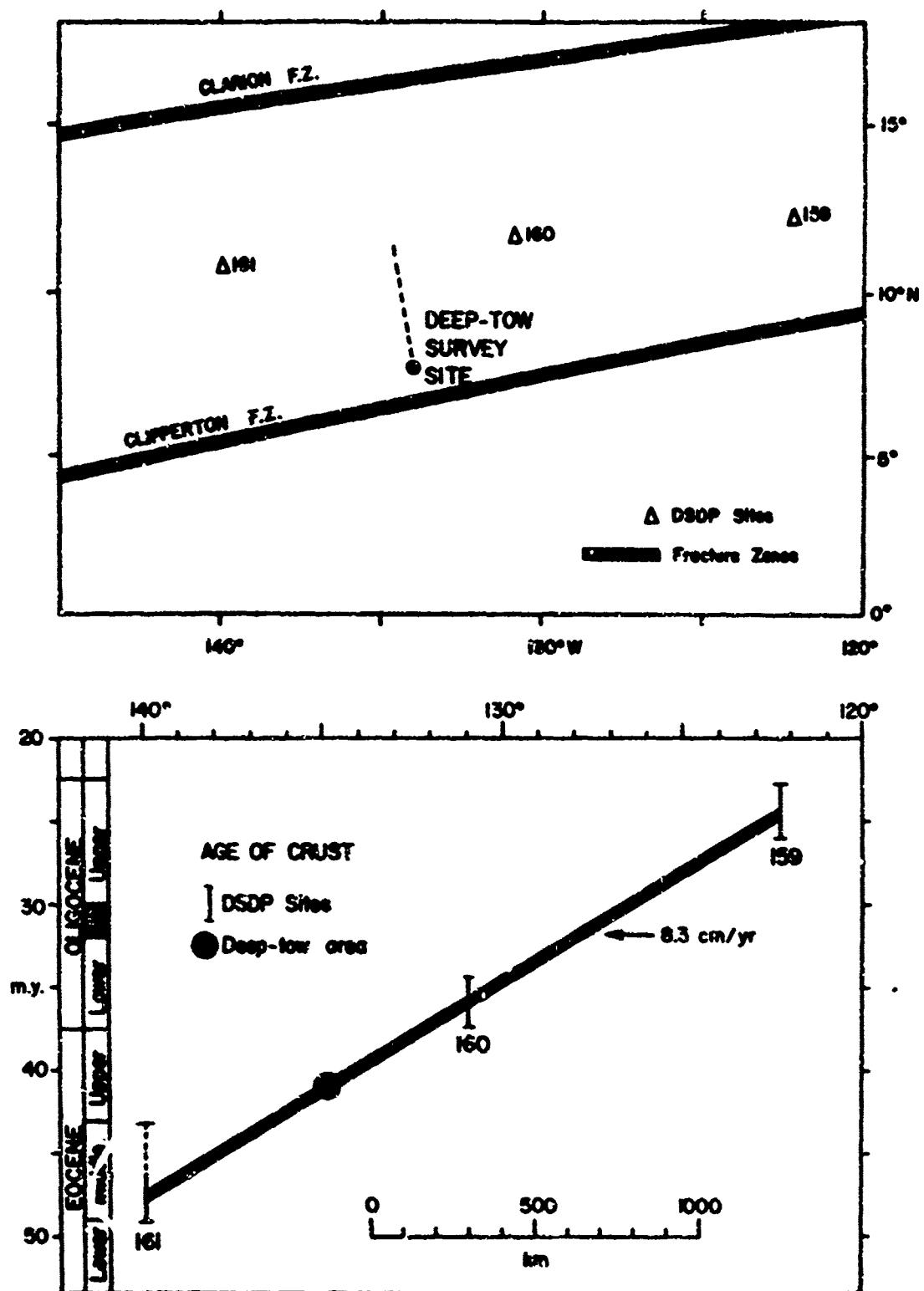
Figure 5 (top) Location of Deep Sea Drilling Project sites in the vicinity of the deep-
tow survey area. Basalt was cored at each of these drilling locations.
(bottom) Age of oldest sediment obtained at the drilling sites shown above
(after Van Andel et al., 1971). The age of the oceanic crust at the deep-tow
site can be estimated by interpolating from the drilling results. The half-
spreading rate during this period of crustal formation was around 8.3 cm/yr.

represented by this portion of oceanic crust, then by interpolation
one can estimate that the crustal age at the deep-tow survey site
is approximately 41 million years, or within the Upper Eocene (Fig.5).
The average half-spreading rate during this interval of crustal
formation was around 8 cm/yr, a rate which was predicted by Riedel
(1967) on the basis of core data alone.

Bathymetry

The site of detailed study centers around a flat-topped
plateau and an adjacent trough, both of which are elongated in a
north-south direction (Fig.7). The plateau is up to 5 km in width,
and rises 200 to 300 m above the surrounding sea floor. The summit
is bordered by a well defined break in slope, which deepens toward
the northern end. The western flank of the plateau is smooth and
gently sloping near the crest, with some escarpments 10-20 m in height
near the base (Fig. 10). A topographic depression lies between the
plateau and the surrounding sea floor to the west. The eastern
flank is characterized by escarpments with slopes which locally are
60° or greater; some of these escarpments are up to 50 m in height
(Fig. 12). The plateau narrows to the north until it is indistin-
guishable from the surrounding sea floor. To the south the plateau
becomes part of a steep basement ridge.

A north-south trending trough lies to the east of the plateau
(Figs. 7 and 8). The trough, which is 5 to 10 km in width, is
apparently closed at the northern end of the survey area (Fig. 7).
It deepens in a southward direction, and continues beyond the
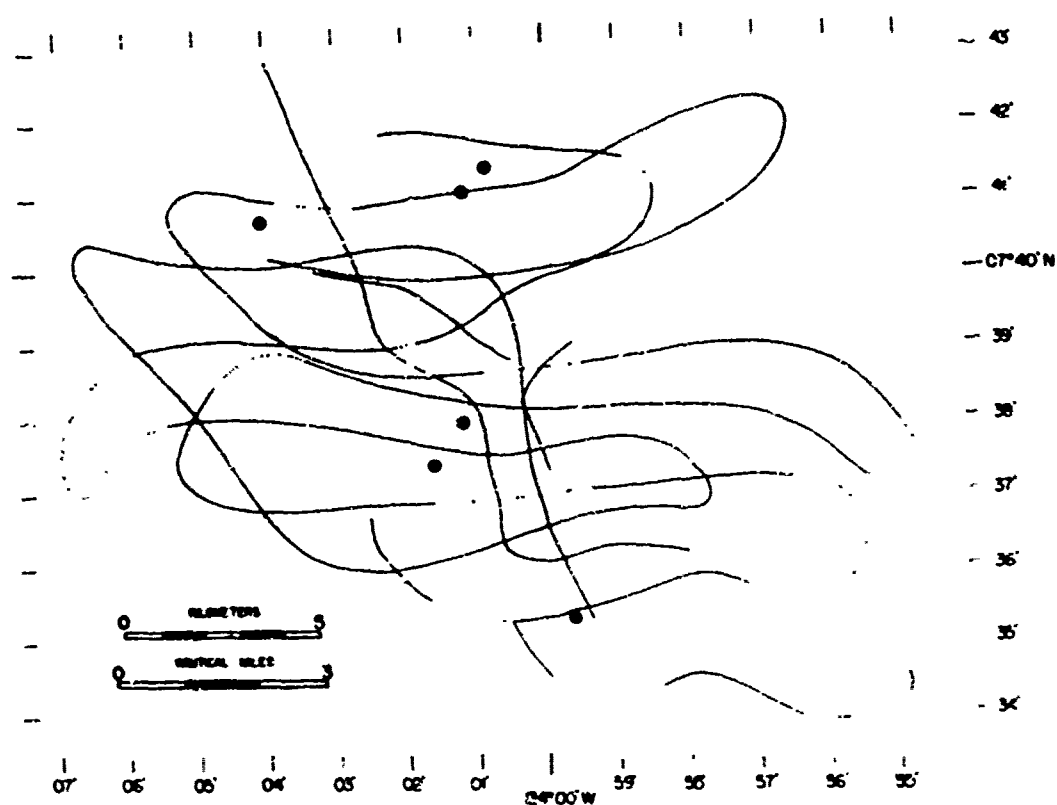
FIGURE 6   Path of the deep-towed instrument within the region of
            detailed study. Quartered circles show the location of
            anchored acoustic transponders. Ranges to two or more
            transponders were obtained along the portion of the
            track shown in solid lines.
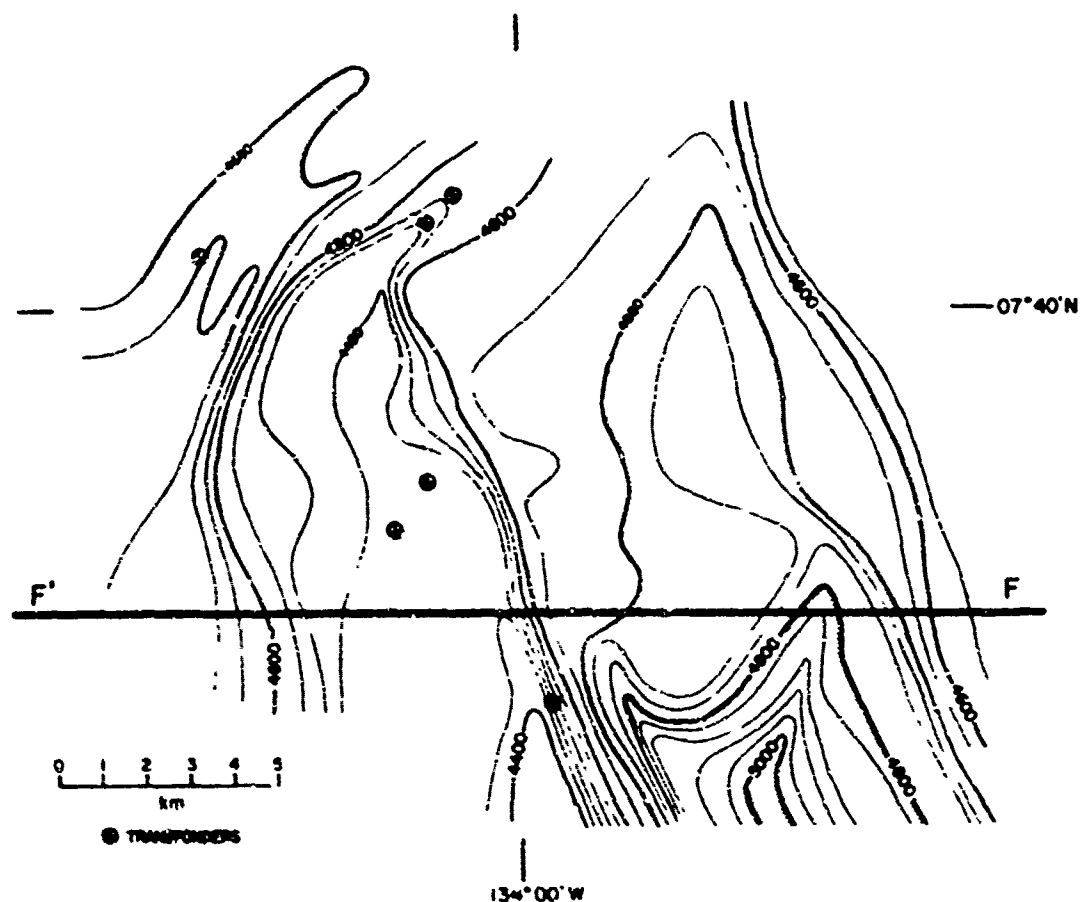
FIGURE 7   Bathymetry of the deep-tow survey area. Contour interval
            is 40 meters. Line F'F indicates the location of the
            seismic reflection profile shown at the top of Figure 8.
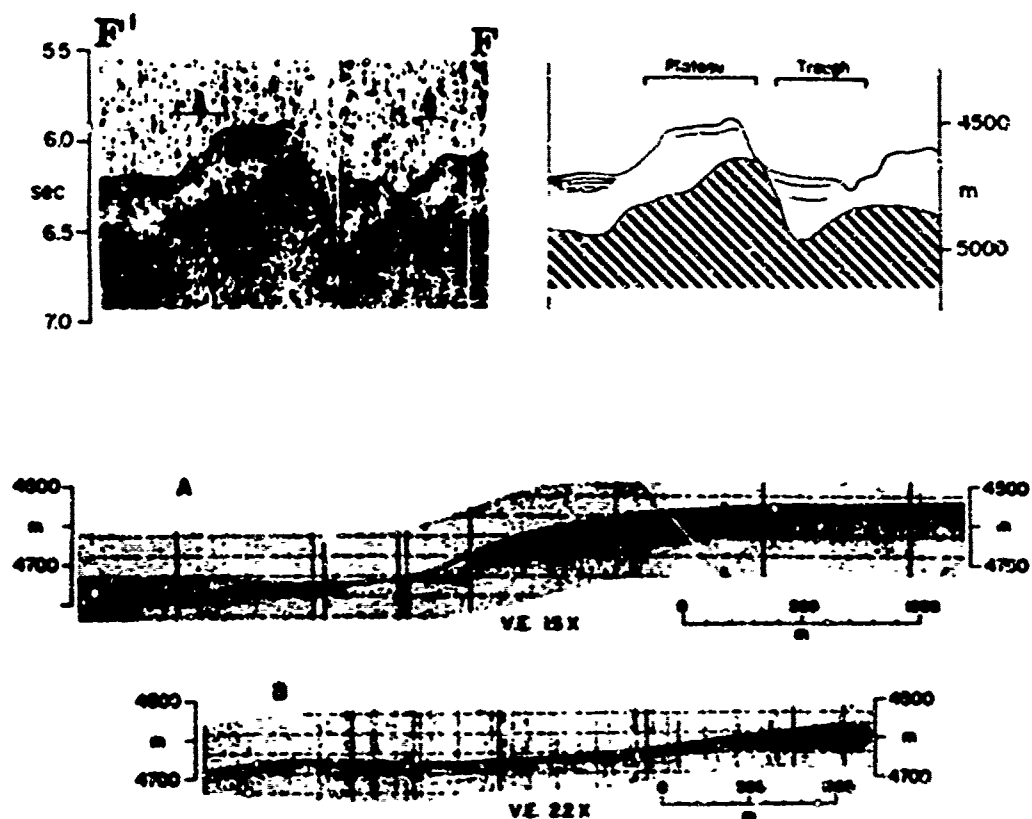
Figure 8 Comparison of surface and near-bottom reflection profiles.
(upper left) East-west seismic reflection profile across the deep-
tow survey area. Vertical exaggeration 16 X.
(upper right) Line drawing of profile F'F. The acoustic basement
appears to outcrop at the base of the plateau's east flank. A promi-
ment erosional channel can be seen on the floor of the trough.
(bottom) Reflection profiles (3. 5 kHz) obtained from the deep-towed
instrument. The approximate locations of these profiles along F'F
are indicated. Profile A is from the west flank of the plateau, and
profile B is from the east side of the trough. There is relatively
little vertical exaggeration on the deep-tow profiles. The trun-
cation of sub-bottom reflectors is clear on the deep-tow profiles,
but cannot be resolved on the profile obtained from the sea surface.

southernmost limit of the area of detailed study. A major channel
extends southward along the axis of the trough, with at least one
secondary channel entering from the plateau to the west. The princi-
pal channel is bordered by broad, smooth terraces, several km in
width, which parallel the channel along the floor of the trough.

Structure

Air gun profiles from surface ship

Seismic reflection profiling techniques from the surface
ship were utilized to estimate the sediment thickness and distribu-
tion pattern within the deep-tow survey area and in the surrounding
region. The plateau in the area of detailed study is composed of
0.3 to 0.4 sec of sediment which overlies an irregular acoustic
basement (Fig. 8). On the plateau's eastern flank the basement
appears to outcrop locally. In the trough, to the east of the
plateau, sediments are 0.2 to 0.3 sec in thickness. The relief of
the sea floor bears some relation to that of the acoustic basement,
but the total sediment thickness is highly variable over distances
of a few kilometers or less.

The air gun profiles obtained by the ship are insufficient
for resolving the sedimentation pattern around small features and
for detecting fine-scale layering within the sedimentary unit.
These profiles commonly show few or no internal reflectors within
the sedimentary material. Considerably more detail appears when
low frequency profiling techniques are used from the towed instrument
operating near the sea floor (see Fig. 8 for comparison of surface

and near-bottom reflection profiles). Continuous reflection profiles obtained by the 3.5 kHz system on the deep-towed instrument show stratification within the sediment which could not be resolved by the air gun profiling techniques. These near-bottom profiles are the basis for identifying the relative ages of outcropping strata, and determining the fine-scale sediment distribution pattern within the survey area.

3.5 kHz profiles from deep-towed instrument

Near-bottom reflection profiling shows that the plateau is underlain by horizontal to gently dipping sedimentary layers which outcrop on both the east and west flanks. The relief on the plateau's west flank is characteristically smooth near the crest, and profiles from these regions (Fig. 10) clearly show outcropping strata which appear to be progressively older down the flank. The layers which outcrop near the base appear to be 100 to 200 m stratigraphically beneath those which outcrop near the crest (Profile 2). There is evidence on Profile 1 (Fig. 10) that folding of the sediments has taken place; this interpretation is supported by results of sediment coring along this profile (Fig. 17, Profile II).

A topographic depression separates the plateau from the surrounding sea floor to the west. In this region the relief is often irregular (Fig. 10, Profiles 3 and 4), and identification of sub-bottom reflectors is more difficult. The profiles suggest that this depression is an erosional channel. Locally the channel is bordered by escarpments up to 50 m in height with near-horizontal
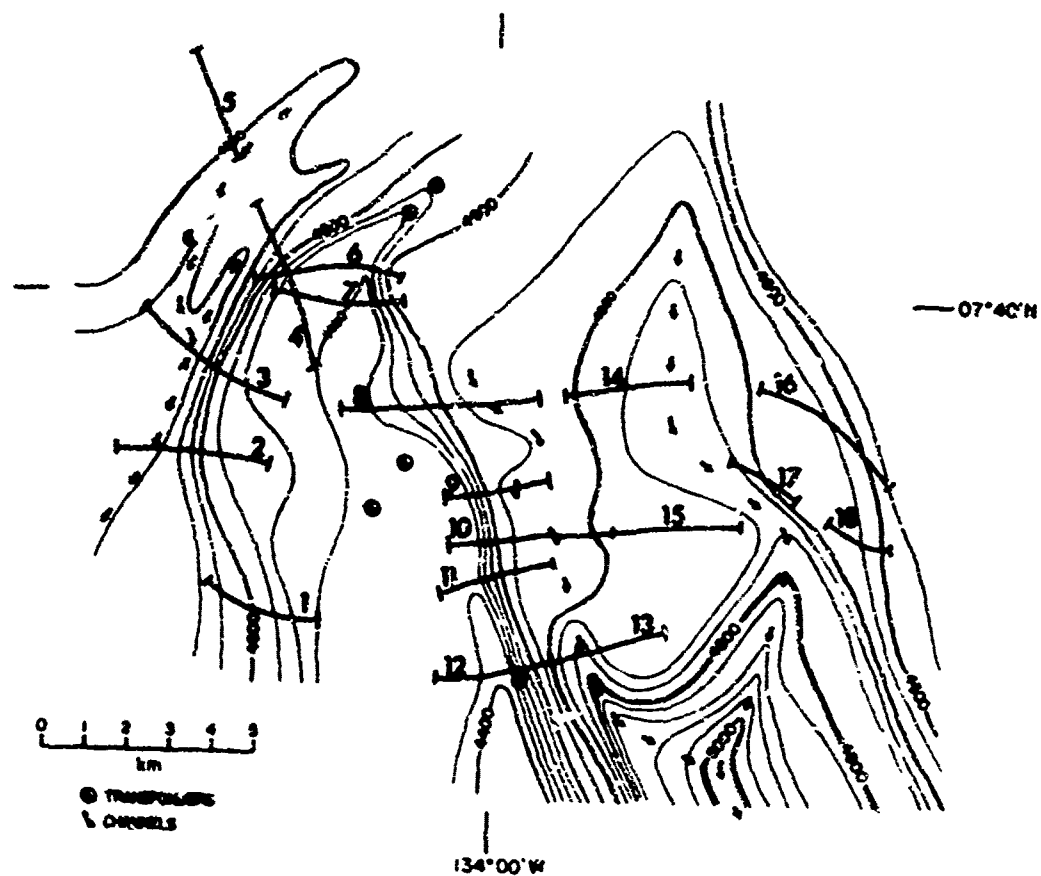
FIGURE 9   Locations of near-bottom reflection profiles shown in
            Figures 10 through 14. Arrows indicate erosional
            channels which appear on the profiles.
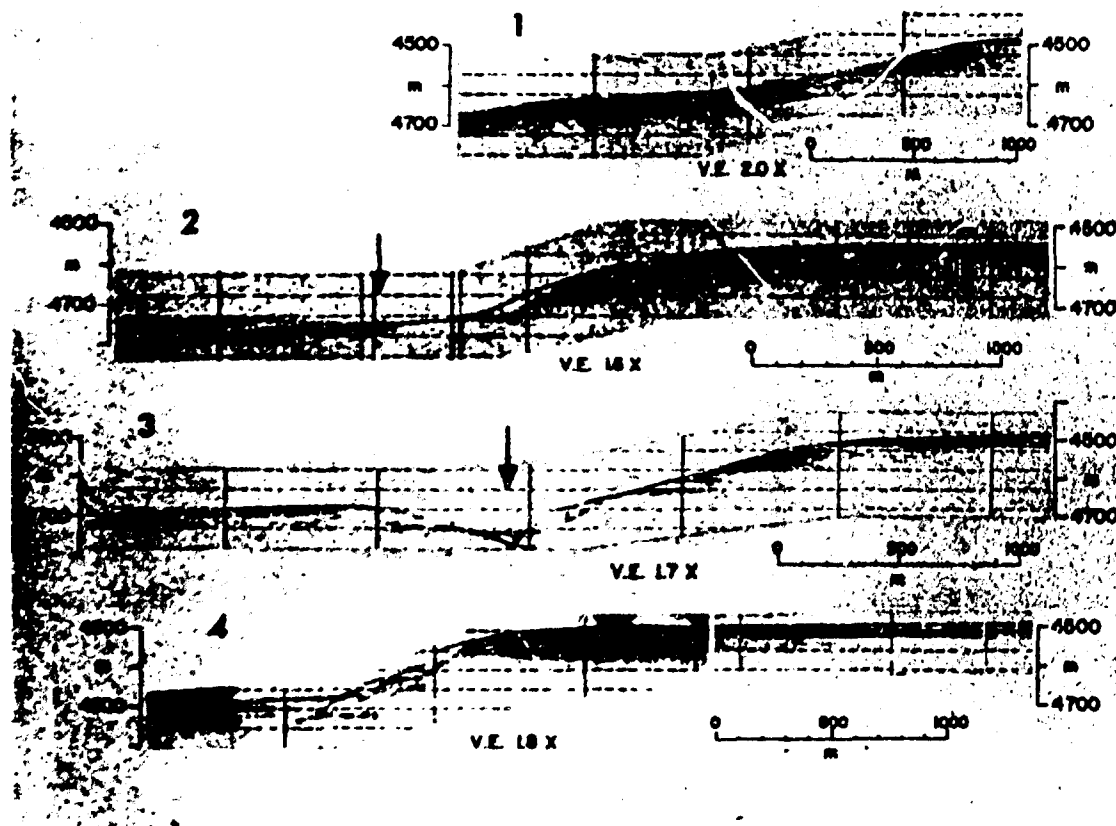
Figure 10   Near bottom reflection profiles from the west flank of the pla-
teau.   Outcropping horizontal strata can be seen on the upper
flank.   Topographic and structural details at the base of the
slope on profile 3 are obscure because of the height of the
instrument at this point.   Arrows indicate the location of a
principal erosional channel which extends southward along the
base of the slope.

sedimentary strata outcropping at the walls on both sides (Fig. 10,
Profile 3; Fig. 17, Profile I). Elsewhere the relief at the base
of the plateau is relatively smooth (Fig. 10, Profile 2).

The sea floor to the west of the plateau is characterized
by gently dipping strata which are abruptly truncated at the sea
floor interface. Fig. 11 shows an eroded synclinal structure in
which layers that are 100-200 m apart stratigraphically appear to
outcrop within a distance of one or two kilometers. This sharp
angular unconformity is widespread throughout the surveyed area
and results in outcropping strata of markedly different ages over a
small area. Beneath the sea floor, however, the strata appear to
be conformable, with no evidence of similar unconformities at depth.

The topography on the east flank of the plateau is irregular,
with steep (>60°) escarpments 20 to 100 m in height in some regions
(Fig. 12, Profiles 8, 9, and 11), and smooth slopes elsewhere (Pro-
files 10, 12). Near the crest the strata dip gently toward the west,
and in the trough beyond the base of the plateau the layers dip
eastward, suggesting an eroded anticlinal structure (Profiles 8,
9, and 10). On the intervening lower slopes the topography is
irregular and the sea floor is acoustically opaque to the 3.5 kHz
profiler, commonly obscuring the details of the subsurface structure.
Near the southern end of the survey area a strong acoustic reflector
outcrops at the sea floor (Fig. 12), which probably corresponds to
the acoustic basement identified by reflection profiling from the
ship (Fig. 8).
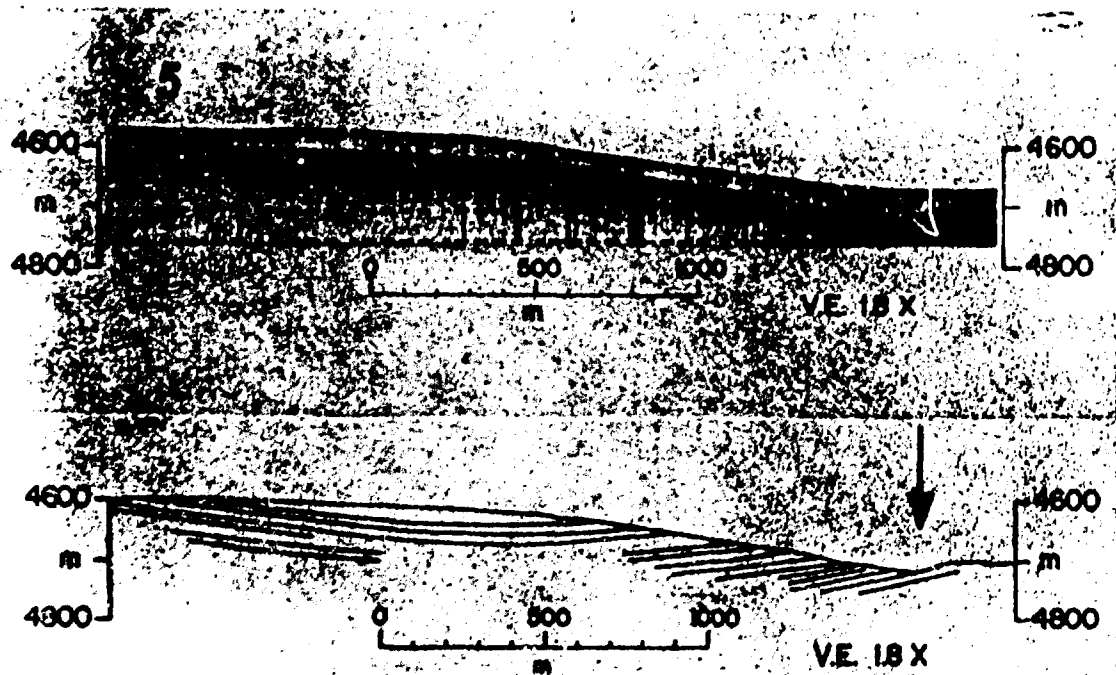
FIGURE 11   (top) Near-bottom reflection profile showing an eroded
             synclinal structure.
             (bottom) Line drawing interpretation of Profile 5
             shown above. The arrow marks the axis of an erosional
             channel.
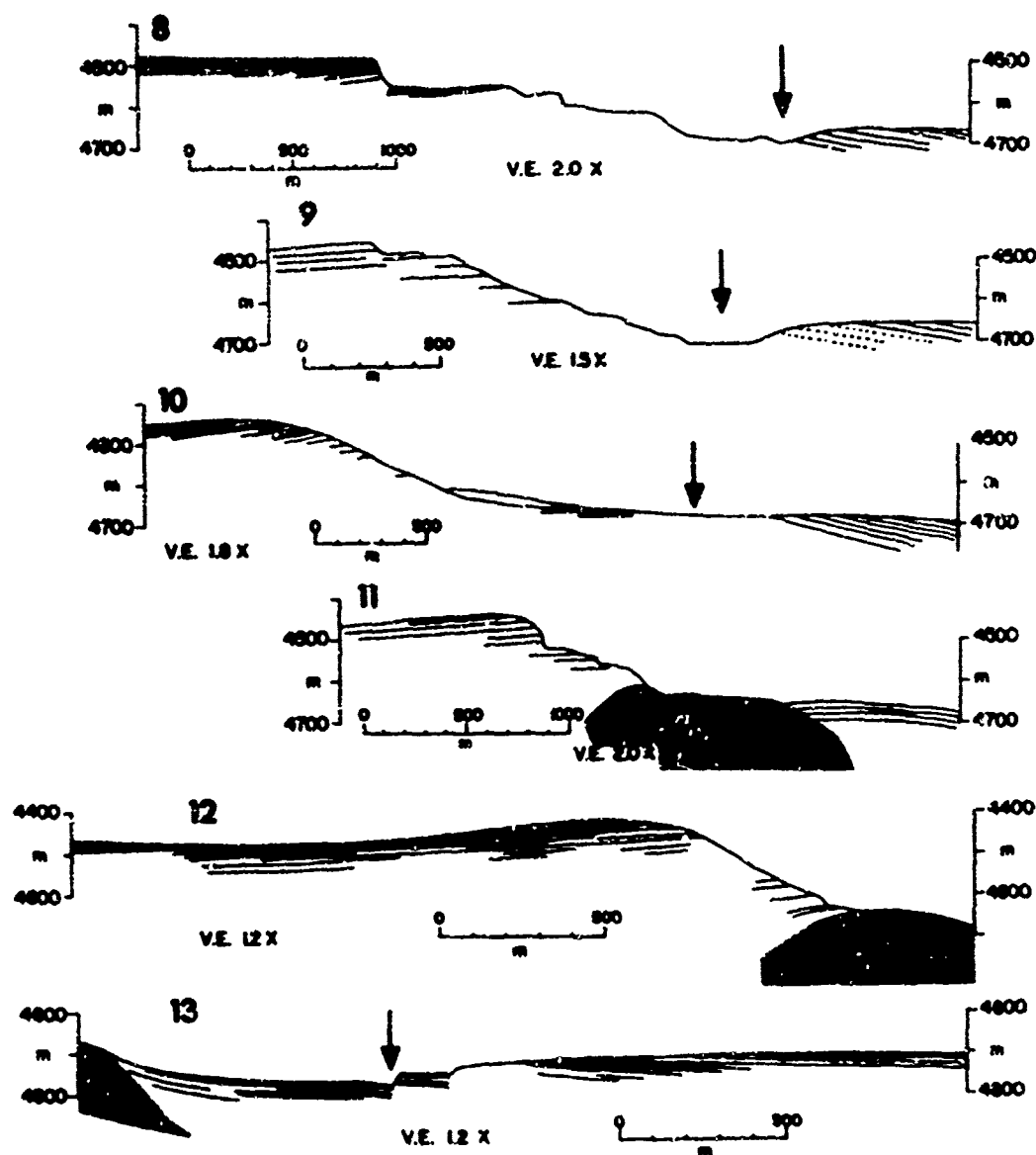
FIGURE 12   Line drawings based on near-bottom reflection profiles
from the east flank of the plateau. Apparent outcrops
of the acoustic basement are shown on the scuthernmost
profiles. The arrows indicate the axis of a channel
at the base of the plateau.

A channel extends southward along the base of the plateau's
east flank (see arrows on profiles in Fig. 12). The oldest sediment
recovered from the area was cored at two locations within the axis
of the channel (Fig. 18, Cores E-10 and E-19). Near the southern end
of the deep-tow survey area this channel joins a larger one which
extends down the axis of the trough to the east (Fig. 9).

The plateau becomes increasingly narrow toward its northern
end until it is indistinguishable from the surrounding sea floor.
Profiles across the northern end (Fig. 13) show that the strata be-
neath the plateau are synclinal, and that the depth is shallower
at the plateau's edges than in the center. The relief on the pla-
teau's flanks in this region is steep and irregular, and the towed
instrument was not sufficiently close to the bottom to delineate
the fine-scale topographic features.

The trough to the east of the plateau has gentle relief,
with no steep escarpments except locally along the axis of the channel.
Broad smooth terraces border the channel on either side (Fig. 14).
Beneath the surface of the terraces the layers are horizontal to
gently dipping. Here, as elsewhere within the study area, the sea
floor topography bears little relation to the structure of the under-
lying strata. On the terraces to the west of the channel the strata
are near horizontal, and increasingly older layers are outcropping
in the direction of the channel axis (arrow on Profile 14). East
of the channel the strata are gently dipping and show evidence of
compressional folding (Profiles 16-18). The structures have been
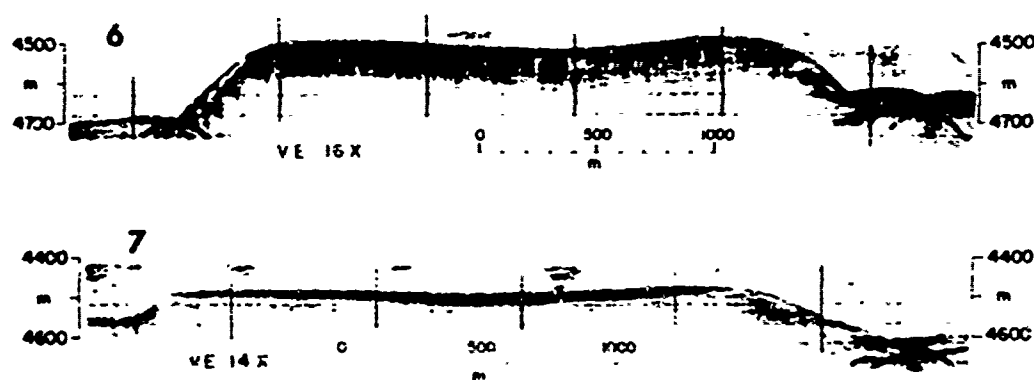
FIGURE 13   Near-bottom reflection profiles across the northern end
             of the plateau. Horizontal strata can be seen beneath
             the plateau's surface. Topographic details on the
             slopes are obscure because of the height of the instru-
             ment on these crossings.
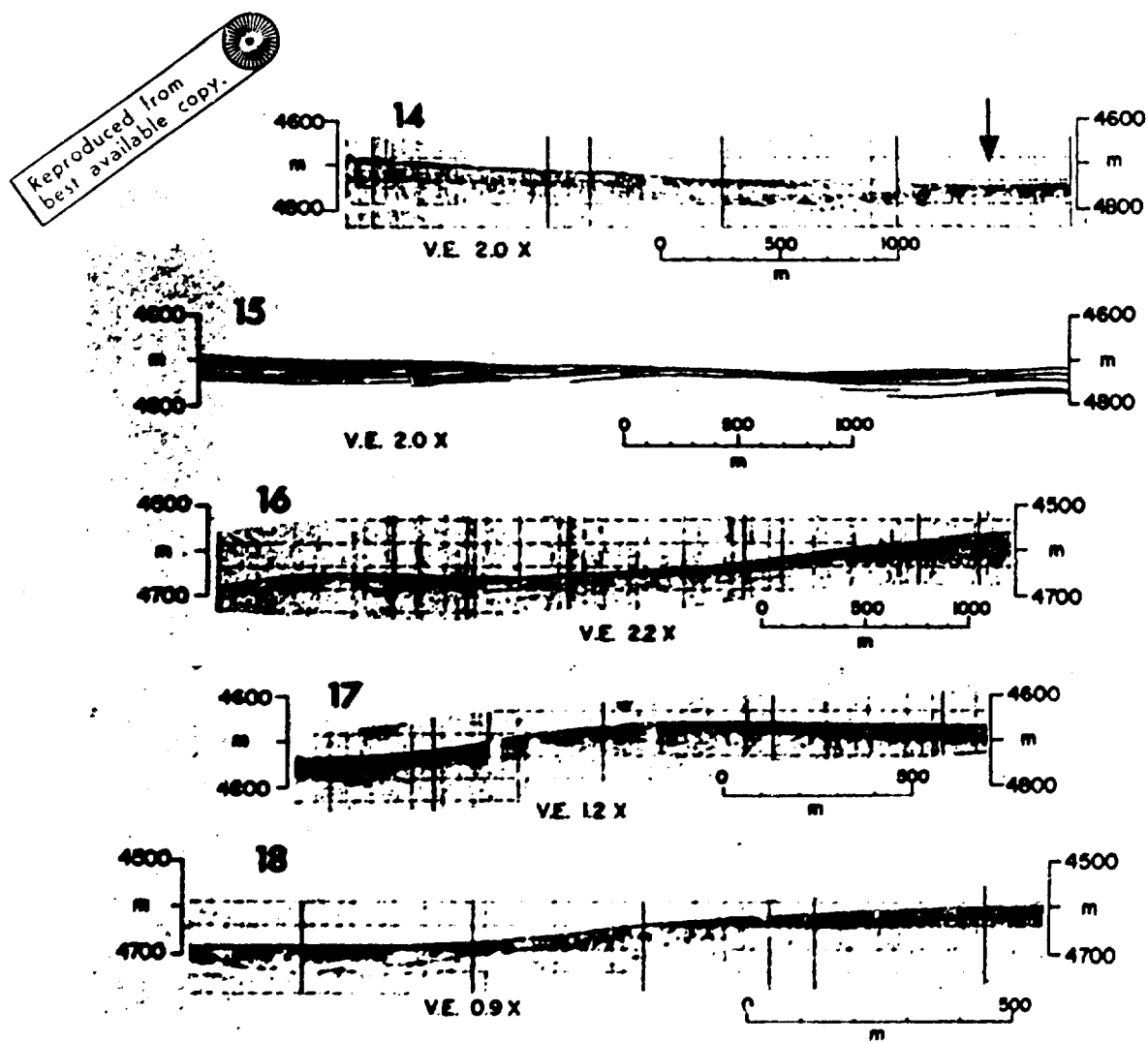
FIGURE 14   Near-bottom reflection profiles from the gently
             undulating region east of the plateau. All profiles
             show strata which are truncated at the sea floor
             interface. The arrow on profile 14 indicates the
             axis of the channel which extends southward along
             the floor of the trough.

sharply truncated at the sea floor by erosion, both on the slopes
and on the relatively level terraces themselves. As elsewhere there
is no indication of similar unconformities at depth.

Sediment Types

Forty-two free-fall cores and two piston cores were obtained
within the survey area (Fig. 15). The principal objective of the
coring was to determine the age of the outcropping sediment layers
which were identified by reflection profiling from the towed instru-
ment. All except one of the cores (Core E-22, Fig. 18) penetrated
through a thin covering of Holocene sediment and recovered signi-
ficantly older material corresponding to the outcropping accustic
reflectors.

There are two distinct sediment types represented in the
cores; these major units are separated by a marked unconformity
(Fig. 16; Plates 4-9):

a. The upper unit is a dark brown (10 YR 4/3) siliceous cal-
careous ooze, consisting largely of biogenous skeletal debris, but
with a small amount (<15%) of clay-size nonbiogenous material. The
ooze has a high water content (Fig. 16; Table 3), and is markedly
different in texture from the underlying material. The upper unit
is up to a few centimeters thick in most of the cores, but in a few
cores the unit is missing entirely.

b. The lower unit is a white (N9) to yellowish brown
(10 YR 5/6) chalk, consisting almost entirely (>98%) of biogenous
skeletal debris. The chalk has a stiff texture and a significantly
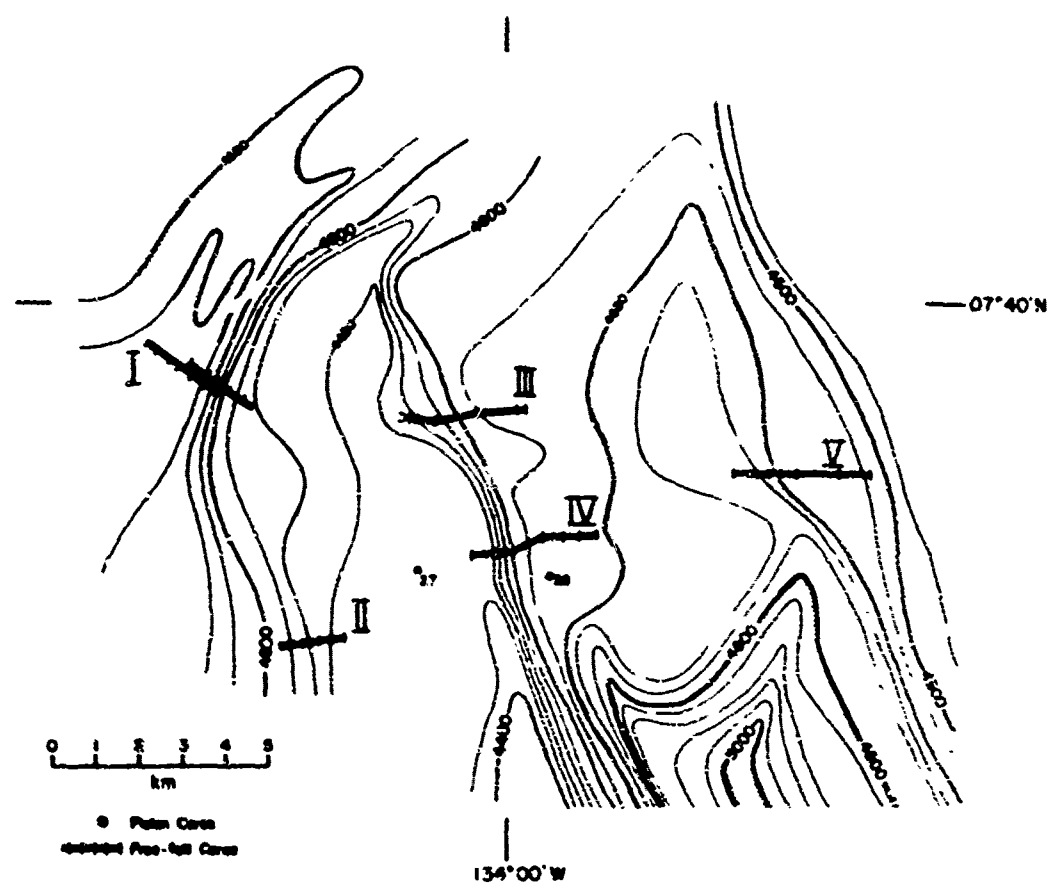
FIGURE 15   Locations of sediment cores from the area of detailed
             study. The circles labeled "27" and "28" indicate the
             locations of piston cores E-27 and E-28, respectively.
             Coring procedures are discussed in the text.
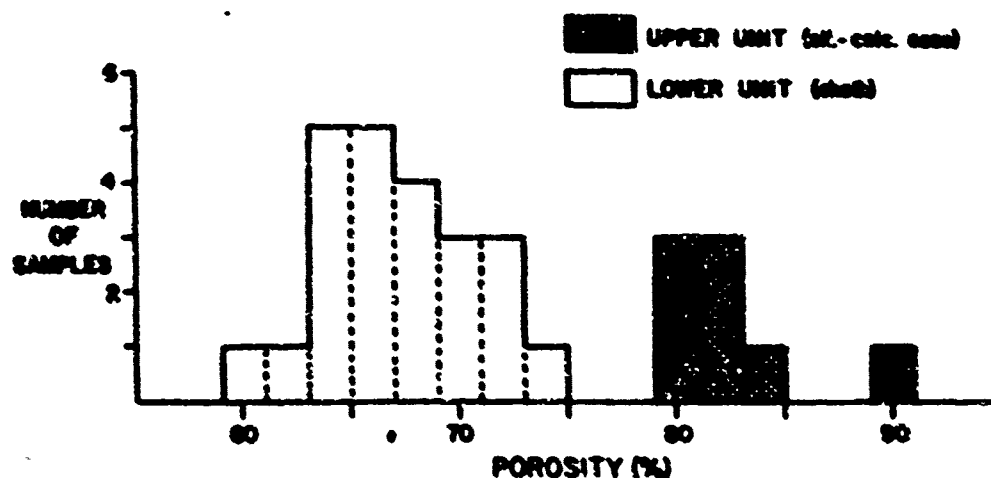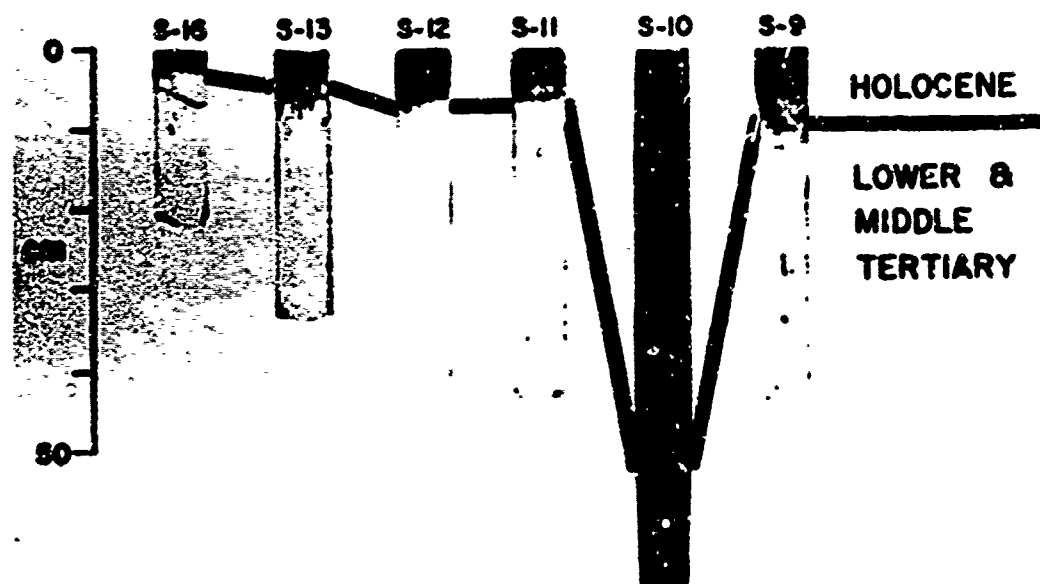
Figure 16 (top) Free-fall cores from Profile II, showing the sharp uncon-
formity between Holocene ooze and the chalk of Tertiary age.
This unconformity was penetrated in 43 of the 44 cores obtained.
(bottom) Histogram summarizing results of porosity determina-
tions. The chalk beneath the unconformity has a significantly
lower porosity and water content than the overlying Holocene sedi-
ment. The stiff texture of the chalk prevented deeper penetration
of the cores.

TABLE 3   Physical properties of several of the cores

Core No.	Level (cm)	Mean diam. (mm)	Percent: Sand	Silt	Clay	Saturated bulk density	Grain density	Porosity (%)	V (m/sec)
E-6	0-5	.0050	6.6	49.3	44.1	1.299	2.597	82.5	----
E-6	25-33	.0122	0.9	72.3	26.8	1.610	2.731	65.7	1523
E-11	12-20	.0043	0.7	56.1	43.2	1.530	2.702	63.9	1542
E-15	0-5	.0092	11.3	56.4	22.3	1.335	2.635	80.7	----
E-16	36-44	.0043	1.0	56.8	42.2	1.536	2.751	70.4	1537
E-17	11-19	.0137	1.4	71.9	26.7	1.541	2.687	68.9	1527
E-19	18-26	.0052	1.0	65.5	33.5	1.295	2.748	84.3	1519
E-20	18-26	.0051	2.4	57.2	40.4	1.575	2.680	66.7	1523
E-21	14-22	.0051	4.7	62.0	33.3	1.487	2.668	71.8	1526
E-22	4-12	.0043	14.4	32.6	53.0	1.313	2.666	82.4	1527
E-23	3-11	.0053	2.5	57.2	49.3	1.496	2.681	71.5	1519
E-26	13-21	.0052	2.4	60.1	37.5	1.516	2.660	69.9	1524
E-27	0-9	.0052	13.2	39.8	47.0	1.319	2.631	81.6	----
E-27	9-13	.0057	17.0	35.2	47.8	1.368	2.680	79.2	1533
E-27	94-102	.0045	2.8	53.2	44.0	1.171	2.489	90.0	1527
E-27	230-238	.0028	1.5	36.1	62.4	1.683	2.685	60.3	1546
E-27	363-371	.0027	2.3	35.2	62.5	1.627	2.700	64.0	1532
E-28	36-44	.0052	1.2	58.8	40.0	1.597	2.706	65.9	1527
E-28	118-126	.0048	1.0	59.6	39.4	1.604	2.685	65.1	1526
S-2	10-18	.0053	7.2	50.1	42.7	1.615	2.647	63.6	1572
S-4	3-11	.0092	3.0	48.1	48.9	1.556	2.688	66.9	1540
S-6	2-10	.0199	2.6	72.0	25.4	1.589	2.683	65.9	1538
S-8	12-20	.0100	2.1	69.7	28.2	1.651	2.693	62.4	1536
S-9	28-36	.0040	2.0	56.2	41.8	1.554	2.695	68.3	1526
S-10	26-34	.0126	3.8	70.2	26.0	1.352	2.620	79.4	1520
S-11	31-39	.0106	1.4	67.5	31.1	1.570	2.700	67.5	1537
S-12	30-38	.0055	2.0	63.7	34.3	1.618	2.662	63.7	1538
S-13	22-30	.0059	2.1	67.6	30.3	1.623	2.665	63.5	1550
S-17	0-8	.0039	1.2	49.7	49.1	1.506	2.690	71.1	1518
S-19	0-8	.0041	1.2	55.7	43.1	1.552	2.651	69.4	1530
S-21	0-8	.0029	1.4	48.4	50.2	1.416	2.646	75.8	1512

lower water content than the overlying ooze. The chalk appears to
be partially lithified, but microscopic examination indicated that
very little recrystallization had taken place. The stiffness of
the chalk prevented the free-fall core barrels from penetrating
deeper than a few tens of centimeters (Plates 4-8).

There has been significant vertical mixing of material across
the boundary between these two layers. The lower unit in cores
E-4 and S-21 contains burrows several cm in length (Plates 6 and 8),
and these burrows have been filled with sediment from the upper unit.
There is a significant amount of contamination by microfossils
from the underlying chalk into the Holocene sediment.

Biostratigraphy

The upper unit in the cores contains abundant Quaternary
radiolaria, including Ommatartus tetrathalamus, Spongaster tetras,
Euchitonia elegans, Pterocanium praetexum, and Theocorythium
trachelium. The radiolarian assemblage in this unit contains a
considerable proportion of reworked Tertiary species, some of which
have been vertically mixed from the underlying chalk, whereas others
must have been eroded from nearby outcrops and laterally transported
to the site of deposition. The foraminifera present in this unit
include Globorotalia tumida, G. cultrata, Globoquadrina dutertrei,
and Pulleniatina obliquiloculata. The species which are present show
considerable effects of dissolution; the original assemblage may have
included additional species which are more easily dissolved (Berger,
1968a). All of these species are present day low latitude forms

(Bradshaw, 1959; Parker, 1971), and are interpreted as Holocene in age.

The age of the outcropping chalk ranges from Upper Eocene to Middle Miocene within the study area (Figs. 17 and 18). The radiolarian and foraminiferal assemblages within this unit consist of species of uniform age, with no evidence of reworking. The apparent lack of reworking and the excellent preservation of the radiolarian specimens enabled precise age assignments to be made. The foraminiferal assemblages showed considerable effects of dissolution with only the more resistant species remaining. A tabulation of the abundances of radiolaria and occurrences of foraminifera within the lower unit of the cores is shown in Plates 10 and 11.

Profile 1

Fifteen free-fall cores were obtained along this profile, which extends from the crest of the plateau down the west flank, across the slope-base depression, and on to the surrounding sea floor. The nine cores from the plateau's flank are progressively older toward the base (Fig. 17), confirming the evidence from reflection profiling which suggests outcropping layers of near horizontal strata. Within the topographic depression at the base, however, the chalk layers are significantly younger than those on either side (Fig. 17, Profile I), suggesting that the depression and the adjacent escarpments may be in part a result of post depositional normal faulting. Late Tertiary and Quaternary sediment is virtually absent within the axis of the depression, indicating that erosional processes
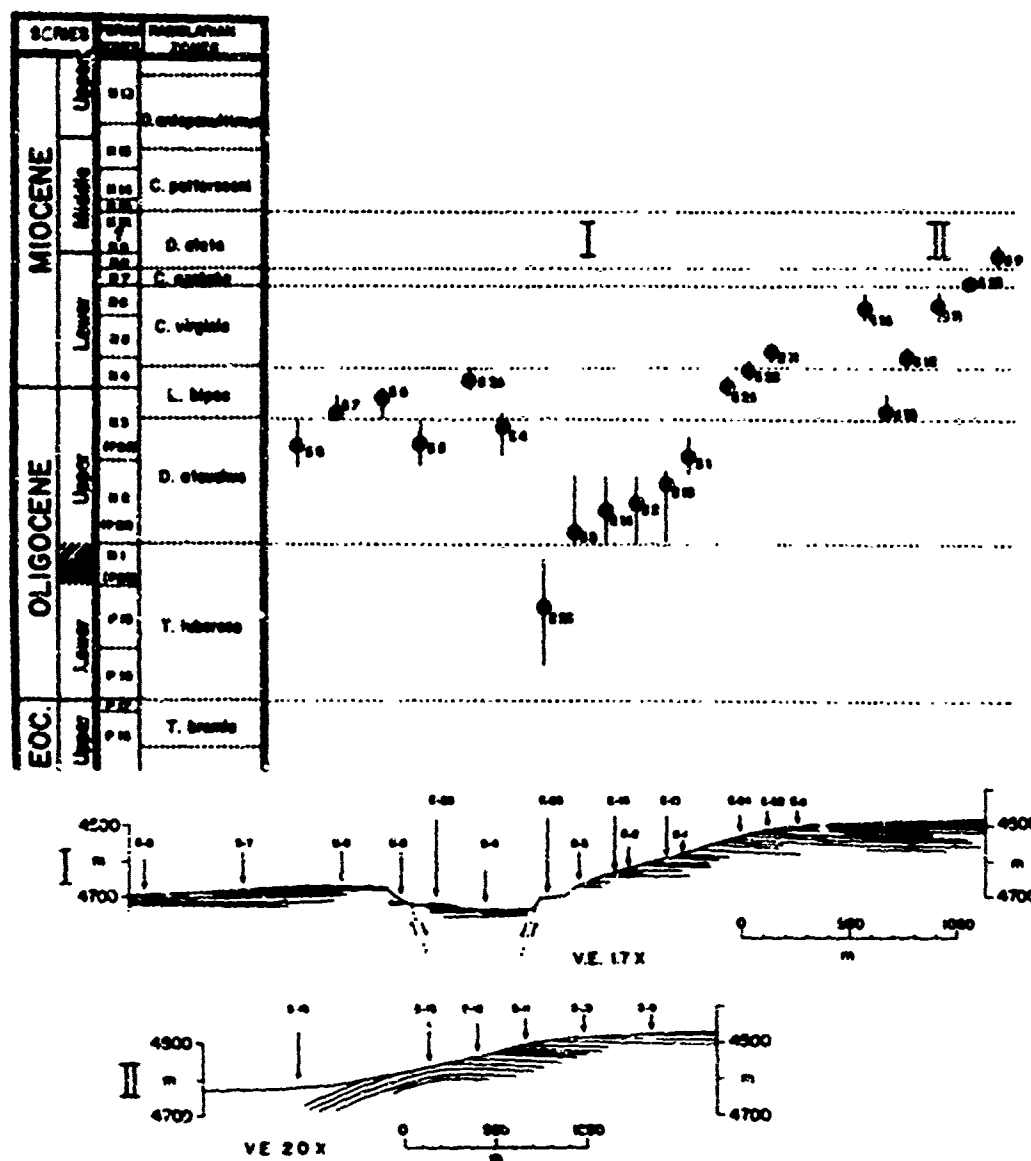
Figure 17   Age of lowermost material in sediment cores from Profiles I and
II. The sub-bottom reflectors shown on the profiles are traced
from 3.5 kHz continuous reflection profiles obtained by the deep-
towed instrument package operating close to the sea floor. Age
assignments are based on radiolarian assemblages, and are shown
relative to the radiolarian zones of Riedel and Sanfilippo (1971).
Vertical lines indicate the uncertainty in age determinations. The
radiolarian zones are correlated with foraminiferal zones and
time-stratigraphic units after Berggren (1971).
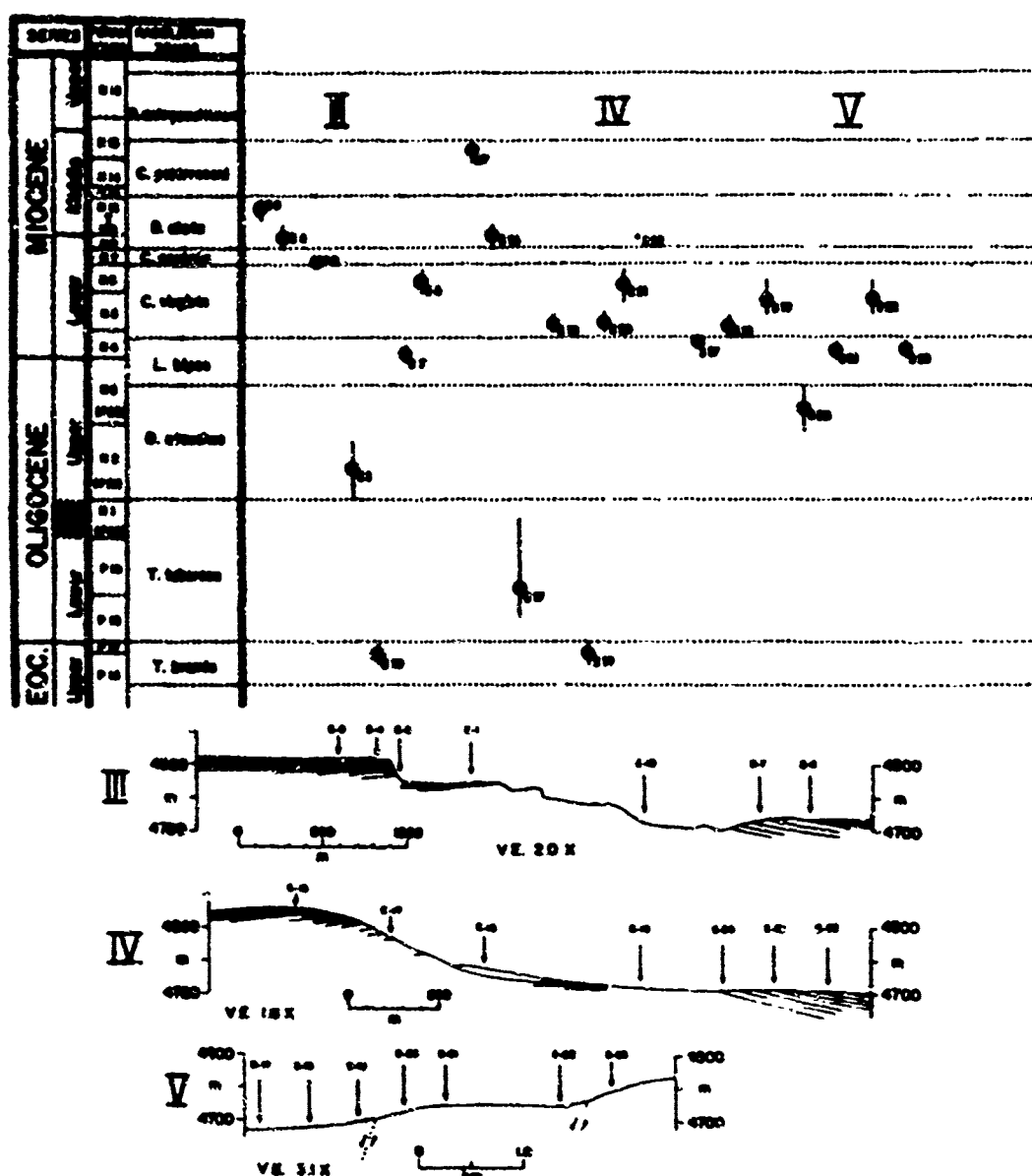
Figure 18 Age of lowermost material in sediment cores from Profiles III,
IV, and V. Profiles III and IV are traced from 3.5 kHz records
obtained by the deep-towed instrumentation. Profile V is from
the ship's echo sounding reco⁻'. Age assignments are based
on radiolarian assemblages (see Plate 11), with vertical lines
indicating the uncertainty in age determinations. Core E-27
is grouped with those of Profile IV. *Core E-22 is Quaternary
throughout its entire length, and consequently the age of the
chalk at this locality is not known.

subsequent to faulting have been influential in shaping and modifying the channel topography.

Profile II

Six cores are from the west flank of the plateau near the crest, at a site where reflection profiling suggested that the sedimentary strata had been folded and subsequently truncated at the sea floor (Fig. 10, Profile 1). The ages of the cores confirm this interpretation (Fig. 17).

Profiles III and IV

Cores along these profiles were taken on the irregular east flank of the plateau. The outcropping strata dip gently to the west near the crest, and are increasingly older at greater depths. Radiolarian ooze of Upper Eocene age outcrops in the channel at the base of the slope (Cores E-10, E-19) in a region where the sea floor is acoustically opaque to the 3.5 kHz profiler. To the east the layered strata reappear, dipping eastward. The presence of escarpments on the east flank is suggestive of faulting. The evidence from the limited number of cores, however, suggests that if faulting occurred, there were no substantial vertical displacements involved.

One of the cores from Profile IV (Core E-18) sampled an irregular mass of sedimentary material which appears to be out of place. Reflection profiling suggests that the mass is lens shaped with no internal bedding structures. The lens is surrounded by substantially older material (Cores E-17, E-19), and may therefore have slumped to its present position at the foot of the slope from a higher

44

elevation on the flank.

Profile V

The seven cores in this sequence were taken in the trough to the east of the plateau. T. profile begins in the axis of the channel and extends eastward onto the adjacent terrace and slope. Near-bottom reflection profiles were not taken at the site of Profile V, hence the dips of the strata along the profile are not known. The age relationships of the cores (Fig. 18), however, suggest that post depositional faulting has been influential to some degree in creating the channel.

Piston cores

One piston core (E-27) was obtained within the topographic depression at the center of the plateau, about 1 km west of Profile IV; the second core (E-28) is from the east flank in a region where the sea floor is acoustically opaque to the 3.5 kHz profiler.

Core E-27 recovered a chalk and siliceous ooze of Miocene age, and approximately 35 cm of Holocene siliceous calcareous ooze (Plate 9). The lowermost two meters of the core is a nannofossil chalk identical in physical properties to that obtained in the free-fall cores (Table 3). The age of the chalk is within the _Cannartus petterssoni_ zone, and is shown in Fig. 18 along with the cores of Profile IV. At a depth of about 150 cm in the core, the chalk grades upward into a siliceous ooze whose age is within the lower _Ommatartus antepenultimus_ zone. The siliceous ooze is unconformably overlain by Holocene sediment at a depth of about 35 cm. The Holocene section

is thicker in this core than in most of the free-fall cores, perhaps

because this site is relatively protected from the effects of erosion.

Core E-28 recovered an outcropping chalk of Lower Miocene

age with no overlying Holocene material present. The age of the chalk

is within the lower Calocycletta virginis zone and is identical to

that of core E-20 of Profile IV.

Sea Floor Environment

Activity of benthic organisms

Sea floor photographs and sediment cores from the survey area

(Fig. 19) indicate that the present sediment surface is a zone of

intense biological activity. Burrowing and mottling structures are

common within cores from locations where Holocene sediment is thickest

(Cores E-22, E-27). In all cores there has been considerable vertical

mixing of material across the Holocene-Middle Tertiary unconformity.

A substantial proportion of the microfossils within the Holocene sed-

iment are older specimens which have been reworked from the under-

lying chalk. In a few cores (E-4, S-21) there is evidence of burrow-

ing into the chalk with Holocene sediment filling the burrows. Most

of the vertical mixing, however, is upward rather than downward;

reworked microfossils are generally absent from the chalk.

Photographs of the sea floor in the study area (see Appendix

I) confirm that organisms are presently active in homogenizing the

upper few centimeters of sediment. Only two of the more than 250

photographs obtained show individual organisms (e.g., Fig. A-3),

but most of the remaining ones contain tracks, trails, mounds, and
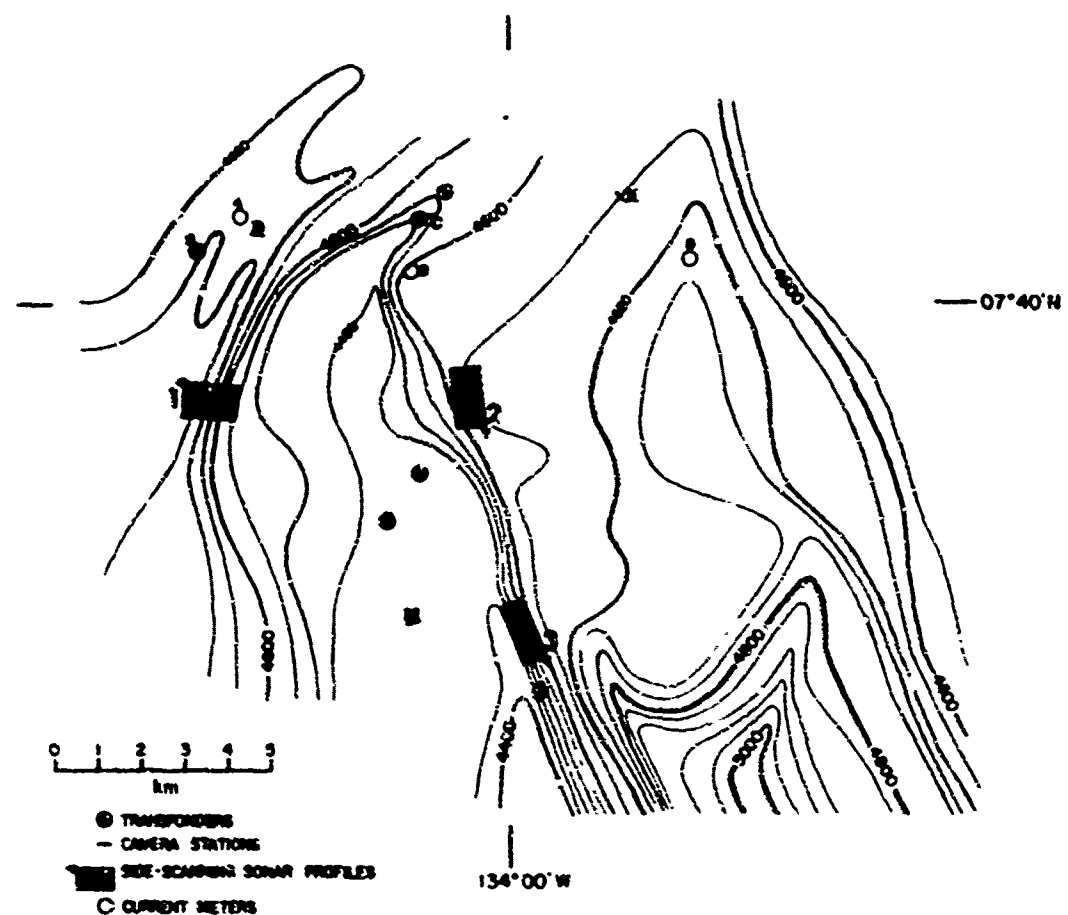
FIGURE 19   Location of camera stations, side-scanning sonar
             profiles, and bottom current meters.

other features indicative of the activity of benthic organisms.
Small trails and mounds are closely spaced in some photographs (Fig.
A-5), and some of the larger mounds (Fig. A-1) and lebensspuren
(Figs. A-6 and A-9) appear to have vertical dimensions of several
centimeters. The presence of the unconformity just beneath the sea
floor (Fig. 16) apparently serves as an effective barrier to deeper
burrowing and mixing, and hence the activity is intense within the
relatively thin layer of Holocene material.

Roughness

The use of side-scanning sonar techniques (Mudie et al, 1970)
in addition to sea floor photography indicates that the relief is
smooth over most of the surveyed area. A few photographs showed
what appeared to be rock outcrops (Figs. A-2, A-8), but the acoustic
ment is at least 0.2 sec beneath the sea floor at these sites.

... of the rocky material was present in any of the sediment cores,
hence the nature of this material is unknown.

Side-scanning sonar profiles show indications of steep local
relief at some points on the flanks of the plateau and in the vicinity
of erosional channels. The west flank of the plateau is generally
smooth, but the channel at the base has prominent relief (Fig. 20a).
Similar features are observed on side-scanning sonar profiles across
other channels within the area. The east flank is generally rough
(Fig. 20b), although there are some locations where smoothing has
created a surface with no prominent features (Fig. 20c).
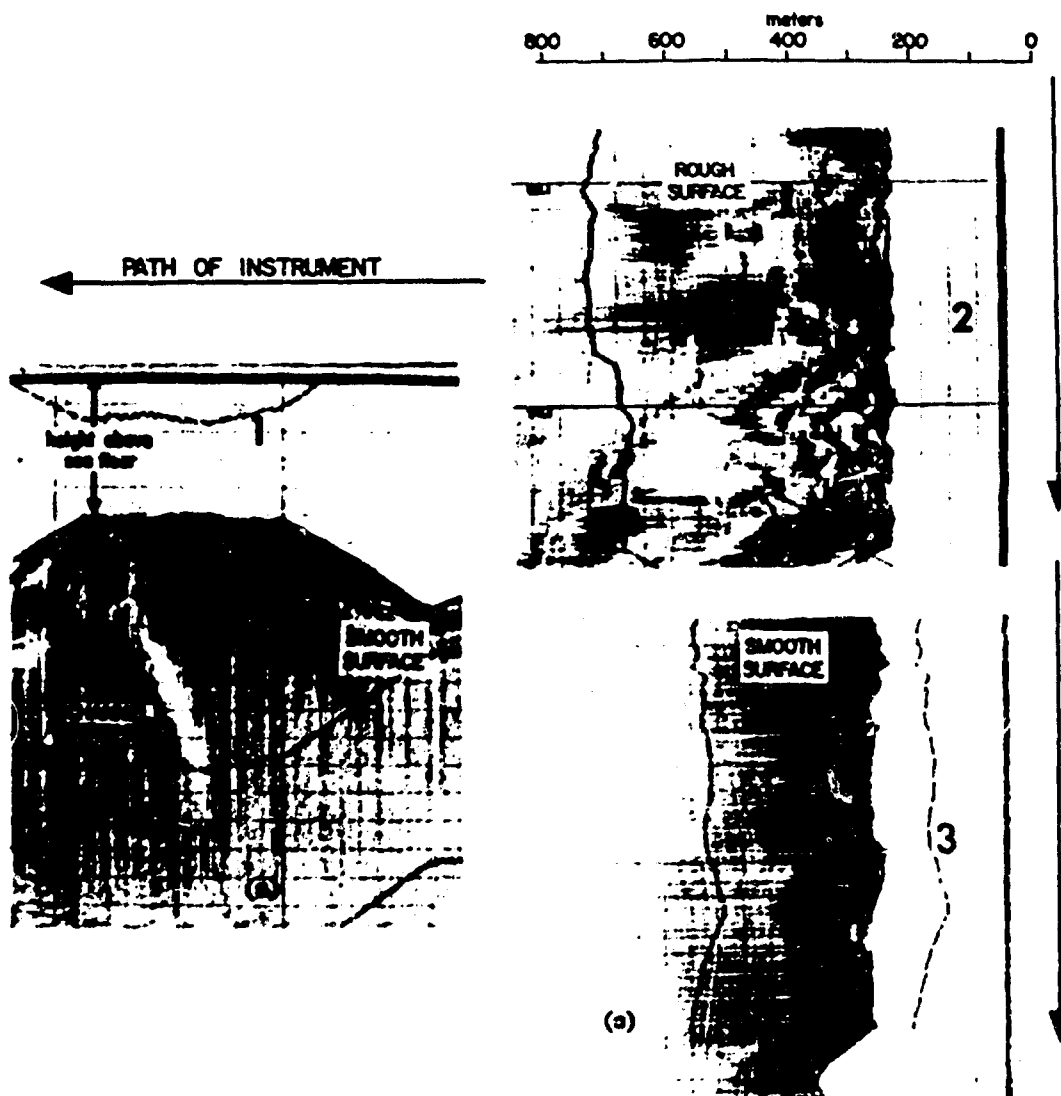
Figure 20   Side-scanning sonar profiles from the west and east flanks of
             the plateau, illustrating the contrasting types of sea floor
             micro-relief within the surveyed area. Locations of the pro-
             files are shown on Figure 19. The arrows indicate the direction
             of travel of the towed instrument package. In each of the pro-
             files the instrument is operating at a height of approximately
             200 meters above the sea floor.

TABLE 4   Summary of current meter data

Instrument Number	Height Above Bottom	Mean Direction	Mean Speed (cm/sec)	Maximum Speed (cm/sec)
2	25 m	056°	4.8	8.3
3	19 m	099°	5.4	9.6
4	5 m	063°	4.5	8.1
5	5 m	102°	---	---
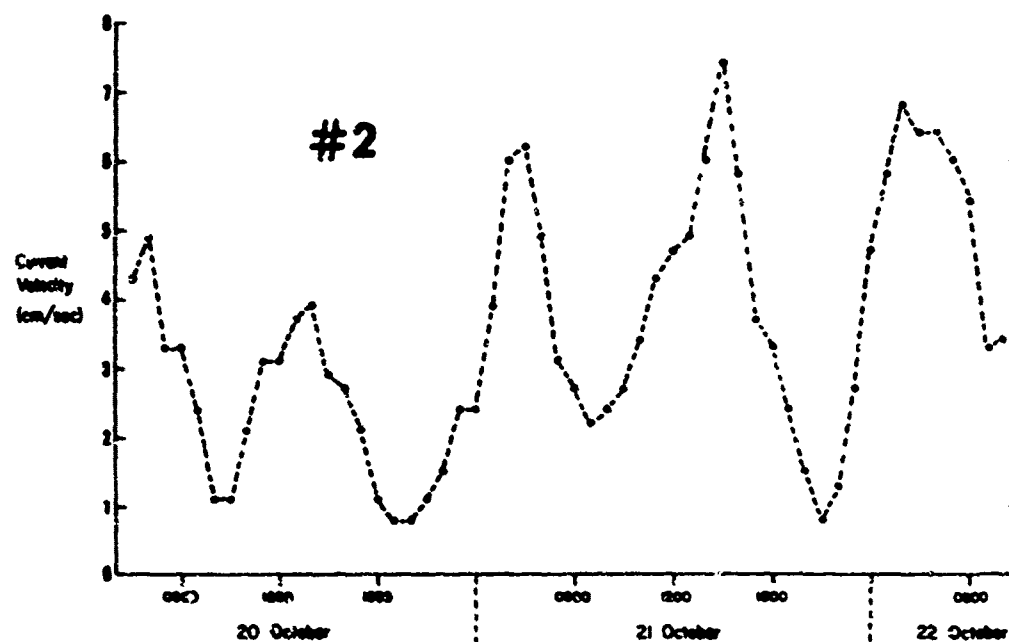
FIGURE 21   Bottom Current measurements obtained by instrument #2
             over a period of approximately two days, illustrating
             the pronounced tidal effect upon deep ocean current
             velocities. Similar tidal variations in speed were
             recorded by the other instruments.

#4 #2   #3   #5
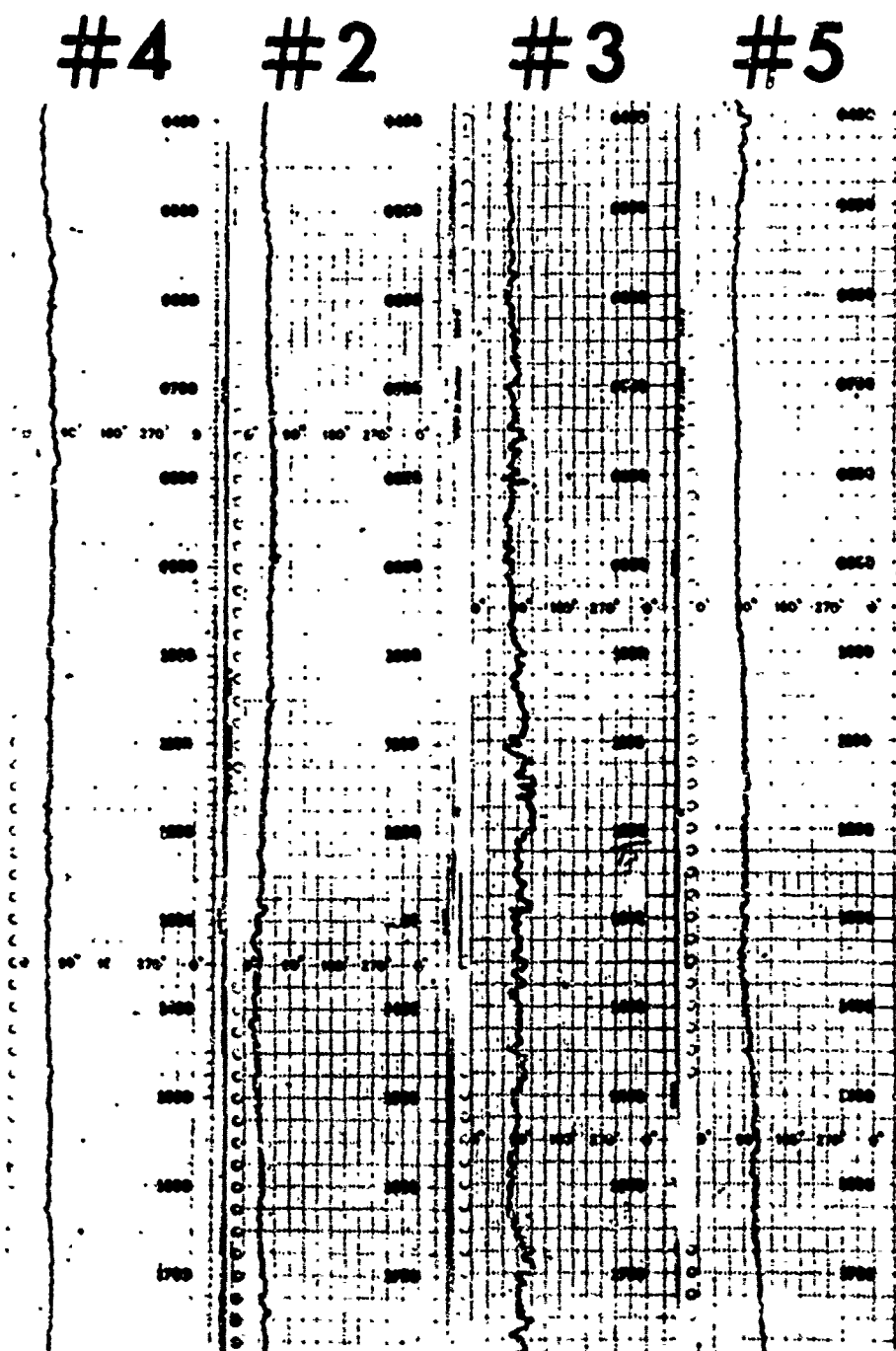
Figure 22 Original current meter records, illustrating the relative uniformity in flow direction at each site. Eastward-flowing currents were recorded at instruments #3 and #5, whereas the flow direction was generally northeastward at instruments #2 and #4.
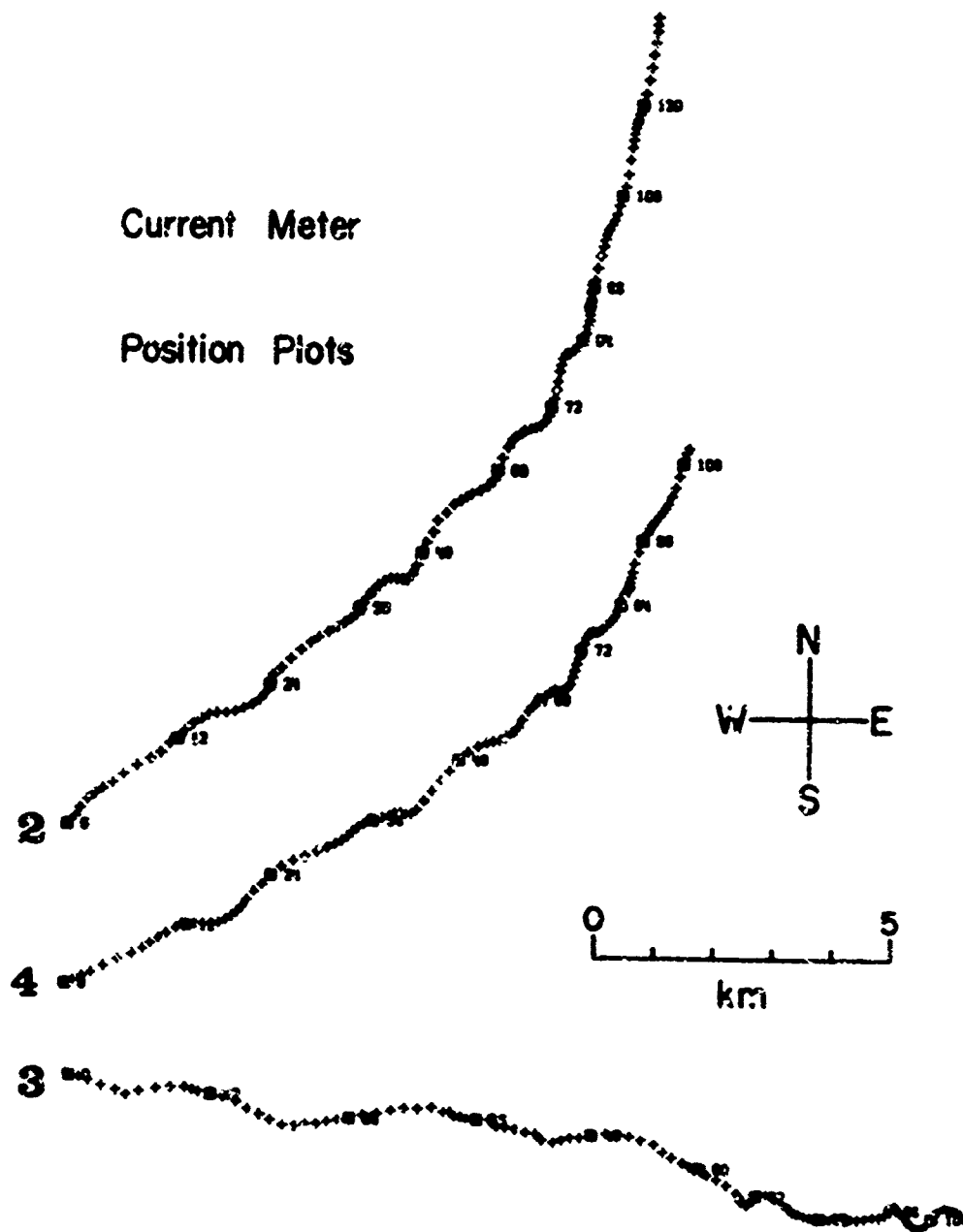
FIGURE 23   Position plots from current meters #2, #3 and #4,
             obtained by vectorially adding consecutive current
             velocities which have been averaged over one-hour
             increments.
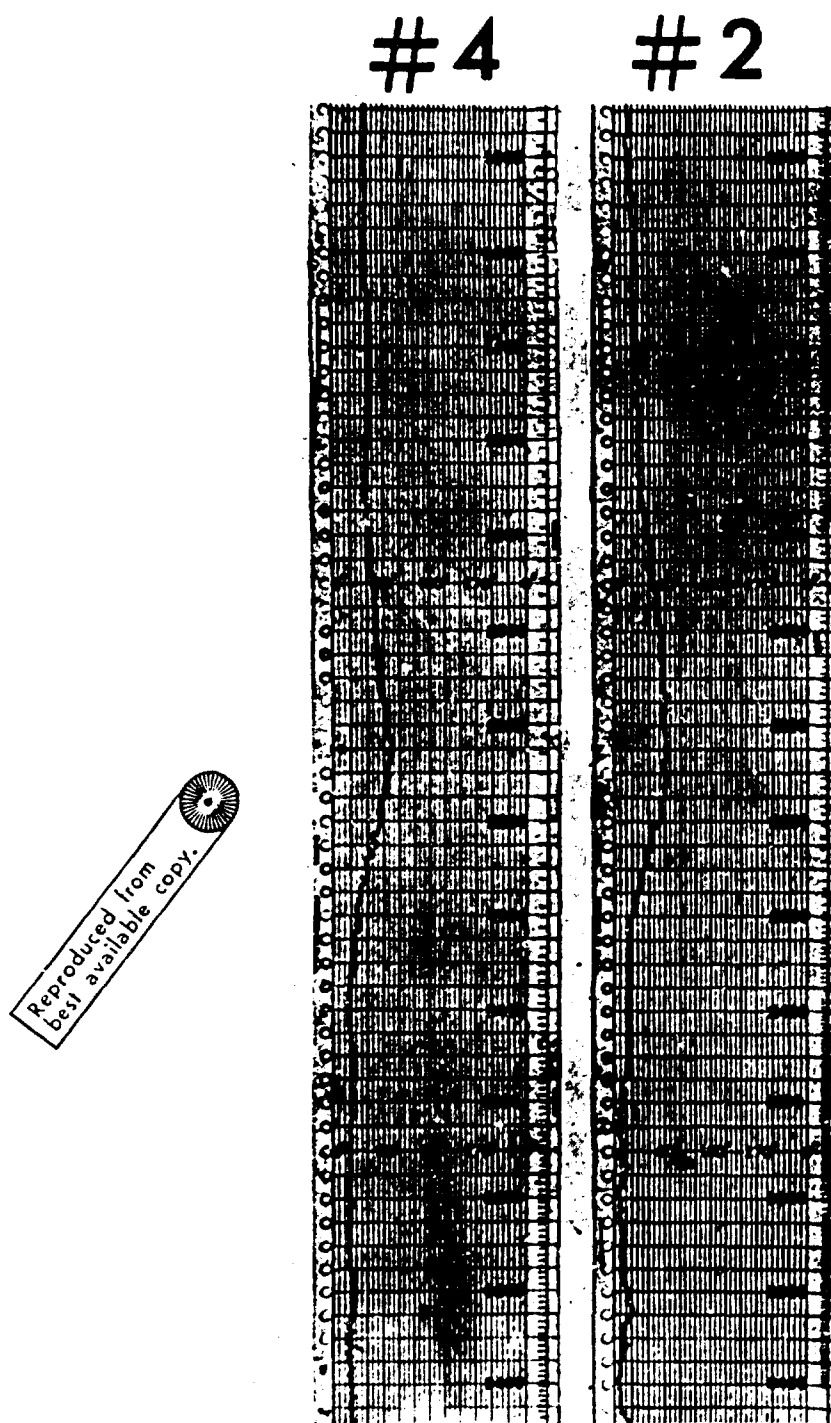
Figure 24   Portions of the original records from current meters #2 and #4, illustrating the close agreement between the two instruments. During the period between 2000 and 2300 the flow changes in direction from northeastward to eastward, and there is a corresponding decrease in current speed.

Bottom currents

Bottom currents were measured at four locations within the survey area (Fig. 19; Table 4). Two of the instruments (#2 and #4) were located in the depression to the west of the plateau. A third instrument (#3) was located near the northern end of the plateau, and a fourth (#5) was located in the trough to the east. Current speed and direction were measured for a period of four days by each instrument except #5, which recorded direction only. Data obtained from the current meters are listed in Table 6.

The observed current speeds were generally low (<10 cm/sec), but fluctuated significantly because of tidal effects. Figure 21 shows the strong semidiurnal tidal component present in the current, as recorded by one of the instruments; similar fluctuations in speed were observed at each of the other instrument locations.

In spite of the fluctuations in speed, the direction of flow at each location was remarkably uniform during the period of observation (Fig. 22). Eastward flowing currents were recorded at instruments #3 and #5, whereas in the depression to the west of the plateau, instruments #2 and #4 recorded a northeastward flow (Figs. 22 and 23). The data suggest that the regional flow of bottom water is toward the east, with local modifications in direction due to topographic effects. The nearby Clipperton Fracture Zone (Fig. 4) may be influential in controlling the direction of flow of bottom water in this part of the Pacific.

There appears to be a correspondence between minor changes

in flow direction and changes in current speed. Figure 24 shows a change in current direction which was recorded by both of the instruments in the channel west of the plateau (#2 and #4). During the period of northeastward flow the current speed was strongest, whereas the speed dropped markedly when the flow direction changed to eastward. The data support the interpretation of a relatively slow eastward flowing bottom current in the region, which at some localities (e.g., at the base of sea floor topographic irregularities) is accelerated in response to tidal influences, and changes direction to conform to the local topography.

Reflection Profiling Survey of Surrounding Area

The region surrounding the site of detailed study was surveyed using continuous seismic reflection profiling techniques from the surface ship. The survey included twelve east-west crossings within an area measuring approximately 50 km by 50 km (Fig. 25). Line drawings of some of the profiles are shown in Fig. 26.

The relief of both the sea floor and the acoustic basement is relatively smooth at the northern end of the area (Fig. 26, Profile I'I), and becomes increasingly irregular toward the south. The plateau within the area of detailed study (Profiles F'F, G'G) terminates to the south against a steep basement ridge, and the trough to the east of the plateau extends southward into an elongated depositional basin approximately 15 km in width and at least 25 km in length (Fig. 25). In the vicinity of this basin the acoustic basement has in excess of 1 km of relief, and basement outcrops
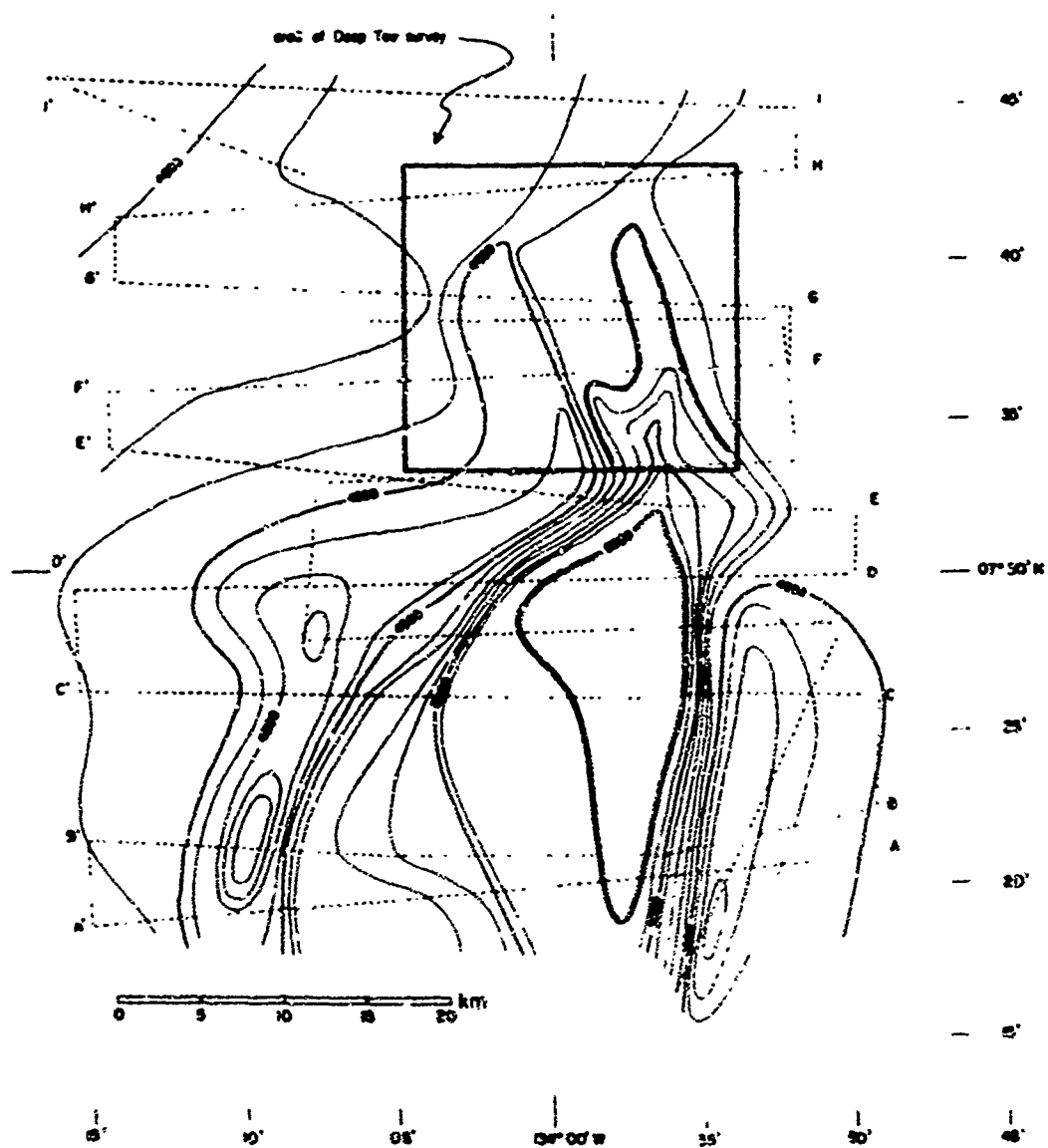
Figure 25   Bathymetry of extended area surrounding the region of detailed
             study. Dotted lines show ship's tracks through the area. Re-
             flection profiles from some of these tracks are shown in
             Figure 26.
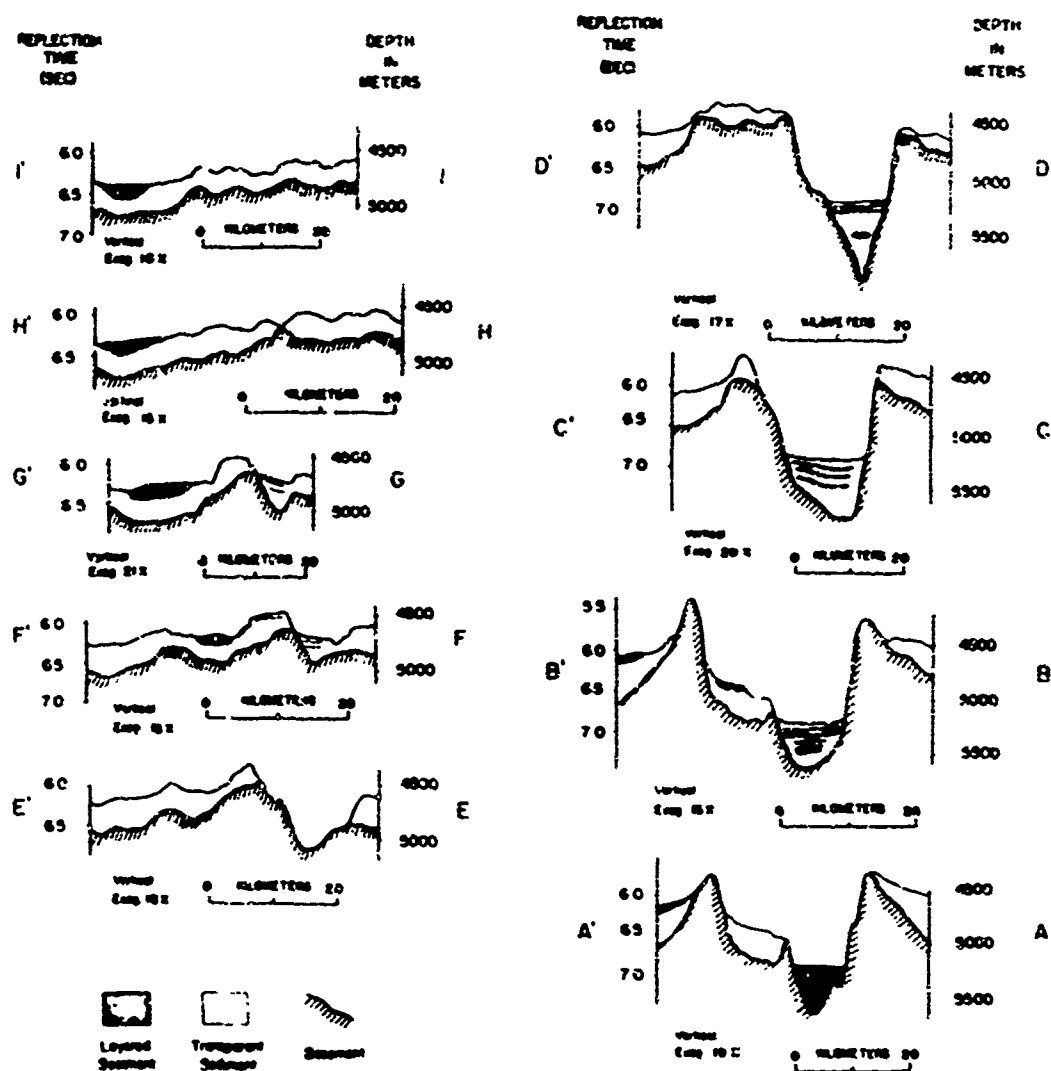
FIGURE 26   Line drawings based on continuous seismic reflection
profiles within the extended survey area. See text
for discussion.

surround the basin and extend northward up the east flank of the
plateau (Fig. 27).

Air gun reflection profiles suggest that two contrasting types
of sedimentary material are distributed over the study area (Fig. 27):
(1) Acoustically transparent sediment covers most of the area. This
"transparent" material shows few or no internal reflectors on the air
gun profiles, although layering within this unit is commonly observed
on near-bottom profiles (Figs. 10-14). The thickness of this unit
varies between 0.3 and 0.4 sec (Fig. 26), and in the northern part
of the area (Profiles H'H and I'I) it is generally conformable with
the relief of the acoustic basement. Toward the south, where the
relief becomes much greater, outcrops of the acoustic basement are
common and the transparent sediment is irregularly distributed.
(2) Relatively thick accumulations of stratified sediment (or layered
sediment) occur elsewhere in the survey area. On the air gun profiles
this material commonly contains near horizontal internal reflectors.
It is generally restricted to relatively deep regions, and is signi-
ficantly thicker than the "transparent" sedimentary material which is
present on the surrounding topographic elevation. A broad area
containing stratified sediment overlying relatively transparent
sediment extends northwestward from the deep-tow survey area (Fig. 27).
The elongated basin to the south of the deep-tow area also contains
relatively stratified sediment, perhaps several hundred meters in
thickness. No samples of this "stratified" unit were obtained, and
therefore its composition is unknown. The profiles suggest, however,
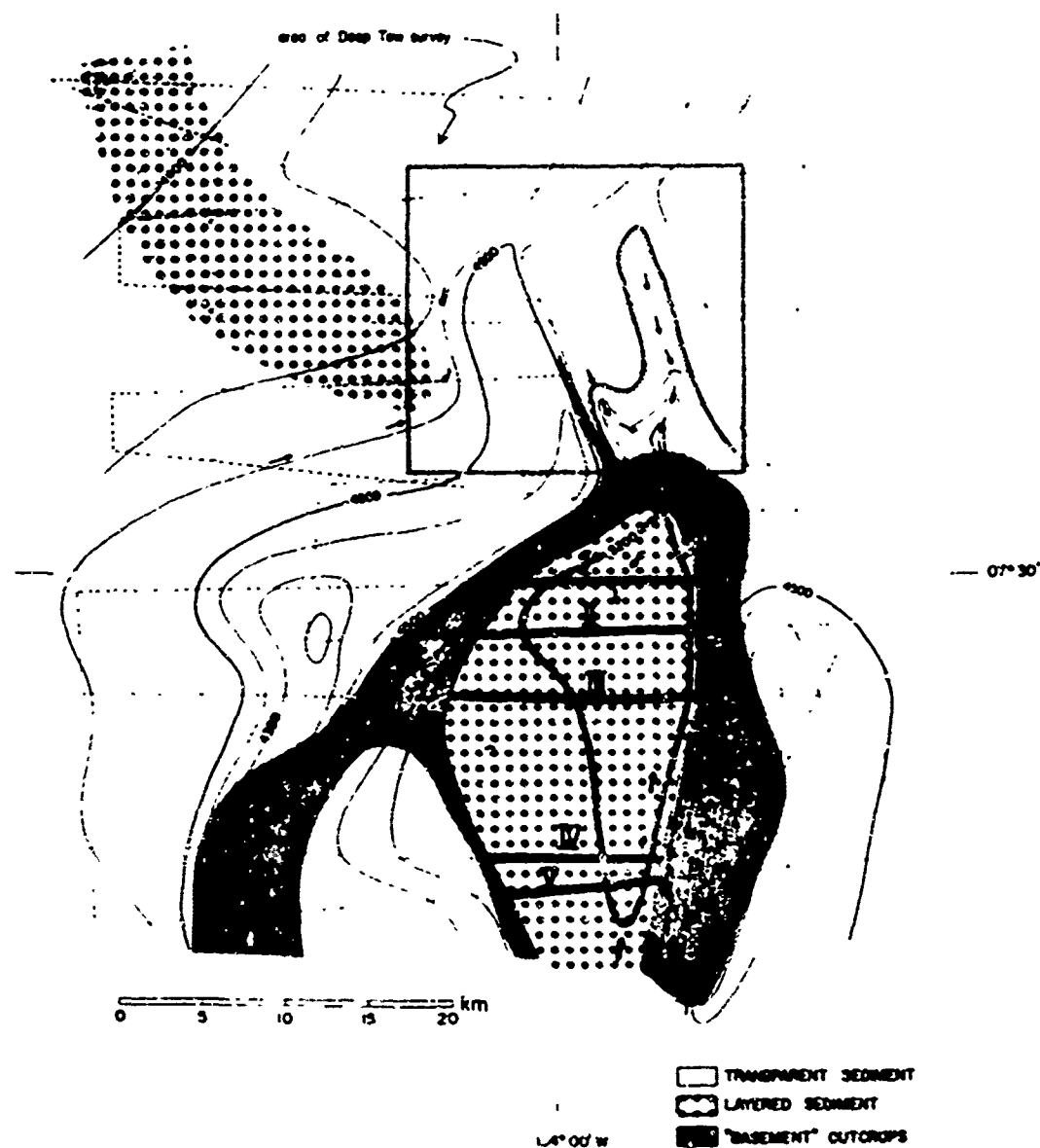
Figure 27   Distribution of major sediment types within the extended area.
            "Transparent" sediment contains no internal reflectors on air
            gun profiles, but generally shows stratification on near-bottom
            profiles. "Stratified" (or layered) sediment commonly contains
            sequences of near-horizontal internal reflectors on air gun
            profiles.
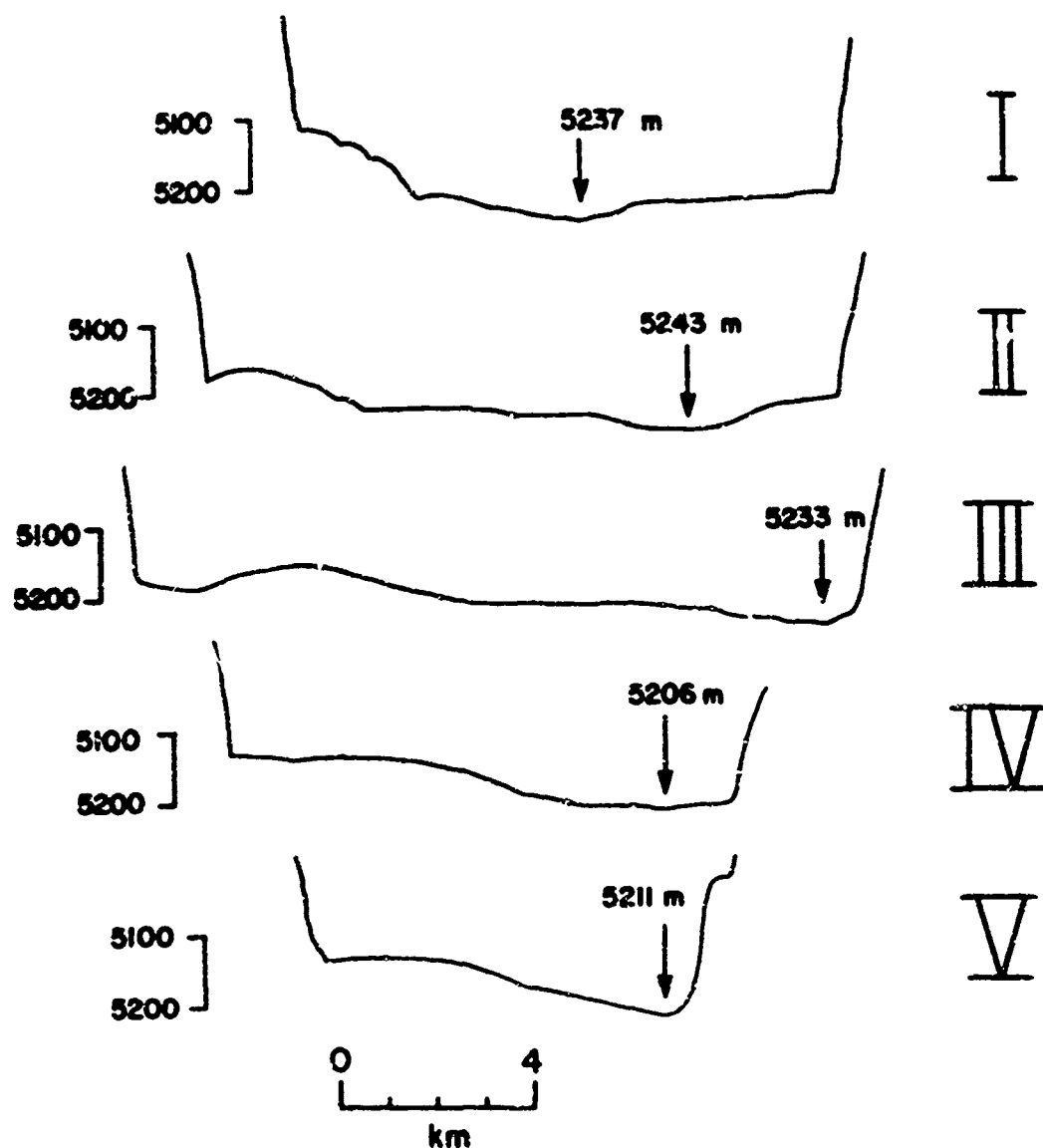
FIGURE 28   Bathymetric profiles across the floor of the basin to
             the south of the deep-tow survey area. The basin is
             fed by major channels from both the northern and
             southern ends. Profile locations are shown in Figure 27.

that much of the sediment which appears stratified on the air gun
profiles has been redeposited from surrounding regions.

INTERPRETATIONS OF RESULTS

Sediment Redistribution in Deep-tow Survey Area

Evidence for erosion

Continuous seismic reflection profiling from the surface
ship gives clear evidence for sediment erosion and redeposition
within the extended survey area (Fig. 27). Each of the two principal
regions where "stratified" sediment is present appears to be a site
where significant volumes of reworked material have accumulated.
The large basin south of the deep-tow area is fed from the north
by two principal channels which join before entering the basin.
Within the deep-tow area (Fig. 9; Fig. 26, Profiles F'F and G'G)
these channels are as much as several tens of meters in depth, and
have eroded deeply into Tertiary chalk. At some locations (Fig. 18,
Cores E-10 and E-19) the channels have exposed Upper Eocene sediments,
whose age is only a few million years younger than the presumed age
of the oceanic crust at this site (Fig. 4). At the southern end of
the deep-tow area these channels join, and substantially more material
is eroded exposing outcrops of the acoustic basement along the
channel axis (Fig. 26, Profile E'E). South of this point the base-
ment deepens abruptly and the region of deposition begins, marked by
the thick accumulation of stratified sediment. The channel appears
to continue meandering southward through the basin itself until it
reaches the deepest part of the basin (Profile II, Fig. 28). A
separate channel enters the basin from the southern end (Fig. 27).

The "fan" of stratified sediment west of the deep-tow area

(Fig. 27) is fed by a major channel which extends southward along
the base of the west flank of the plateau (Fig. 9). A secondary
channel enters the head of the fan from the opposite direction, and
supplies sediment from the region to the southwest of the deep-tow
area. This "fan" overlies 0.2 to 0.3 sec of acoustically transparent
sediment, and appears to have filled a previously existing topographic
depression.

Near-bottom reflection profiles and sediment cores confirm
that significant erosion has taken place, and indicate that erosion
has affected virtually the entire deep-tow survey area (Fig. 27).
Reflection profiles from throughout the area (Figs. 10-14) show an
abrupt truncation of acoustic reflectors at the sea floor interface,
but there is no indication of similar unconformities at depth.
Forty-three of the forty-four cores penetrated an unconformity
between Holocene ooze and Lower to Middle Tertiary chalk, and in
most cores this unconformity is within a few centimeters of the sea
floor (Plates 4-9).

Time of erosion

The presence of the unconformity near the sea floor interface
indicates that erosion processes have occurred relatively recently in
geologic time. The presence of a thin layer of Holocene material
above the unconformity (Fig. 16), however, suggests that substantial
erosion is not taking place today. Bottom current speeds were low
(<10 cm/sec) during the period of observation (Tables 4 and 6),
and bottom photographs showed well preserved sedimentary structures
resulting from the activity of benthic organisms. It is therefore

likely that condition on the sea floor today are relatively quiescent
compared to the conditions which must have existed during the recent
past. During the Pleistocene the circulation patterns of the atmos-
phere and oceanic surface waters are presumed to have undergone
periods of marked intensification in response to the extreme climatic
fluctuations (Arrhenius, 1950; 1966). It may be that the deep cir-
culation was subjected to corresponding pulsations with intensified
current speeds during the glacial stages.

Thickness of material eroded

The minimum quantity of material which has been eroded can
be estimated from the near-bottom reflection profiles (Figs. 10-14).
Profile 5 (Fig. 11) shows a synclinal sedimentary structure which has
been truncated by erosion on both sides of the synclinal axis. The
resulting sea floor relief exposes layers covering a stratigraphic
thickness of 100-200 m within a distance of one kilometer. Similarly,
Profile 15 (Fig. 14) reveals that at least several tens to hundreds
of meters of cover has been removed from a gently folded sequence of
strata.

Coring and near-bottom profiling indicate that the region to
the east of the plateau may be an eroded anticlinal structure (Fig. 12;
Fig. 18). On the plateau's east flank the strata dip westward,
whereas in the trough to the east the layers dip eastward (Fig. 18,
Profiles III and IV). In the intermediate region, near the channel
at the base of the plateau, Eocene sediments outcrop. If the strata
which now outcrop on the east flank of the plateau were formerly

continuous with strata to the east of the channel, then perhaps several hundred meters of material has been eroded in the vicinity of the channel (see arrows on profiles in Fig. 12)

The depositional history at the survey site can be reconstructed by noting the ages of sediment cores in relation to their outcrop pattern, and estimating the amount of material which is missing. Cores from Profile I on the west flank of the plateau (Fig. 17) sampled a continuous sequence of outcropping strata ranging in age from lowermost Oligocene to Middle Miocene. The average accumulation rate for this sequence of strata is approximately 12 to 15 m per million years, or 12 to 15 mm per thousand years. If this accumulation rate were extrapolated from the Middle Miocene to the present, however, it would almost certainly be too high. Rates of supply of sediment to this portion of oceanic crust have varied considerably during the Cenozoic as a result of a northward component in the motion of the Pacific plate (Francheteau et al, 1970; Tracey et al, 1971). Maximum rates of deposition occurred when this region was beneath the biological equator; this may have occurred during the Oligocene (approximately 25 to 30 million years ago) on the basis of recent drilling results which suggest that the Pacific plate has had a northward component of motion of approximately 3 cm/yr during the late Cenozoic (E. L. Winterer, personal communication). Since that time, as the Pacific plate has moved northward, the rate of sediment supply has decreased. Today, sediment is supplied at a significantly lower rate, perhaps 3 to 5 m per million years. Using these figures,

several tens of meters of sediment (representing the Middle Miocene
through Pleistocene) is missing from the deep-tow survey area, and
presumab'y has been redeposited elsewhere.

The stiff texture and relatively low water content of the
outcropping chalk layers (Fig. 16) suggest that the chalk was formerly
under a higher overburden pressure. Modern deep sea sediments common-
ly have porosities of 75% to 85% (Hamilton, 1971), and recent deep
drilling into continuous sections of pelagic carbonate has encountered
low porosity (60%) material only at depths of several tens of meters
or more (Hays et al, 1971). The physical properties of pelagic
sediments, however, are dependent not only upon former overburden
pressures, but upon the entire set of conditions to which the material
has been subjected since original deposition (E. L. Hamilton, per-
sonal communication). Quantitative estimates of former overburden
thicknesses within the deep-tow area on the basis of porosity alone,
therefore, are not justified.

Evidence for Erosion Elsewhere in the Central Pacific

Deep-tow survey of Area K

Another small area in the central Pacific, which will be
designated Area K, was recently surveyed using the deep-towed instru-
mentation (Mudie et al, 1971). This site is located several hundred
kilometers to the northeast of the primary deep-tow survey area des-
cribed above (Fig. 2), and lies within the zone of red clay sedi-
mentation where rates of accumulation are relatively slow. The topo-
graphy at Area K is characterized by lineated abyssal hills and
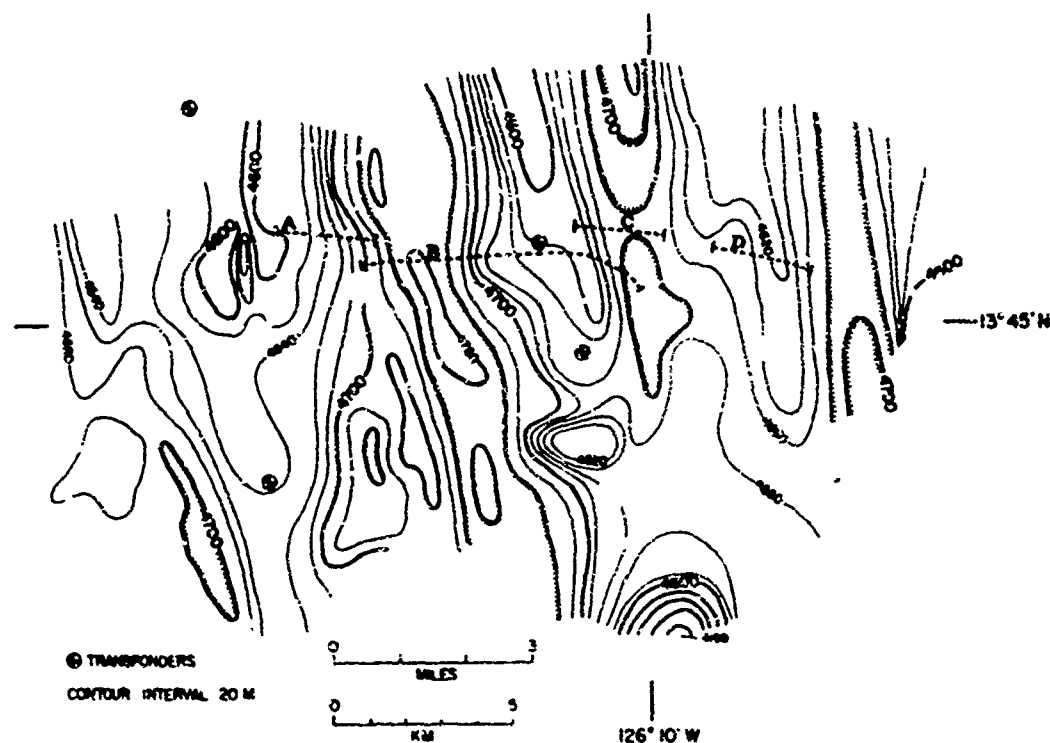
FIGURE 29   Bathymetry of "Area K", after Mudie et al. (1971).
             Lineated abyssal hills and troughs are characteristic
             of this area. Dotted lines indicate the locations of
             near-bottom reflection profiles shown in Figure 30.
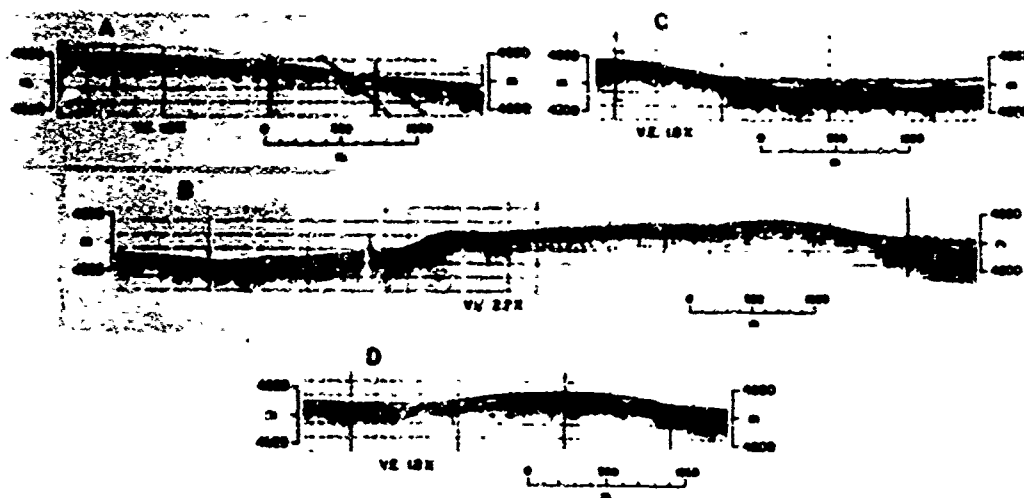
Figure 30   Nea bottom reflectior profiles from Area K. The structural
and erosional features in this area are remarkably similar to
those observed in the primary area studied. See text for
discussion.

troughs (Fig. 29). A large circular abyssal hill is present in the
southern part of the area, and a small trough surrounded by steep
escarpments occurs to the southwest of Profile A. Elsewhere within
the area the relief is smooth with no evidence of faulting.

Continuous seismic reflection profiles were obtained within
the area using the 3.5 kHz system on the deep-tow vehicle. Many of
the profiles from Area K are remarkably similar to those obtained
in the primary deep-tow area in the equatorial region.

Profile A (Fig. 30), which crosses the eastern limb of one
of the abyssal hills, shows sedimentary strata which have been gently
folded into anticlinal and synclinal forms, and subsequently truncated
at the sea floor interface. It is difficult to determine whether
the layering is a reflection of the basement topography or whether
compressional folding of the strata has taken place.

Profile B (Fig. 30) crosses one of the abyssal hills, and
includes the troughs on either side. The structure of the hill itself
is remarkably similar to that of the plateau within the primary survey
area. The hill in Profile B is underlain by near horizontal strata
which outcrop on both the east and west flanks. The sediments in
the trough to the west are also truncated by erosion at the sea
floor, and it appears that these outcropping layers at the deepest
part of the trough are stratigraphically at least 100 m beneath
those which outcrop at the crest of the hill.

Profile C shows in more detail the trough to the east of
the hill shown in Profile B. As before the strata underlying the
hill outcrop along the hill slope. Within the trough, however,

the sea floor is horizontal and smooth, and the relatively transparent sediment is ponded around the acoustic basement. The smoothness of the floor of the trough and the ponded nature of the sediment suggest that the sediment within the trough has b. reworked from surrounding areas, perhaps from the adjacent hill slopes.

Profile D crosses another of the elongated abyssal hills, where essentially horizontal strata underlyir the hill are outcropping on the slopes. A line of ten free-fall cores was dropped along the east flank of the hill shown in Profile B in an attempt to determine the age of the outcropping sediment layers. All of the material within the cores was unfossiliferous, hence the ages of the strata cannot be determined. The reflection profiles, however, indicate that substantial erosion has occurred, and the presence of the unconformity at the sea floor suggests that the erosion occurred relatively recently. The evidence for erosion at Area K is remarkably similar to that observed in the prim y survey area.

Detailed surveys in other abyssal hills regions

Detailed investigations recently have been carried out in two other small areas in the central Pacific, and at each of these sites there is evidence for recent ocean floor erosion. Moore and Heath (1967) surveyed an abyssal hills region south of Hawaii (near 08°20'N, 153°C0'W), and used closely spaced free-fall cores to determine the small-scale sediment distribution pattern. They found that, in each of the cores that penetrated through Quaternary sediment, an unconformity separated the Quaternary section from underlying

sediment of Middle Miocene age or older (Moore, 1970). Johnson and

Johnson (1970) used similar surveying and coring techniques in an

abyssal hills area west of the Line Islands (near 03°50'S, 155°45'W),

and found a similar outcropping or near-outcropping of Lower and Middle

Miocene sediments. The two deep-tow survey areas (Fig. 3) and the

areas surveyed by Moore (1970) and by Johnson and Johnson (1970)

are widely separated (hundreds of kilometers), and evidence for

recent erosion was present in each of the four areas. The presence

of similar features indicative of recent erosion over such a wide-

spread area suggests that the erosion processes may have occurred

on a large scale, and not merely in response to local conditions.

Proposed Mechanisms in Other Regions

Several attempts have been made to explain the irregularities

which are commonly observed in deep sea sedimentation patterns.

Arrhenius (1963, p. 721) noted the abnormal thinness of Quaternary

strata on the crest and slopes of a hill, and proposed that there

is a "continuous process of resuspension and transport downhill ...

probably caused by the churning action of benthic animals, some of

which have bee~   erved forming a suspension cloud which may be

displaced by any horizontal movement of the near-bottom water."

Luyendy' (1969) has recently attempted to express quantitatively

the relation between differential sediment accumulation patterns and

the degree of activity of benthic organisms.

Tareyev (1965) proposed that topographic irregularities at

the sea floor can create standing internal waves, and that the

resulting differences in vertical velocity components in the water

column lead to differential sedimentation rates on a small scale.

In a region of ascending currents, such as hill slopes which face

"upstream", only particles with a settling velocity which is greater

than the vertical component of current velocity are capable of reach-

ing the sea floor. Conversely, sediment deposition will be intensi-

fied in areas where descending currents are maintained.

Moore (1970) suggested that tectonic activity during the

Tertiary created normal fault structures on the sea floor, exposing

Tertiary sediments to erosion by bottom currents and benthic organisms.

Johnson and Johnson (1970), in a study of a small area to the south

and west of the Line Islands Ridge, found that bottom currents have

played an important role in shaping the sea floor topography and in

redistributing sediments. Berger (1967, 1970) and others have

demonstrated that the bottom waters of the Pacific are markedly

undersaturated with respect to $CaCO_3$, and that consequently chemical

dissolution is important in removing the carbonate fraction of the

sediment in abyssal depths. van Andel and Komar (1969), in a de-

tailed study of sediment cores from the crest of the mid-Atlantic

Ridge, suggest that turbidity currents have ponded pelagic sediments

into topographic valleys near the ridge crest. There is a similar

ponding of sediment into lineated valleys near the crest of the East

Pacific Rise (Larson, 1971).

Even in the absence of lateral transport, intensive vertical

mixing is commonly present in the upper few tens of centimeters of

sediment. Glass (1969) has demonstrated that thin microtektite layers
are vertically displaced over distances of tens of centimeters, per-
haps as a result of the activity of benthic organisms. Berger and
Heath (1968) have attempted to predict quantitatively the effects
of vertical mixing as a function of the rate of sedimentation and
the depth of the "mixed" layer at the sea floor interface.

Some of the depositional irregularities have been attributed
to changing conditions on a global scale through geologic time.
Arrhenius (1963; 1966) suggested that fluctuating climatic conditions
during the Quaternary have caused highly variable rates of primary
productivity and chemical dissolution in the equatorial Pacific
yielding variable net rates of sediment accumulation. Rates of
supply of terrigenous debris to the deep sea floor have also varied
considerably during the Quaternary as a result of variable rates
of subaerial erosion and migrating shorelines (Broecker et al, 1958).
This effect commonly obscures the depositional history of pelagic
materials (Ruddiman, 1971). The outcropping pre-Pliocene sediments
of the equatorial Pacific appear to show increasing age northward
from the equator (Hays et al, 1969); this effect has been attributed
to a wider zone of high productivity during pre-Pliocene time. Rates
of chemical dissolution at the sea floor interface may have increased
during the Tertiary in response to decreasing bottom water temper-
atures and increasing rates of production of bottom water in high
latitudes (Heath, 1969). Large-scale motions of crustal plates
(McKenzie and Parker, 1967; Morgan, 1968) across biogeographic

boundaries produce further complications, such as the north-south
asymmetry of sediment accumulation in the equatorial Pacific (Tracey
et al, 1971).

Probable Mechanisms Influential in Deep-tow Area

Tectonic activity

Significant horizontal and vertical crustal displacements
appear to have taken place in the vicinity of the study area. The
basement relief to the south of the site of detailed study is re-
markably steep (Fig. 26), and may be a result of tectonic activity
along the Clipperton Fracture Zone lying 50 to 100 km to the south
(Fig. 3). The north-south trending basement ridge which outcrops
along the east flank of the plateau (Fig. 12) appears to have been
displaced 10 to 20 km in a right-lateral direction at the south end
of the deep-tow survey area (Fig. 25). The elongated depositional
basin to the south of the deep-tow area (Fig. 27) may be a result
of crustal extension which provided a site for thick sediment ac-
cumulation.

There is evidence that tectonism and vulcanism have occurred
in the vicinity of other fracture zones in the northeast Pacific.
Andrews (1971) suggests that differential crustal spreading rates
across fracture zones are important in producing secondary topo-
graphic features which may be lineated at an oblique angle to the
lineated hills which are created near spreading centers. It may
be that the steep, irregular topography south of the deep-tow area
is a consequence of differential crustal motion along the Clipperton

Fracture Zone.

The eroded anticlinal structure on the east side of the
plateau (Fig. 12) coincides in position with that of a basement
ridge (Fig. 8; Fig. 12). This elevation in the acoustic basement
may represent a post depositional intrusive which deformed the over-
lying sediments. There is evidence for deep ocean vulcanism at
locations which are far from active spreading centers (Spiess et al,
1969), and basaltic material obtained by deep drilling has been dated
and determined to be significantly younger than the probable age
of the underlying oceanic crust (Macdougall, 1971). It may be that
volcanic and intrusive activity is common at great distances from
plate boundaries, and that the "basement" at some places within the
surveyed area represents a relatively recent igneous event.

Vertical crustal displacements of several tens of meters
have occurred within the survey area. Bathymetric profiles obtained
with the towed instrument show that small regions of the sea floor
with slopes in excess of 60° are widespread (Figs. 10 and 12), and
closely spaced sediment cores demonstrate that at least some of these
relatively steep slopes must have been formed by post depositional
normal faulting (Fig. 17, Profile I). At one location (Fig. 18,
Profile V) an active erosional channel was initially created by nor-
mal faulting, and subsequent erosional processes apparently have
reshaped the topography so that prominent escarpments are no longer
present.

There is no evidence that reworked sediment has accumulated

at the base of topographic escarpments on the plateau's flanks, or
that sediment movement was initiated by tectonic processes. If
gravitational slumping did occur as a result of tectonic activity,
then the slumped material must have been removed subsequently by
bottom currents. One possible exception is the lens of sediment
at the site of core E-18 which appears to be stratigraphically out
of place (Fig. 18, Profile IV), and may have slumped to its present
position from a higher elevation on the plateau's flank.

Tectonic processes, therefore, have facilitated sediment
erosion and redeposition within the area studied. Sediments have
been deformed by post depositional vulcanism and perhaps by lateral
compression as well. Normal faulting on a small scale has created
channels within which eroded sediment can be preferentially trans-
ported. Transcurrent faulting and perhaps igneous activity has
created topographic depressions within which eroded sediment can
accumulate.

Erosion by currents

There is considerable evidence that bottom currents which
are now present in the deep ocean may be capable of eroding and
transporting modern sea floor sediments (Hollister and Heezen, 1966).
Bottom photographs commonly show features indicative of sediment trans-
port (Laughton, 1963; 1968; Heezen and Hollister, 1964; Hollister
and Elder, 1969), and direct measurements have detected bottom
currents with appreciable speeds (McCoy, 1969; Reid, 1969;
Schwartzlose and Isaacs, 1969).

It is difficult to determine precisely the critical erosion velocities for the sediment types present at the deep-tow survey site. Numerous observations have been made of the flow conditions required to move various types of sediment (e.g., Rubey, 1938; Hjulstrom, 1939), but relatively few experiments have been performed on pelagic deep sea sediment. Generally the sediment types used in laboratory flumes have a relatively simple geometry, such as quartz grains of uniform size or artificial glass beads (Vanoni, 1964). The components of deep ocean sediments, however, are highly complex in morphology; this is especially true of biogenous skeletal debris. Therefore it is hazardous to estimate erosion velocities for pelagic sediments on the basis of studies performed upon other types of material.

An additional source of uncertainty in determining critical erosion velocities for deep ocean sediment is the differing boundary layer conditions which are present during different experiments and observations. A smooth deposit of fine-grained sediment which remains unaffected in the presence of moderate current speeds might be readily eroded if, due to the activity of benthic organisms, small perturbations were created along the sediment surface. The effects of small-scale topographic irregularities and an active benthic fauna are no doubt of great importance in facilitating sediment transport. These effects, however, are difficult to observe directly, and consequently there is considerable uncertainty in studying quantitatively the effect of perturbations within the boundary layer.

Southard et al, (1971) have recently performed laboratory

flume experiments on an argillaceous carbonate silt from the deep
ocean, composed principally of foraminiferal tests and coccolitho-
phorid debris. The critical erosion velocity for this material was
determined for flow conditions in a shallow (6 cm depth) channel
using sea water at room temperature. They observed that velocities
for erosion are 7 to 10 cm/sec for a bed which has been recently
stirred (simulating conditions of recent deposition), and 15 to 20
cm/sec for a bed which has been allowed to settle for several tens
of hours. These experimental velocities should be multiplied by a
correction factor of ~1.8 in order to obtain erosion velocities for
the same material if measured 1 m above the ocean bottom (Southard
et al, 1971). Thus the critical erosion velocities for this sediment
in deep ocean conditions would range from about 15 to 35 cm/sec.

Maximum current velocities recorded in the deep-tow survey area
were approximately 10 cm/sec (Appendix II). These current speeds
apparently are insufficient for eroding the Holocene sediment, since
this thin layer appears to be widespread throughout the survey area
(Plates 4-9). The Holocene material is not of uniform thickness,
however, and in some cores it is missing entirely. There may be
local intensification of currents at these locations, and here the
currents may attain speeds substantially greater than those recorded
by current meters. Alternatively, the uneven distribution of Holocene
material may be due to a relatively recent event of intensified
current flow, perhaps a monthly or a seasonal effect, which was
not detected due to the relatively limited duration of the survey.

Critical erosion velocities for fine-grained sediment (i.e.,

constituent particles smaller than about 0.05 mm) are strongly depen-

dent upon the degree of consolidation of the material. The layer of

Holocene ooze within the survey area has a high water content (80% to

90%), and is apparently not eroded in the presence of current speeds

up to 10 cm/sec. This observation is consistent with experimentally

determined erosion velocities of 15 to 30 cm/sec for fine silts and

clays with water contents of 80% to 90% (Postma, 1967, Figs. 1 and 2).

As sediment becomes more consolidated the critical erosion velocity

increases significantly. Current speeds on the order of 100 cm/sec

are required to erode fine silt and clay with a water content of 60%

to 70% (Postma, op. cit.). It therefore appears that, if the erosion

into the Tertiary chalk were accomplished by means of current action

alone, current speeds much greater than those present today must have

been required.

Chemical dissolution

The sediment types and their net rate of accumulation in much

of the deep ocean are determined primarily by the rate of corrosion of

skeletal debris at the sea floor interface. Dissolution in the deep

ocean affects primarily the calcareous microfossils, and foraminiferal

species are particularly susceptible (Berger, 1967). Calcareous

nannofossils, by contrast, are relatively protected from corrosion

by a thin proteinaceous outer layer (E. D. Milow, personal com-

munication). There is evidence that significant dissolution of

siliceous material also can take place (Berger, 1968b). Radiolarian

species have become increasingly more fragile during the Cenozoic,
and relatively recent species are preferentially corroded within
mixed assemblages (Riedel and Funnell, 1964; Moore, 1969).

Sediments of all ages within the survey area show substantial
effects of dissolution; only the more resistant foraminiferal species
have been preserved, and the specimens present are highly corroded.
The depth where rapid carbonate solution begins (the lysocline)
corresponds to the top of the Antarctic Bottom Water (Berger, 1970;
Edmond et al, 1971). There is evidence that in the Atlantic, the
lysocline was several hundred meters shallower during the glacial
stages than it is now (Berger, 1968a), suggesting that during this
time bottom water was being formed more rapidly. One might anticipate
increased solution of both siliceous and calcareous debris during
periods of rapid formation of bottom water. The CO_2-rich and SiO_2-
deficient surface water wr   be supplied to the sea floor interface
at a faster rate, and the increased respiration of benthic animals
would furnish additional CO_2 to the sea floor interface (Arrnenius,
1963).

Chemical dissolution alone, however, is not a sufficient
explanation to account for all of the erosional features observed.
If dissolution alone were initiated in a region of low relief and
near horizontal strata, one would anticipate that it should proceed
downward at a relatively uniform rate within a small area. At the
deep-tow site, however, material has been preferentially removed
on a small scale, creating a sharp angular unconformity at the

sea floor. Perhaps differential erosion and dissolution on a small scale has occurred in response to local intensification of the flow of bottom water within the area

Activity of benthic organisms

Intensive reworking of the upper few centimeters of sediment by deposit-feeding benthic organisms produces significant changes in the physical stability of the sediment surface. The water content and the roughness of the sediment surface are increased, and the critical erosion velocity for the sediment is lowered. Rhoads and Young (1970) recently conducted experiments on shallow water muds to determine the effects that deposit-feeding organisms have on the sediment stability. Equal volumes of sieved mud were introduced into two halves of a wave tank, and specimens of a deposit-feeding bivalve (Nucula proxima) were introduced into one half of the tank and allowed to rework the sediment surface until it developed a granular, burrowed texture. Then the water above the sediment surface in both tanks was oscillated at velocities ranging up to 13 cm/sec, and differential resuspension was determined by noting the turbidity in each half of the tank:

> Little turbidity was developed in either tank at veloci-
> ties up to 3 and 4 cm/sec. But at velocities greater than
> 4 cm/sec, there was greater resuspension of sediment and
> greater turbidity above the burrowed sediment than over the
> unburrowed sediment. Fecal pellets and mud clasts in the
> burrowed sediment were preferentially eroded and suspended
> at velocities greater than 4 cm/sec. These particles soon
> disintegrated into silt-size and clay-size grains, producing
> high turbidity. During erosion of the loose granular sed-
> iment, the roughness of the sediment surface was increased,
> producing turbulence, which accelerated the erosion process.
> (Rhoads and Young, 1970, pp. 166-168).

Bottom photographs from the deep-tow area (Appendix I) demon-
strate that the upper few tens of centimeters of sediment is a zone
of intense biological activity. Any sedimentary material which is
put into suspension will be transported laterally if any current
whatsoever is present. Under conditions of intense biological activ-
ity and relatively low rates of sediment supply, a sedimentary particle
might travel great distances as a result of repeated resuspension
and lateral drift. Within the deep-tow area, rates of supply of
material are relatively low (several mm per thousand years), and
some species of benthic organisms are evidently capable of burrowing
several centimeters beneath the sea floor. A sedimentary particle
need be resuspended only once every few thousand years in order to
remain within the "mixed layer" and thereby subject to continual
lateral movement.

Interaction of various mechanisms

It appears that erosion has been accomplished by all of the
mechanisms discussed above. Tectonic processes have created various
copographic features which facilitated sediment redistribution,
including: (a) steep, irregular basement relief; (b) faults within
the strata along which channels could develop for the subsequent
transport of eroded sediment; and (c) wide, deep depressions to serve
as sites for sediment redeposition. The activity of benthic organ-
isms has undoubtedly served to disturb the boundary layer at the sea
floor, and thereby provide for the lateral transport of sedimentary
material which, in the presence of low currents, would have been

otherwise buried and unaffected by erosion.

The principal mechanisms responsible appear to be (a) erosion by intensified bottom currents, together with (b) differential chemical solution in response to these currents. Either of these two processes alone is probably insufficient to explain the features observed. Chemical dissolution has occurred during the entire depositional history of the area, and probably at increased rates during the late Tertiary and the Pleistocene glacial stages. Solution alone, however, would be unlikely to produce the widespread angular unconformity and the irregular outcrop pattern which is observed. Erosion by currents alone is a possible explanation, but unreasonably high current speeds might be required in order to erode into the chalk because of the chalk's stiff texture and high cohesiveness. In the presence of solution processes, however, individual fragments within the chalk would become disaggregated at the sea floor interface, and erosion would be accomplished more easily.

The form which the erosion surface assumes may have been controlled by former topographic irregularities which became accentuated during the erosional episodes. It is suggested that small-scale topographic features served to create regions where the current flow became intensified locally, and that in these regions both chemical solution and mechanical erosion could proceed more rapidly than in more protected regions nearby. For example, a minor depression initially created by faulting may have become eroded preferentially, and gradually became a channel which grew as eroded material

was transported along it. There were probably numerous episodes of intensified current flow and ocean floor erosion during the Pleistocene, and during successive stages the erosion surface became increasingly complex. The prominent unconformity which is observed today (Fig. 16) represents only the shape of the erosion surface when the current speeds most recently decreased to the point where erosion could no longer take place.

The extensive areas of outcropping Tertiary strata in the central Pacific (Hays et al, 1969; Riedel, 1971) may be explained most satisfactorily in terms of regional erosion and redeposition. Nondeposition or local erosional events appear to be inadequate explanations.

PELAGIC SEDIMENTATION IN THE EQUATORIAL PACIFIC
DURING THE PLEISTOCENE

It has been suggested here and elsewhere (e.g., Arrhenius, 1952; Olausson, 1969) that the extreme climatic fluctuations during the Pleistocene had a profound effect upon the deep ocean circulation, and upon depositional conditions on the sea floor. In particular, it has been proposed that substantial ocean floor erosion occurred during the glacial stages in response to intensified bottom currents. The following discussion attempts to predict how various oceanographic processes would change in response to glaciation, and how these processes might interact to create conditions favoring increased sediment redistribution on the sea floor (Figs. 31 and 32).

Surface Circulation

The intensity of the atmospheric circulation and the wind-driven oceanic circulation is controlled by the rate of heat exchange between low and high latitudes (Fairbridge, 1962; Arrhenius, 1966). When the major climatic belts migrate toward the equator or toward the poles, there are corresponding increases and decreases in the north-south temperature gradient, and in the intensity of the surface circulation. During the Tertiary, for example, there was a steady climatic deterioration in middle and high latitudes as a result of the migration of the geographic poles to regions of thermal isolation (Donn and Ewing, 1966). Consequently the circulation intensified, and upwelling and productivity were increased in the equatorial

86

EFFECTS OF GLACIATION UPON OCEANIC CIRCULATION
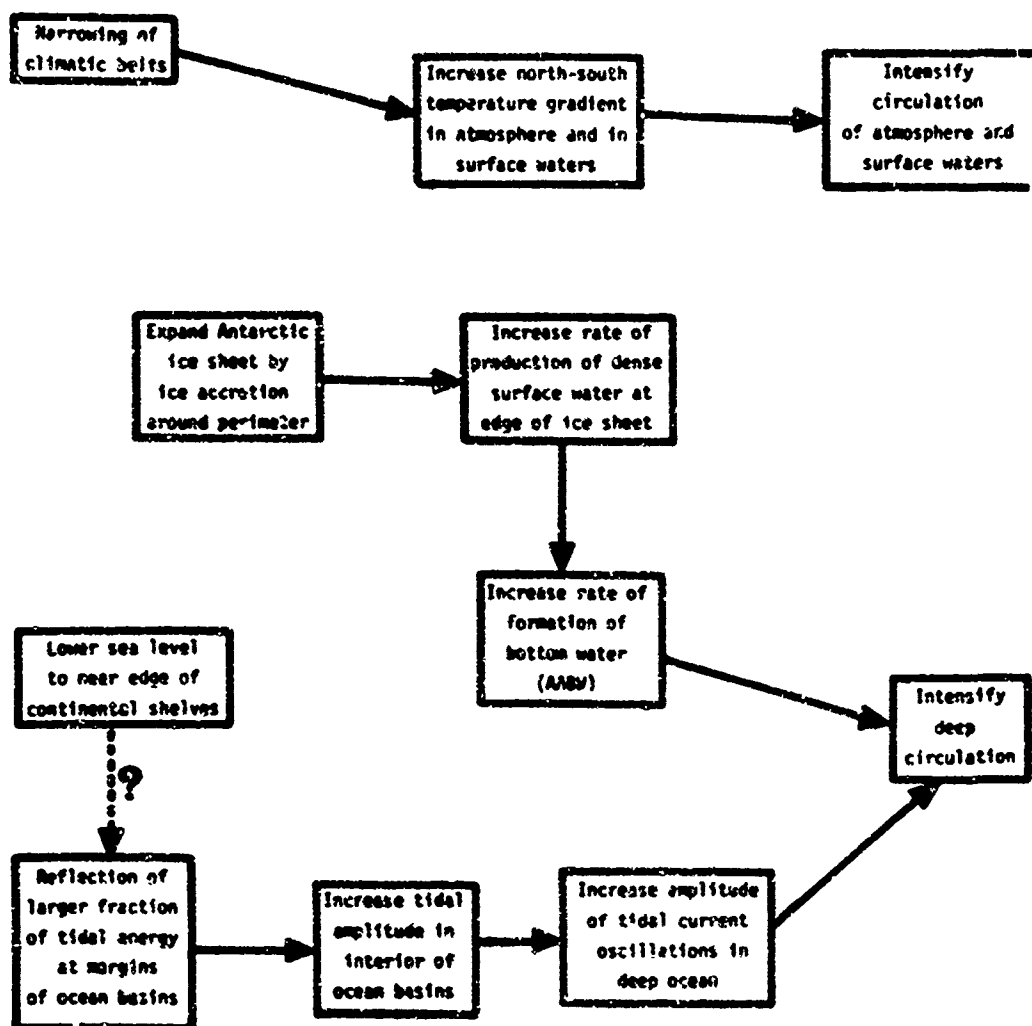
Figure 31   A schematic representation of how various climatic and oce-
            anographic factors might interact to produce intensified oceanic
            circulation during the glacial stages of the Pleistocene. See
            text for discussion.

zone (Arrhenius, 1950).

With the onset of extensive glaciation at the end of the
Tertiary, the climatic conditions began to undergo major oscillations.
The climatic fluctuations which characterize the Pleistocene are
probably best explained in terms of a variability in the moisture
supply for glacial growth (Donn and Ewing, 1966). Since glaciation
was probably synchronous in the northern and southern hemispheres
(Epstein et al, 1970), the earth's climatic belts expanded during the
interglacials and contracted during the glacials (Fairbridge, 1962;
Lamb and Woodroffe, 1970). There were corresponding increases
(glacials) and decreases (interglacials) in the intensity of the
trade winds, and in the rates of upwelling and primary productivity
(Arrhenius, 1966). These migrations of climatic belts and the ac-
companying variations in rates of circulation and primary productivity
are commonly observed in the depositional record (e.g. Emiliani,
1966; Ericson and Wollin, 1968; Hays et al, 1969; McManus, 1970).

<center>Deep Circulation</center>

Production of bottom water

The deep ocean circulation as well as the surface circulation
may have been affected substantially by glacial conditions. For
example, the rate of production of bottom water in high latitudes
may have increased. Today the deep water of the Pacific Ocean (Ant-
arctic Bottom Water) originates in the shallow seas surrounding the
Antarctic continent, principally the Weddell Sea and the Ross Sea
(Jacobs et al, 1970; Seabrooke et al, 1971). The formation of

<center>88</center>

Antarctic Bottom Water occurs when relatively cold surface water
mixes with warmer intermediate water near the shelf edge. These
two parent water masses have approximately the same density, but
significantly different temperatures and salinities (Seabrooke et al,
1971). Because of the nonlinear equations of state of sea water
the resulting mixture is denser than either of the two original water
masses (Fofonoff, 1956), and a cabbeling instability develops to
transport the Antarctic Bottom Water which is produced downward to
the deep ocean floor (Foster, 1971).

Several attempts have been made to explain how the cold sur-
face water is brought to a condition which allows mixing with warmer
intermediate water to produce bottom water (AABW). Seabrooke et al,
(1971) have proposed that the surface water of the westward flowing
Antarctic Coastal Current is modified in temperature and salinity
as it flows beneath the wide shelves of the Weddell Sea, and that it
eventually reaches a state (-1.9°C; 34.60 $^o/oo$) where it is suffic-
iently dense to form an appropriate mixture with warmer intermediate
water. Theoretical studies by Foster (1971), however, suggest that
the cooling and freezing of sea water on the underside of an ice
shelf occurs at too slow a rate to produce any significant modifi-
cation of the shelf water. He suggests that the required changes
in the properties of the surface water which are necessary for bottom
water production are provided by haline convection induced by the
direct freezing of sea water. In spite of considerable uncertainty
in determining the mechanism by which the surface water is modified,

it appears likely that the process is seasonal, and that consequently the maximum production of AABW occurs during the southern winter during the accretion of ice around the perimeter of the Antarctic ice cap (Foster, 1971).

During the glacial stages of the Pleistocene conditions favoring the formation of cold, saline surface water around the Antarctic ice cap were extended in time and space beyond the normal seasonal expansions and contractions. As ice accretion proceeded during the glacial stages, there was an increasingly greater area of ice cover around which cold and relatively saline surface water could form. The subsequent production of bottom water was probably directly proportional to the rate of ice formation. Munk (1966) has attempted to approach quantitatively the problem of bottom water production rates, and estimates that 43 grams of bottom water are formed for each gram of ice that freezes. It therefore appears likely that conditions of an expanding ice cap around the Antarctic continent favor a steadily increasing rate of production of bottom water.

Dissipation of tidal energy

The velocities of deep ocean currents are characteristically periodic. Semidiurnal tidal components are commonly recorded during measurements of several days' duration (Nowroozi et al, 1968; Doebler, 1967; Winbush and Munk, 1970; Lonsdale et al, 1971), and monthly variations also have been reported (Schmitz et al, 1970). It is likely, therefore, that deep ocean currents in some localities are

a reflection of the dissipation of tidal energy as well as a net
transport of bottom water from one region of the ocean basin to
another.

Tidal energy in the ocean basins is dissipated at a rate
of 2.7×10^{19} ergs/sec, a rate which is determined from precise
observations of the moon's acceleration (Munk, 1968). This dissipa-
tion rate is quite high, and is such that all of the energy stored
in the tides at any instant is dissipated in several days
(Hendershott, personal communication). A substantial fraction of
this total dissipation, between 1.4 and 1.7×10^{19} ergs/sec, takes
place along the continental margins and in shallow seas (Miller, 1966).

Frictional dissipation in shallow seas is not the only
possible mechanism to serve as a sink for tidal energy. Cox and
Sandstrom (1962) show that tidal energy flowing over a rough ocean
bottom is converted to internal waves, and that the subsequent
dissipation of these waves may be important in accounting for the
total rate of dissipation of tidal energy. Miller (1966) attempted
to estimate the frictional dissipation in the deep ocean using an
empirical expression for the rate of energy loss per unit area
($\gamma \rho u^3$ where $\gamma = .002$ and $u =$ current speed). He estimated that for
the entire area of the deep oceans the dissipation is on the order
of 10^{16} ergs/sec, or three order of magnitude less than the total
dissipation rate required. He assumed, however, that tidal current
speeds in the deep ocean are on the order of 1 cm/sec. By assuming
tidal current oscillations on the order of 10 cm/sec, which is

consistent with recent observations, the deep ocean dissipation is on the order of 10^{19} ergs/sec. This value compares favorably with the energy dissipated in shallow seas and with the total dissipation rate required.

One might consider the possibility that the pattern of tidal energy dissipation was substantially different during the glacial stages. Sea level was approximately 130 m lower than at present during the most recent glacial advance (Curray, 1965), and consequently many of the world's continental shelves and shallow seas were subaerial and no longer available for the dissipation of tidal energy. One possible consequence of lowering sea level to near the shelf edge is a greater reflection of tidal energy at the oceanic boundaries. This condition would result in higher tidal amplitudes at the sea surface in the interior of the ocean basins, and a corresponding increase in the amplitude of tidal oscillations on the deep sea floor (Hendershott, personal communication).

It is by no means clear, however, that the oceanic boundaries would become less dissipative to tidal energy as the shore line migrates seaward across the continental shelves. The continental slopes of the world vary considerably in steepness, but in many extensive regions the slopes average no more than two or three degrees (Shepard, 1963). In these regions the slopes may be insufficiently steep to reflect significant tidal energy. The energy which is absorbed at the continental margins during interglacial times may continue to be absorbed at the shelf edges during glacial stages,

resulting perhaps in intensified erosion of sediment on the contin-
ental slopes. The mechanisms controlling tidal currents in the deep
ocean today are poorly understood; consequently there is much un-
certainty in attempting to predict the tidal oscillations on the
ocean floor during periods of markedly different geographic and cli-
matic cond'tions.

Depositional Environment

Assuming that both the surface circulation and deep circula-
tion were intensified during glacial stages, one can then predict the
effect of these changes upon depositional conditions on the ocean
floor (Fig. 32). First of all, there was more material supplied to
the sea flour from the overlying waters. Large quantities of ter-
rigenous sediment were transported to the deep ocean as a result of
the effects of lower sea level. Apart from this effect, there re-
mained a substantial increase in the rate of supply of pelagic
sediment as well. Some of this material was derived from arid or
semi-arid continental regions (Damuth and Fairbridge, 1970; Frenzel,
1968) and transported to the open ocean by intensified wind systems
(Bonatti and Arrhenius, 1965). In addition, the rate of supply of
biogenous skeletal material was increased as a result of increased
primary productivity (Arrhenius, 1963). This increase in productivity
occurred primarily in regions where productivity is high today, such
as the equatorial zone and certain coastal regions. Productivity
may have been increased in the central water masses as well. Today
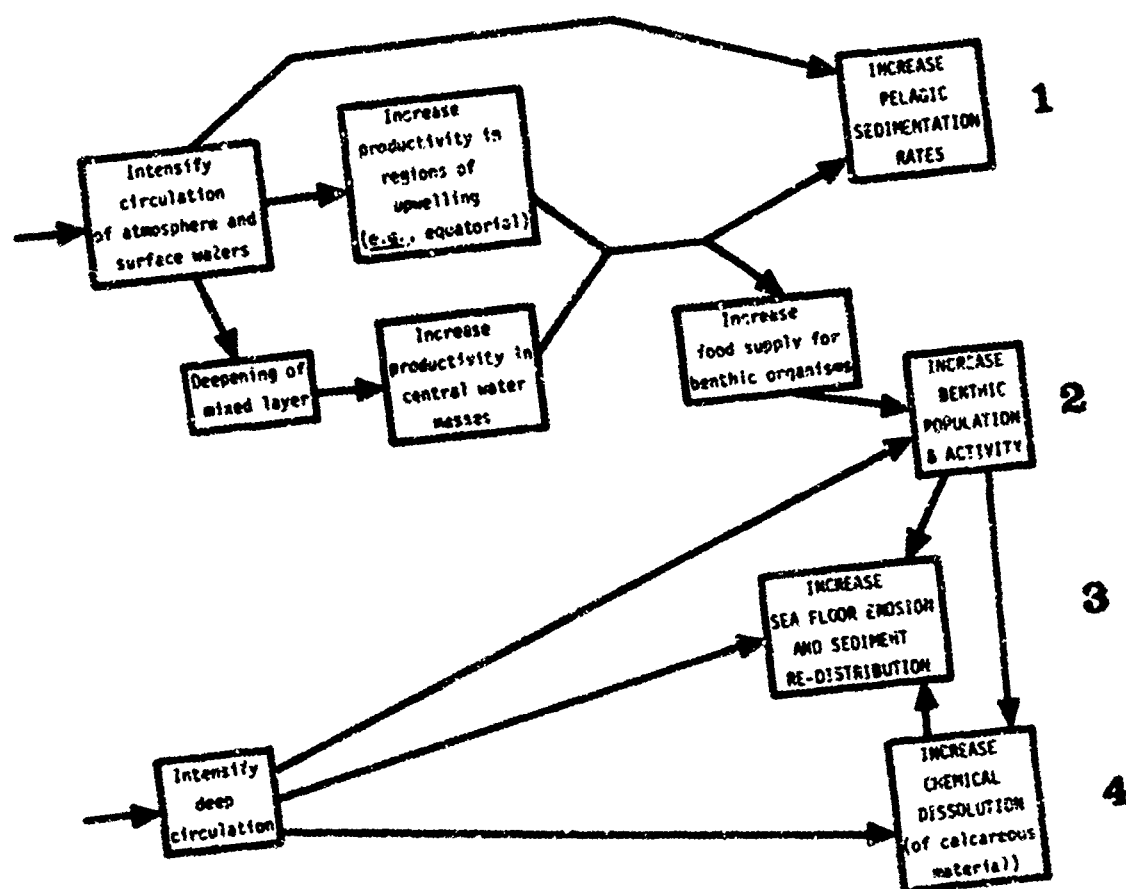the production of bottom water in high latitudes is compensated

Figure 32   Effects of intensified oceanic circulation upon environmental conditions at the sea floor. The four principal effects are of varying degrees of importance, depending upon the topographic features in the area of interest.

quantitatively by vertical upwelling within the Pacific at a rate averaging 1.2 cm/day (Munk, 1966). An increased rate of production of deep water during glacial stages would then be accompanied by a compensating increased rate of upwelling throughout the Pacific basin.

A second change which might be anticipated is a more abundant population of benthic organisms, particularly in protected regions where deposition rates are highest. Since the size of a benthic population is limited principally by food supply (Sanders and Hessler, 1969; Griggs et al., 1969), a higher planktonic population in the surface waters should support a more abundant benthic population on the sea floor beneath. If oxygen supply were an additional limiting factor to benthic activity, glacial conditions should provide oxygenated surface waters to the sea floor at a higher rate, and thereby allow a more active benthic fauna. In addition, the deposit-feeding and suspension-feeding organisms might show a marked spatial separation. Experiments and observations in shallow water (Rhoads and Young, 1970, Figs. 6 and 7) suggest that the sea floor in relatively protected environments is abundantly populated by deposit feeders which produce a granular, burrowed sediment surface. At nearby sites which are relatively exposed, deposit feeders are less abundant, and the sediment surface is less disturbed by burrowing. The frequent resuspension of sediment where deposit-feeders are present produces sediment instability and water turbidity, and thereby serves as a limiting factor for most suspension-feeders at these locations (Rhoads and Young, 1970). Third, glacial conditions should facilitate

the dissolution of calcareous skeletal material at the sea floor.
The presence of an active benthic population would favor rapid solu-
tion by providing more CO_2 to the waters near the sea floor interface
(Arrhenius, 1963; Berger, 1968a). In addition, the sediment components
might be mechanically disintegrated during the feeding activities
of benthic organisms, thereby facilitating both chemical solution and
erosion by currents. The most profound solution effects. however,
would be due to the increased rates of production of bottom water in
high latitudes. Extensive studies (Berger, 1970; Parker and Berger,
1971) have shown that there is a continuous destruction of almost all
calcareous sediment exposed on the Pacific Ocean floor, and that the
regions where solution is most intense are in contact with Antarctic
Bottom Water. Olausson (1969) indicates that dissolution of carbonate
sediment in the North Atlantic was intensified during the glacial
stages, and suggests that the bottom waters were more corrosive as
a result of either a lower temperature or a more rapid rate of flow.
Kennett (1970) has found evidence of intense solution of glacial-age
carbonate sediments in the sub-Antarctic region, probably a result
of increased production of bottom water. Kaye (1957) performed lab-
oratory experiments on calcite crystals and limestone blocks, and
determined that fluid motion is of considerable importance in con-
trolling the rate of solution of carbonate materials. Edmond (1971)
has reinterpreted the results of the buoy experiment in which the
rates of solution of calcite spheres (Peterson, 1966) and foramini-
feral tests (Berger, 1967) were determined at several depths in the

water column. He demonstrates that the variable rate of solution of $CaCO_3$ is not a reflection of the carbonate chemistry of the water, but rather is a consequence of the water's flow rate. This correspondence supports the interpretation that more intense solution during glacial stages was due to stronger bottom currents, in response to increased rates of production of bottom water in high latitudes.

Finally, physical erosion and redistribution of sediment should increase during glacial stages. There is evidence that sediment reworking increased progressively during the Tertiary, and may have been particularly intense during the glacial stages. Heath (1969) has pointed out that the early and middle Tertiary sediments of the equatorial Pacific are much more uniform and better sorted than the late Tertiary and Quaternary sediment, and suggests that intensified bottom currents and benthic activity would be expected as increasing volumes of bottom water are formed beneath the growing Antarctic ice cap. Studies of sediment cores (Riedel and Funnell, 1964; Riedel, 1971) show that Quaternary sediments generally contain a substantial proportion of reworked material, but the outcropping or near-outcropping Tertiary sediments often contain relatively homogeneous faunal assemblages, indicating very little mixing. Recent deep drilling at several sites in the equatorial Pacific (Table 6) has recovered tens to hundreds of meters of Tertiary sediment containing no apparent unconformities and little evidence of reworking. The evidence supports the interpretation that substantial ocean floor

TABLE 5   Continuous Cenozoic sections recovered by Deep Sea
            Drilling Project in equatorial Pacific

DSDP Site	Location	Age of Sediments	Depth below Sea Floor
69	06°00'N 152°52'W	L. Mioc. - U. Eoc.	52 m to 162 m
70	06°20'N 140°22'W	U. Mioc. - L. Olig.	8 m to 325 m
71	04°28'N 140°19'W	L. Pleist. - M. Olig.	0 m to 436 m
77	00°29'N 133°14'W	U. Pleist. - L. Olig.	0 m to 470 m
78	07°57'N 127°21'W	M. Mioc. - L. Olig.	0 m to 315 m

erosion in the Pacific may be characteristic only of the late Cenozoic
and particularly the glacial stages of the Pleistocene.

Of the four principal effects which glaciation may produce
on the deep sea floor (Fig. 32), only the first (increased sediment
supply) tends to accumulate sediment more rapidly at a given locality;
the last three act to remove or at least redistribute material.
Local topographic irregularities probably determine which of these
effects will predominate at any given site. One might expect, for
example, that increased sediment supply should predomiate in regions
relatively protected from strong currents, and that solution and ero-
sion should be most important in exposed regions where strong currents
are present. The benthic population would be most abundant where
food supply is greatest, with perhaps a small benthic population of
suspension-feeders in the exposed regions.

As an example of variable sea floor conditions on a small
scale, Fig. 33 shows a line drawing based on a reflection profile
from the basin south of the deep-tow area, and indicates that local
areas might conveniently be classified as either exposed or protected.
This arbitrary classification might be applied to any region of the
sea floor, depending on whether or not local topographic effects
exposed the region to erosional processes. Fig. 34 summarizes the
depositional conditions which one might expect at the sea floor in
both exposed and protected regions during glacial and interglacial
stages. In the exposed region, any material which accumulates during
the relatively quiet interglacials is likely to be removed during the
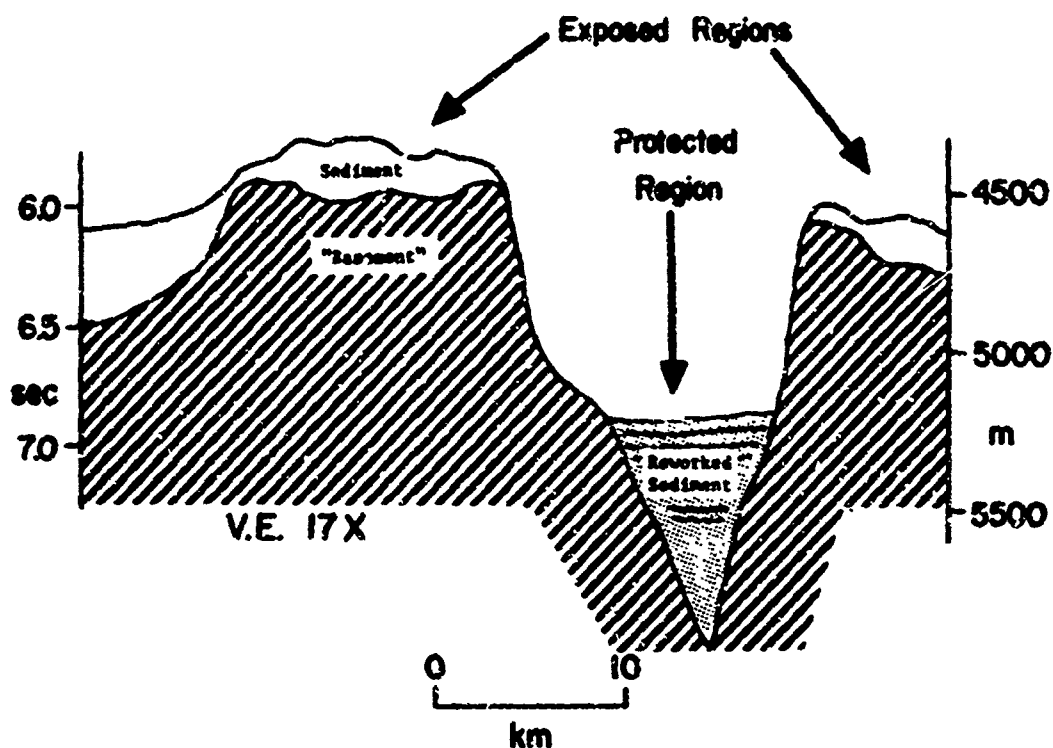
FIGURE 33   Line drawing of reflection profile from the vicinity
             of the deep-tow survey area, indicating the small-
             scale variability in depositional environments which
             may be characteristic of many regions where the
             topography is irregular.

FIGURE 34   Hypothetical conditions of deposition during glacial
             and interglacial stages in an area consisting of
             relatively protected and relatively exposed regions.
             See text for discussion.

following glacial stage. Consequently the depositional record in
exposed regions may contain hiatuses. In protected regions, however,
the depositional record should be relatively complete. Depositional
conditions at protected sites should alternate between periods of
intense vertical and lateral mixing and high sediment supply (glacials)
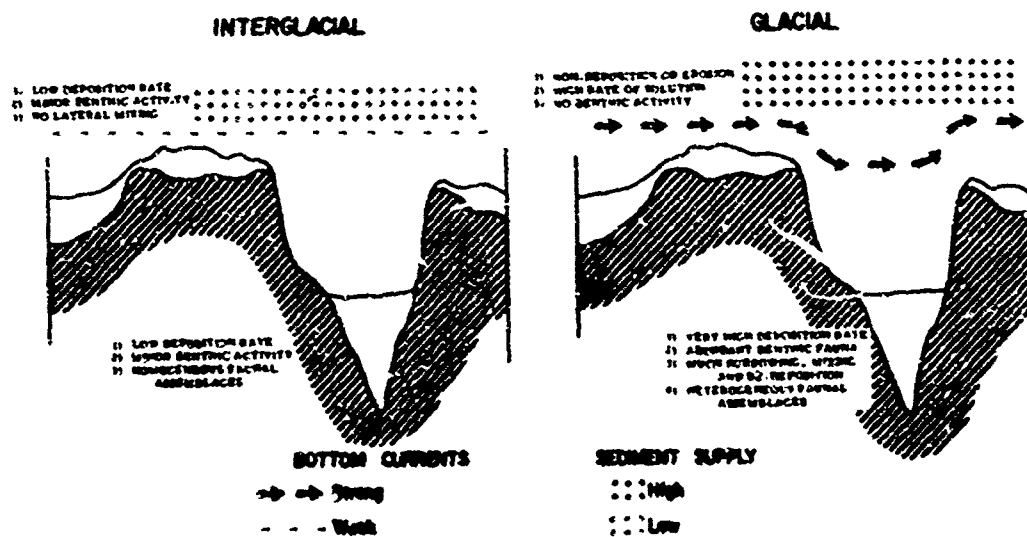and relatively quiescent periods of little mixing and low deposition
rates (interglacials). Sediment cores from protected regions such
as this should clearly show such alternations if highly variable
deposition conditions did indeed exist during the Pleistocene.

Duration of erosional events

Subaerial erosional processes commonly occur during infrequent
episodic events of relatively short duration (perhaps several hours
or days), and not at a uniform rate in response to a set of "average"
conditions. During the time intervals which separate these events
there may be little or no erosion taking place. One might consider
whether the proposed intensification of bottom water flow and sedi-
ment reworking during the Pleistocene also may have been episodic
in nature.

The deep ocean is relatively remote from those regions on the
earth's surface where the major climatic conditions are determined.
Because of its remoteness, and because of the relatively long time
required for complete mixing of the world's oceans (several hundred
years), surface climatic conditions are probably integrated over
hundreds of years in determining the effects of these changing con-
ditions on the deep sea floor. As a result, a brief interval of

markedly unusual climatic conditions at the surface may have no effect
at all upon the deep ocean if the event is of sufficiently short
duration.

It therefore appears that relatively long-term events, such
as glacial/interglacial climatic oscillations, may be required in
order to create significant changes in the depositional conditions
on the deep sea floor. The conditions favoring intensified ocean
floor erosion during glacial stages probably developed gradually,
over a time scale of 10,000 to 100,000 years. The individual ero-
sional episodes may well have occurred during brief periods, per-
haps in response to tidal oscillations similar to those observed
today. But the conditions which allowed intensified erosion to occur
must have developed over a relatively long period of time.

REFERENCES

Andrews, J. E., Abyssal hills as evidence of transcurrent faulting
        on North Pacific fracture zones, Geol. Soc. Amer. Bull., 82,
        463-470, 1971.

Arrhenius, G. O. S., Late Cenozoic climatic changes as recorded by
        the equatorial current system, Tellus, 2, 83-88, 1950.

Arrhenius, G., Sediment cores from the East Pacific, Repts. Swed.
        Deep Sea Exp., 5, 1952.

Arrhenius, G. O. S., Pelagic sediments, in The Sea, 3, M. N. Hill,
        ed., Interscience, New York, 655-727, 1963.

Arrhenius, G., Sedimentary record of long-period pheonomena, in
        Advances in Earth Science, P. M. Hurley, ed., M.I.T. Press,
        Cambridge, 155-174, 1966.

Atwater, T. and H. W. Menard, Magnetic lineations in the northeast
        Pacific, Earth and Planet. Sci. Letters, 7, 445-450, 1970.

Ballard, R. D. and K. O. Emery, Research submersibles in oceanography, Mar. Tech. Society, Washington, 1970.

Berger, W. H., Foraminiferal ooze: solution at depths, Science, 186, 383-385, 1967.

Berger, W. H., Planktonic foraminifera: selective solution and paleo-climatic interpretation, Deep-Sea Res., 15, 31-43, 1968a.

Berger, W. H., Radiolarian skeletons: solution at depths, Science, 159, 1237-1238, 1968b.

Berger, W. H., Planktonic foraminifera: selective solution and the lysocline, Mar. Geology, 8, 111-138, 1970.

Berger, W. H. and G. R. Heath, Vertical mixing in pelagic sediments, Jour. Mar. Res., 26, 134-143, 1968.

Berggren, W. A., A Cenozoic time scale: some implications for re-gional geology and paleobiogeography, Jour. Foram. Res., in press, 1971

Boegeman, D. E., G. J. Miller and W. R. Normark, Precise positioning for bottom samples using a relay transponder, in preparation, 1971.

Bonatti, E. and G. Arrhenius, Eolian sedimentation in the Pacific off northern Mexico, Mar. Geology, 3, 337-348, 1965.

Bradshaw J. S., Ecology of living planktonic foraminifera in the north and equatorial Pacific Ocean, Contr. Cushman Found. Foram. Res., 10 (2), 25-64, 1959.

Bramlette, M. N. and W. R. Riedel, Observations on the biostratigraphy of pelagic sediments, in Micropalaeontology of the Oceans. SCOR Symposium, Cambridge Univ. Press, 665-668, 1971.

Broecker, W. S., K. K. Turekian and B. C. Heezen, The relation of deep-sea sedimentation rates to variations in climate, Amer. J. Sci., 256, 503-517, 1958.

Chase, T. E., H. W. Menard, and J. Mammerickx, Bathymetry of the North Pacific, Institute of Marine Resources, Scripps Inst. of Oceanography, 10 sheets, 1970.

Cox, C. S. and H. Sandstrom, Coupling of internal and surface waves in water of variable depth, J. Oceanog. Soc. Japan, 18, 499-513, 1962.

Curray, J. R., Late Quaternary history, continental shelves of the United States, in The Quaternary of the United States, H. E. Wright and D. G. Frey, eds., Princeton Univ. Press, 723-735, 1965.

Damuth, J. E. and R. W. Fairbridge, Equatorial Atlantic deep-sea arkosic sands and ice-age aridity in tropical South America, Geol. Soc. Amer. Bull., 81, 189-206, 1970.

Doebler, H. J., Savonius current meter measurements of deep ocean currents on the slope of Plantagenet Bank, Bermuda, J. Geophys. Res., 72, 511-519, 1967.

Donn, W. L. and M. Ewing, A theory of ice ages III, Science, 152, 1706-1712, 1966.

Edmond, J. M., An interpretation of the calcite spheres experiment (abstract), Trans. Am. Geophys. Union, 52, 256, 1971.

Edmond, J., Y. Chung and J. G. Sclater, Pacific bottom water flow: implications of continuous deep water temperature profiles from the central North Pacific, J. Geophys. Res., in press, 1971.

Emery, K. O. and D. A. Ross, Topography and sediments of a small area of the continental slope south of Martha's Vineyard, Deep-Sea Res., 15, 415-422, 1968.

Emiliani, C., Isotopic paleotemperatures, Science, 154, 851-857, 1966.

Epstein, S., R. P. Sharp and A. J. Gow, Antarctic ice sheet: stable isotope analyses of Byrd Station cores and interhemispheric climatic implications, Science, 168, 1570-1572, 1970.

Ericson, D. B., M. Ewing and B. C. Heezen, Turbidity currents and sediments in the North Atlantic, Amer. Assoc. Petrol. Geol. Bull., 36, 489-512, 1952.

Ericson, D. B., G. Wollin, M. Ewing and B. C. Heezen, Atlantic deep-sea sediment cores, Geol. Soc. Amer. Bull., 72, 193-286, 1961.

Ericson, D. B. and G. Wollin, Pleistocene climates and chronology in deep-sea sediments, Science, 162, 1227-1234, 1968.

Evans, M. W. and W. White, Internal length and time scales of motion in the Pacific North Equatorial Current, in preparation, 1971.

Ewing, J., M. Ewing, T. Aitken and W. J. Ludwig, North Pacific
      sediment layers measured by seismic profiling, in The Crust
      and Upper Mantle of the Pacific Area, Geophys. Monograph #12,
      Am. Geophys. Union, Washington, 147-173, 1968.

Fairbridge, R. W., World sea-level and climatic changes, Quaternaria,
      IV, 111-134, 1962.

Fell, H. B., Biological applications of sea-floor photography, in
      Deep Sea Photography, J. B. Hersey, ed., Johns Hopkins Press,
      Baltimore, 207-221, 1967.

Fofonoff, N. P., Some properties of sea water influencing the form-
      ation of Antarctic Bottom Water, Deep-Sea Res., 4, 32-35,
      1956.

Foster, T. D., An analysis of the cabbeling instability in sea water,
      Deep-Sea Res., in press, 1971.

Francheteau, J., C. G. A. Harrison, J. G. Sclater and M. L. Richards,
      Magnetization of Pacific seamounts: a preliminary polar
      curve for the northeastern Pacific, J. Geophys. Res., 75,
      2035-2061, 1970.

Frenzel, B., The Pleistocene vegetation of northern Eurasia, Science,
      161, 637-649, 1968.

Glass, B. P., Reworking of deep-sea sediments as indicated by the
      vertical dispersion of the Australasian and Ivory Coast micro-
      tektite horizons, Earth and Planet. Sci. Letters, 6. 409-415,
      1969.

Gordon, A. L. and R. D. Gerard, North Pacific bottom potential
      temperatures, in Geological Investigation of the North Pacific,
      Geol. Soc. Amer. Memoir 126, J. D. Hays, ed., 23-39, 1971.

Griggs, G. B., A. G. Carey and L. D. Kulm, Deep-sea sedimentation
      and sediment-fauna interaction in Cascadia Channel and on
      Cascadia Abyssal Plain, Deep-Sea Res., 16, 157-170, 1969.

Hamilton, E. L., Elastic properties of marine sediments, J. Geophys.
      Res., 76, 579-604, 1971.

Hays, J. D., T. Saito, N. D. Opdyke and L. H. Burckle, Pliocene-
      Pleistocene sediments of the equatorial Pacific: their paleo-
      magnetic, biostratigraphic and climatic record, Geol. Soc.
      Amer. Bull., 80, 1481-1513, 1969.

Hays, J. D. et al., Initial Reports of the Deep Sea Drilling Project,
        vol. 9, U. S. Govt, Printing Office, Washington, in press,
        1971.

Heath, G. R., Carbonate sedimentation in the abyssal equatorial Pacific
        during the past 50 million years, Geol. Soc. Amer. Bull., 80,
        689-694, 1969.

Heath, G. R. and T. C. Moore, Jr., Subbottom profile of abyssal sedi-
        ments in the central equatorial Pacific, Science, 149, 744-746,
        1965.

Heezen, B. C., Dynamic processes of abyssal sedimentation: erosion,
        transportation, and redeposition on the deep-sea floor,
        Geophys. J. Roy. Astr. Soc., 2, 142-163, 1959.

Heezen, B. C., Turbidity currents, in The Sea, 3, M. N. Hill, ed.,
        Interscience, New York, 742-771, 1963.

Heezen, B. C., D. B. Ericson and M. Ewing, Further evidence for a
        turbidity current following the 1929 Grand Banks earthquake,
        Deep-Sea Res., 1, 193-202, 1954.

Heezen, B. C. and C. D. Hollister, Deep-sea current evidence from
        abyssal sediments, Mar. Geology, 1, 141-174, 1964.

Heezen, B. C., C. D. Hollister and W. F. Ruddiman, Shaping of the
        continental rise by deep geostrophic contour currents,
        Science, 152, 502-508, 1966.

Hjulstrom, F., Transportation of detritus by moving water, in Recent
        Marine Sediments, P. D. Trask, ed., Amer. Assoc. Petrol.
        Geol., Tulsa, 5-31, 1939.

Hollister, C. D. and R. B. Elder, Contour currents in the Weddell Sea,
        Deep-Sea Res., 15, 99-101, 1969.

Hollister, C. D. and B. C. Heezen, Ocean bottom currents, in The
        Encyclopedia of Oceanography, R. W. Fairbridge, ed., Reinhold
        Publ. Co., New York, 576-583, 1966.

Isaacs, J. D., J. L. Reid, Jr., G. B. Schic and R. A. Schwartzlose,
        Near-bottom currents measured in 4 kilometers depth off the
        Baja California coast,   J. Geophys. Res., 71, 4297-4303,
        1966.

Jacobs, S. S., A. F. Amos and P. M. Bruckhausen, Ross Sea oceanography
          and Antarctic Bottom Water formation, Deep-Sea Res., 17,
          935-962, 1970.

Johnson, D. A. and T. C. Johnson, Sediment redistribution by bottom
          currents in the central Pacific, Deep-Sea Res., 17, 157-169,
          1970.

Jones, E. J. W., M. Ewing, J.Ewing and S. l Eittreim, Influences
          of Norwegian Sea overflow water on sedimentation in the
          northern North Atlantic and Labrador Sea, J. Geophys.
          Res., 75, 1655-1680, 1970.

Kaye, C. A., The effect of solvent motion on limestone solution,
          J. Geol., 65, 35-46, 1957.

Kennett, J. P., Pleistocene paleoclimatic and foraminiferal bio-
          stratigraphy in subantarctic deep-sea cores, Deep-Sea Res.,
          17, 125-140, 1970.

Knauss, J. A., Equatorial current systems, in The Sea, 2, M. N.
          Hill, ed., Interscience, New York, 235-252, 1963.

Krause, D. C., Interpretation of echo sounding profiles, Int. Hydrog.
          Rev., 39, 65-123, 1962.

Lamb, H. H. and A. Woodroffe, Atmospheric circulation during the
          last ice age, Quaternary Res., 1, 29-58, 1970.

Larson, R. L., Near-bottom geologic studies of the East Pacific
          Rise crest, Geol. Soc. Amer. Bull., 82, 823-842, 1971.

Laughton, A. S., Microtopography, in The Sea, 3, M. N. Hill, ed.,
          Interscience, New York, 437-472, 1963.

Laughton, A. S., New evidence of erosion on the deep ocean floor,
          Deep-Sea Res., 15, 21-23, 1968.

Lonsdale, P. F., W. R. Normark and W. A. Newman, Sedimentation and
          erosion on Horizon Guyot, in preparation, 1971.

Lowenstein, C. D., Position determination near the sea floor, in
          Marine Sciences Instrumentation, 4, Plenum Press, New York,
          319-324, 1968.

Luyendyk, B. P., Geological and geophysical observations in an
          abyssal hill area using a deeply towed instrument package,
          Ph.D. thesis, University of California, San Diego, 212 pp.,
          1969.

Luyendyk, B. P., Origin and history of abyssal hills in the northeast
        Pacific ocean, Geol. Soc. Amer. Bull., 81, 2237-2260, 1970.

Macdougall, D., Deep sea drilling: age and composition of an
        Atlantic basaltic intrusion, Science, 171, 1244-1245, 1971.

McCoy, F. W., Bottom currents in the western Atlantic ocean between
        the lesser Antilles and the mid-Atlantic Ridge, Deep-Sea
        Res., 16, 179-184, 1969.

McKenzie, D. P. and R. L. Parker, The north Pacific: an example
        of tectonics on a sphere, Nature, 216, 1276-1280, 1967.

McManus, D. A., Criteria of climatic change in the inorganic compon-
        ents of marine sediments, Quaternary Res., 1, 72-102, 1970.

Menard, H. W. and R. L. Fisher, Clipperton Fracture Zone in the
        northeastern equatorial Pacific, J. Geol., 66, 239-253, 1958.

Miller, G. R., The flux of tidal energy out of the deep oceans,
        Jour. Geophys. Res., 71, 2485-2489, 1966.

Moore, D. G., The free corer: sediment sampling without wire and
        winch, J. Sed Petrol., 31, 627-630, 1961.

Moore, T. C., Jr., Radiolaria: change in skeletal weight and resist-
        ance to solution, Geol. Soc. Amer. Bull., 80, 2103-2108,
        1969.

Moore, T. C., Jr., Abyssal hills in the central equatorial Pacific:
        sedimentation and stratigraphy, Deep-Sea Res., 17, 573-593,
        1970.

Moore, T. C., Jr., Radiolaria, in Initial Reports of the Deep Sea
        Drilling Project, vol. 8, in press, 1971.

Moore, T. C., Jr., and G. R. Heath, Abyssal hills in the central
        Pacific: detailed structure of the sea floor and sub-bottom
        reflectors, Mar. Geology, 5, 161-179, 1967.

Morgan, W. J., Rises, trenches, great faults, and crustal blocks,
        J. Geophys. Res., 73, 1959-1982, 1968.

Mudie, J. D., W. R. Normark and E. J. Gray, Jr., Direct mapping of
        the sea floor using side-scanning sonar and transponder
        navigation, Geol. Soc. Amer. Bull., 81, 1547-1554, 1970.

Mudie, J. D., J. A. Grow and J. R. Hutt, Microtopographic, magnetic, and bottom penetration survey of a small area of abyssal hills in the equatorial Pacific, in preparation, 1971.

Munk, W. H., Abyssal recipes, Deep-Sea Res., 13, 707-730, 1966.

Munk, W. H., Once again -- tidal friction, Quart. J. Roy. Astr. Soc., 9, 352-375, 1968.

Nowroozi, A. A., M. Ewing, J. E. Nafe and M. Fleigel, Deep ocean current and its correlation with the ocean tide off the coast of northern California, J. Geophys. Res., 73, 1921-1932, 1968.

Olausson, E., Le climat au Pleistocene et la circulation des oceans, Rev. Geogr. Phys. et Geol. Dyn., 11, 251-264, 1969.

Owen, R. W. and B. Zeitzschel, Phytoplankton production: seasonal change in the oceanic eastern tropical Pacific, Mar. Biol., 7, 32-36, 1970.

Parker, F. L., Distribution of planktonic foraminifera in recent deep-sea sediments, in Micropalaeontology of Marine Bottom Sediments, SCOR symposium, Cambridge Univ. Press, 289-307, 1971.

Peterson, M. N. A., Calcite: rates of dissolution in a vertical profile in the central Pacific, Science, 154, 1542-1544, 1966.

Phleger, F. B, Displaced foraminifera faunas, Soc. Econ. Paleont. Mineral., Spec. Publ. 2, 66-75, 1951.

Postma, H., Sediment transport and sedimentation in the estuarine environment, in Estuaries, G. H. Lauff, ed., Publ. No. 83, Am. Assoc. Adv. Sci. (Washington), 158-179, 1967.

Reid, J. L., Jr., ed., Oceanic Observations of the Pacific: 1955, the NORPAC Atlas, Univ. of Calif. Press, Berkeley, 1960.

Reid, J. L., Jr., Preliminary results of measurements of deep currents in the Pacific Ocean, Nature, 221, 848, 1969.

Reid, J. L., Jr., H. Stommel, E. D. Stroup and B. A. Warren, Detection of a deep boundary current in the western south Pacific, Nature, 217, 937, 1968.

Rhoads, D. C. and D. K. Young, The influence of deposit-feeding organisms on sediment stability and community trophic structure, J. Mar. Res., 28, 150-178, 1970.

Riedel, W. R., Radiolarian evidence consistent with spreading of
        the Pacific floor, Science, 157, 540-542, 1967.

Riedel, W. R., The occurrence of pre-Quaternary radiolaria in deep-
        sea sediments, in Micropalaeontology of Marine Bottom Sed-
        iments, SCOR symposium, Cambridge Univ. Press, 567-594, 1971.

Riedel, W. R. and B. M. Funnell, Tertiary sediment cores and micro-
        fossils from the Pacific Ocean floor, Quart. J. Geol. Soc.
        Lond., 120, 305-368, 1964.

Riedel, W. R. and A. Sanfilippo, Radiolaria, in Initial Reports of
        the Deep Sea Drilling Project, vol. 4, 503-575, 1970.

Riedel, W. R. and A. Sanfilippo, Cenozoic radiolaria from the western
        tropical Pacific, in Initial Reports of the Deep Sea Drilling
        Project, vol. 7, in press, 1971.

Rubey, W. W., The force required to move particles on a stream bed,
        U. S. Geol. Survey Prof. Paper 189-E, 121-140, 1938.

Ruddiman, W. F., Pleistocene sedimentation in the equatorial Atlantic:
        stratigraphy and faunal paleoclimatology, Geol. Soc. Amer.
        Bull., 82, 283-302, 1971.

Sachs, P. L. and S. O. Raymond, A new unattached sediment sampler,
        J. Mar. Res., 23, 44-53, 1965.

Sanders, H. L. and R. R. Hessler, Ecology of the deep-sea benthos,
        Science, 163, 1419-1424, 1969.

Sanfilippo, A. and W. R. Riedel, Post-Eocene "closed" theoperid
        radiolarians, Micropaleontology, 16, 446-462, 1970.

Seabrooke, J. M., G. L. Hufford and R. B. Elder, Formation of Antarctic
        Bottom Water in the Weddell Sea, Jour. Geophys. Res., 76,
        2164-2178, 1971.

Schick, G. B., J. D. Isaacs and M. H. Sessions, Autonomous instruments
        in oceanographic research, in Marine Sciences Instrumentation,
        4, Plenum Press, New York, 203-230, 1968.

Schmitz, W. J., A. R. Robinson and F. C. Fuglister, Bottom velocity
        observations directly under the Gulf Stream, Science, 170,
        1192-1194, 1970.

Schwartzlose, R. A. and J. D. Isaacs, Transient circulation event
        near the deep ocean floor, Science, 165, 889-891, 1969.

Shepard, F. P., Submarine Geology (2nd ed.), Harper and Row, New York, 1963.

Snodgrass, F., Deep sea instrument capsule, Science, 162, 78-87, 1971

Southard, J. B., R. A. Young and C. D. Hollister, Experimental erosion of fine abys al sediment, J. Geophys. Res., 76, in press, 1971.

Spiess, F. N., M. S. Loughridge, M. S. McGehee and D. E. Boegeman, An acoustic transponder system, Navigation, 13, 154-161, 1966.

Spiess, F. N., B. P. Luyendyk, R. L. Larson, W. R. Normark and J. D. Mudie, Detailed geophysical studies on the northern Hawaiian arch using a deeply towed instrument package, Mar. Geology, 7, 501-528, 1969.

Spiess, F. N. and J. D. Mudie, Small scale topographic and magnetic features, in The Sea, 4, Part I, A. E. Maxwell, ed., Interscience, New York, 205-250, 1970.

Tareyev, B. A., Internal baroclinic waves in flow round irregularities on the ocean floor and their effect on sedimentation processes, Oceanology, 5, 31-37, 1965.

Tracey, J. I., Jr., et al., Initial Reports of the Deep Sea Drilling Project, vol. 8, U.S. Govt. Printing Ofc., Wash., in press, 1971.

van Andel, Tj. H. and P. D. Komar, Ponded sediments of the mid-Atlantic Ridge between 22° and 23° north latitude, Geol. Soc. Amer. Bull., 80, 1163-1190, 1969.

van Andel, Tj. H. et al., Deep Sea Drilling Project, Leg 16, Geotimes, 16, 12-14, 1971.

Vanoni, V. A., Measurements of critical shear stress for entraining fine sediments in a boundary later, Calif. Inst. of Tech., Keck Lab. of Hydraulics and Water Resources, Rept. #KH-R-7, 47 pp., 1964.

Wimbush, M. and W. Munk, The benthic boundary layer, in The Sea, 4, Part I, A. E. Maxwell, ed., Interscience, New York, 731-763, 1970.

Wooster, W. S. and G. H. Volkmann, Indications of deep Pacific circulation from the distribution of properties at five kilometers, J. Geophys. Res., 65, 1239-1249, 1960.

PLATE 1

All figures are at a magnification of X 140.

Fig. 1   Tnyrsocyrtis triacantha (Ehrenberg)   E-10, 57-58 cm

Fig. 2   Thyrsocyrtis tetracantha (Ehrenberg)   E-10,   0-1 cm

Fig. 3   Sethochytris babylonis (Clark and Campbell) E-10,   5-7 cm

Fig. 4   Cycladophora turris Ehrenberg   E-10,   0-1 cm

Fig. 5   Thyrsocyrtis bromia Ehrenberg   E-10,   5-7 cm

Fig. 6   Thyrsocyrtis bromia Ehrenberg   E-10,   5-7 cm

Fig. 7   Thyrsocyrtis tetracantha (Ehrenberg)   E-10, 57-58 cm

Fig. 8   Theocampe mongolfieri Ehrenberg   E-10,   0-1 cm

Fig. 9   Artophormis barbadensis (Ehrenberg)   E-17, 20-21 cm

Fig. 10   Artophormis gracilis Riedel   S-8, 22-24 cm

Fig. 11   Dorcadospyris quadripes Moore   S-8, 22-24 cm

Fig. 12   Theocerys sp.   E-17, 20-21 cm

Fig. 13   Lithocyclia aristotelis (Ehrenberg) group   E-10,   0-1 cm

Fig. 14   Lithocyclia angustum (Riedel)   E-25, 17-18 cm

Fig. 15   Lithocyclia aristotelis (Ehrenberg) group   E-10, 50-51 cm

Fig. 16   Dorcadospyris triceros (Ehrenberg)   E-19, 26-27 cm
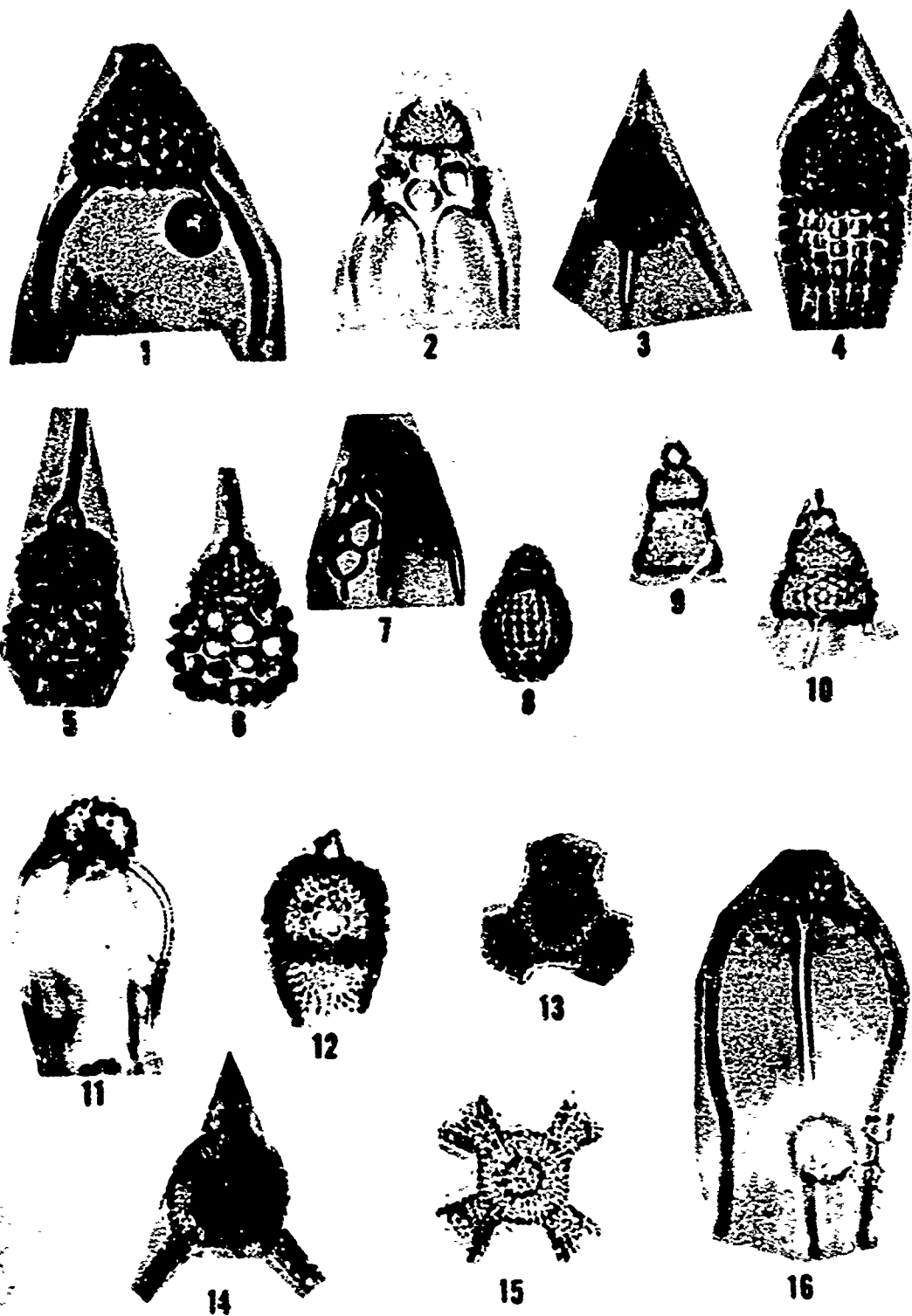
PLATE 2

Figures 1 through 10 are at a magnification of X 140.
Figures 11 through 15 are at a magnification of X 95.

Fig. 1   Cannartus prismaticus (Haeckel)   S-8, 22-24 cm

Fig. 2   Cannartus tubarius (Haeckel)   E-6, 45-46 cm

Fig. 3   Cannartus violina Haeckel   E-3, 40-42 cm

Fig. 4   Cannartus laticonus Riedel   E-5, 31-33 cm

Fig. 5   Ommatartus antepenultimus Riedel and Sanfilippo

E-27, 110-112 cm

Fig. 6   Ommatartus hughesi (Campbell and Clark)   E-27, 110-112 cm

Fig. 7   Cyclampterium (?) milowi Riedel and Sanfilippo   E-14, 1-2 cm

Fig. 8   Cyclampterium pegetrum Sanfilippo and Riedel   S-8, 22-24 cm

Fig. 9   Cyclampterium leptetrum Sanfilippo and Riedel   E-6, 45-46 cm

Fig. 10 Cyclampterium tanythorax Sanfilippo and Riedel E-5, 31-33 cm

Fig. 11 Dorcadospyris ateuchus (Ehrenberg)   S-8, 22-24 cm

Fig. 12 Dorcadospyris simplex (Riedel)   E-6, 45-46 cm

Fig. 13 Dorcadospyris alata (Riedel)   E-5, 31-33 cm

Fig. 14 Dorcadospyris papilio (Riedel)   S-7, 11-13 cm

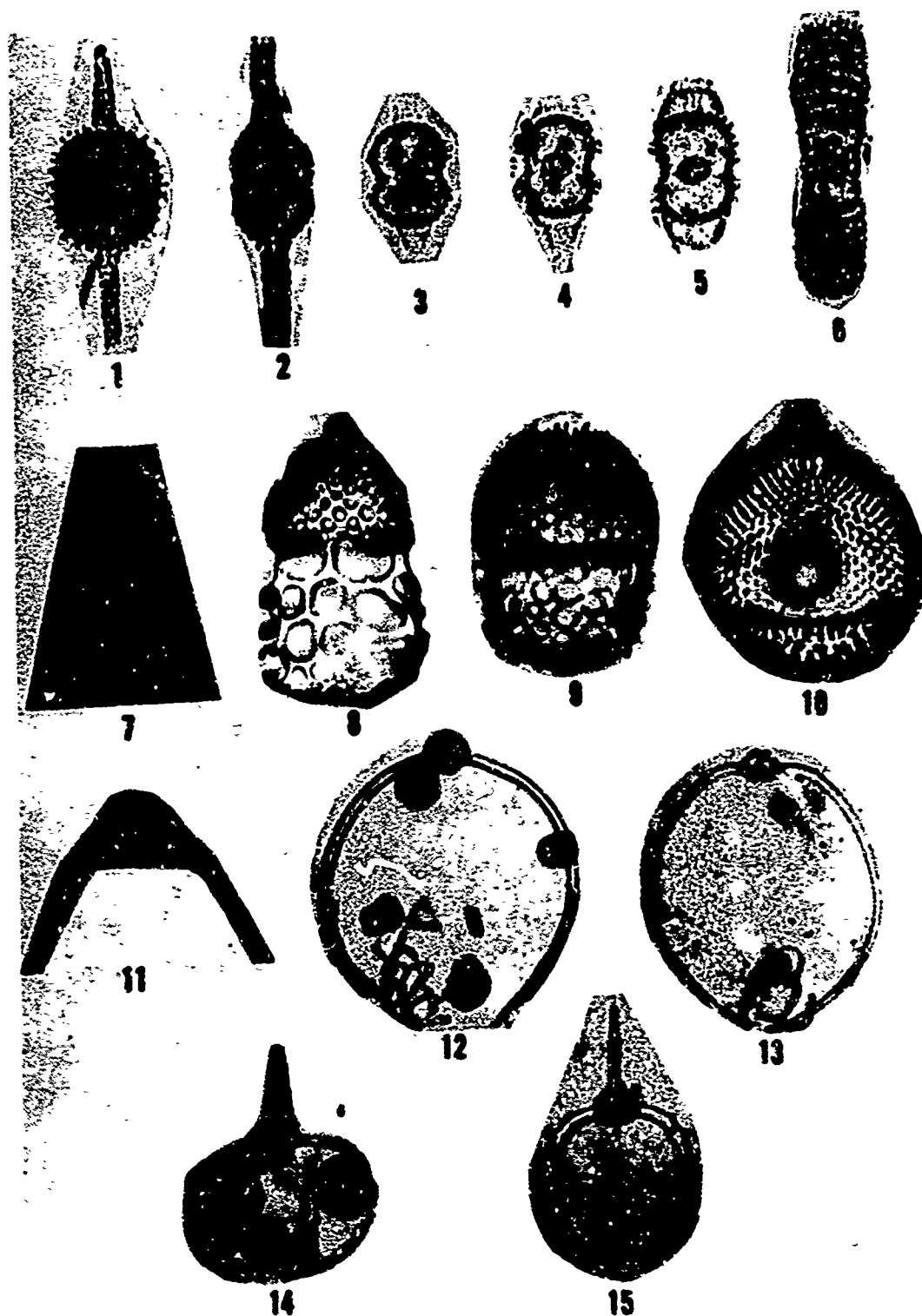Fig. 15 Dorcadospyris dentata Haeckel   E-3, 40-42 cm

PLATE 3

All figures are at a magnification of X 140.

Fig. 1   Theocyrtis tuberosa Riedel   E-10, 0-1 cm

Fig. 2   Theocyrtis annosa (Riedel)   S-23, 3-5 cm

Fig. 3   Calocycletta robusta Moore   S-6, 17-19 cm

Fig. 4   Calocycletta costata (Riedel)   E-4, 41-42 cm

Fig. 5   Lychnocanium bipes Riedel   S-7, 11-13 cm

Fig. 6   Calocycletta virginis Haeckel   E-11, 21-22 cm

Fig. 7   Calocycletta virginis Haeckel   E-18, 7-8 cm

Fig. 8   Stichocorys delmontensis (Campbell and Clark)

                                                              E-27, 110-112 cm

Fig. 9   Stichocorys wolffii Haeckel   E-3, 40-42 cm

Fig. 10   Cyrtocapsella cornuta Haeckel   E-6, 45-46 cm

Fig. 11   Cyrtocapsella tetrapera Haeckel   E-5, 31-33 cm

Fig. 12   Stichocorys delmontensis (Campbell and Clark) E-16, 45-46 cm

Fig. 13   Lithopera renzae Sanfilippo and Riedel   E-5, 14-16 cm

Fig. 14   Lithopera renzae Sanfilippo and Riedel   E-5, 31-33 cm

Fig. 15   Lithopera neotera Sanfilippo and Riedel   E-27, 140-142 cm
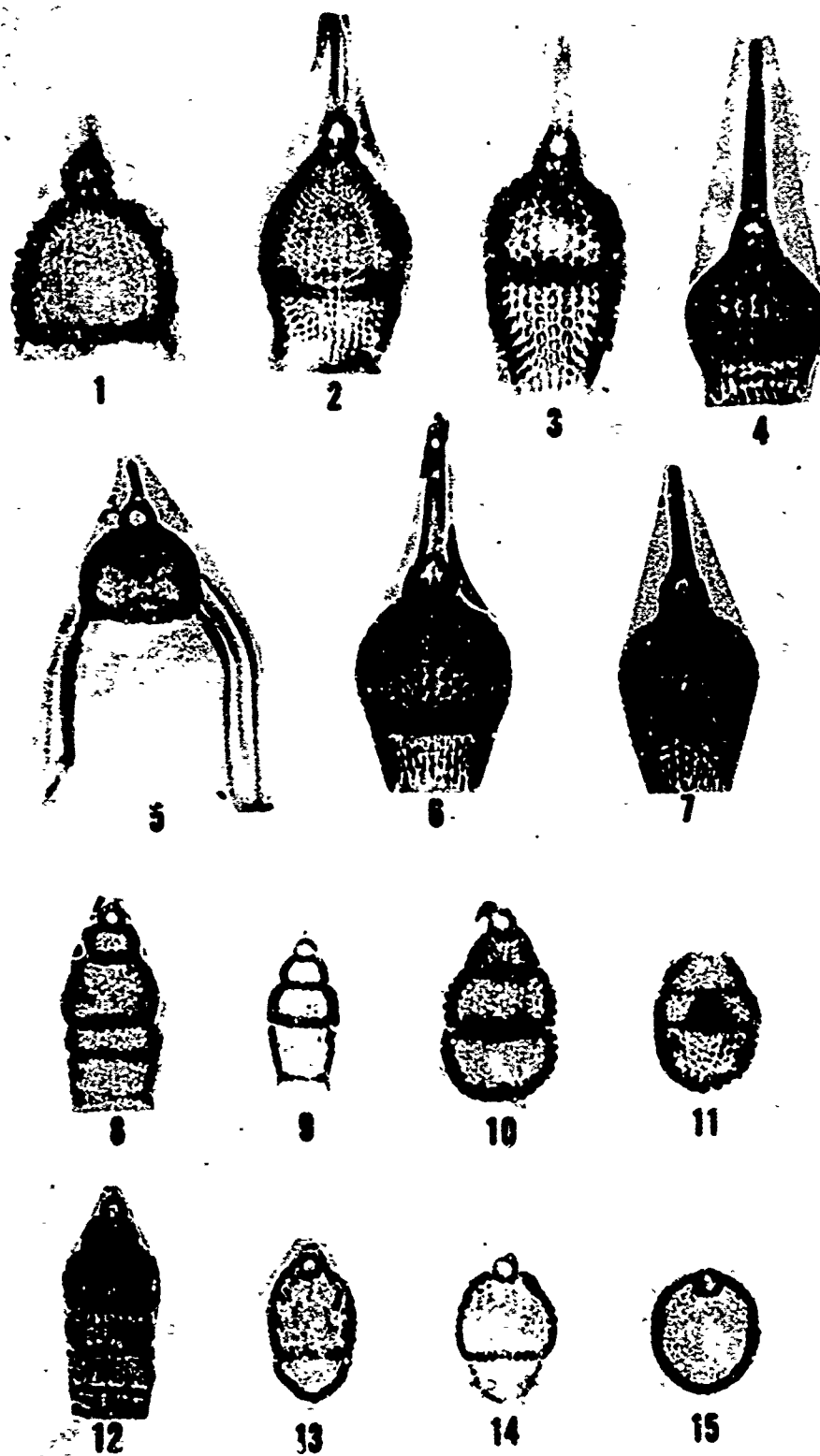
PLATE 4

FREE-FALL CORES: PROFILE I
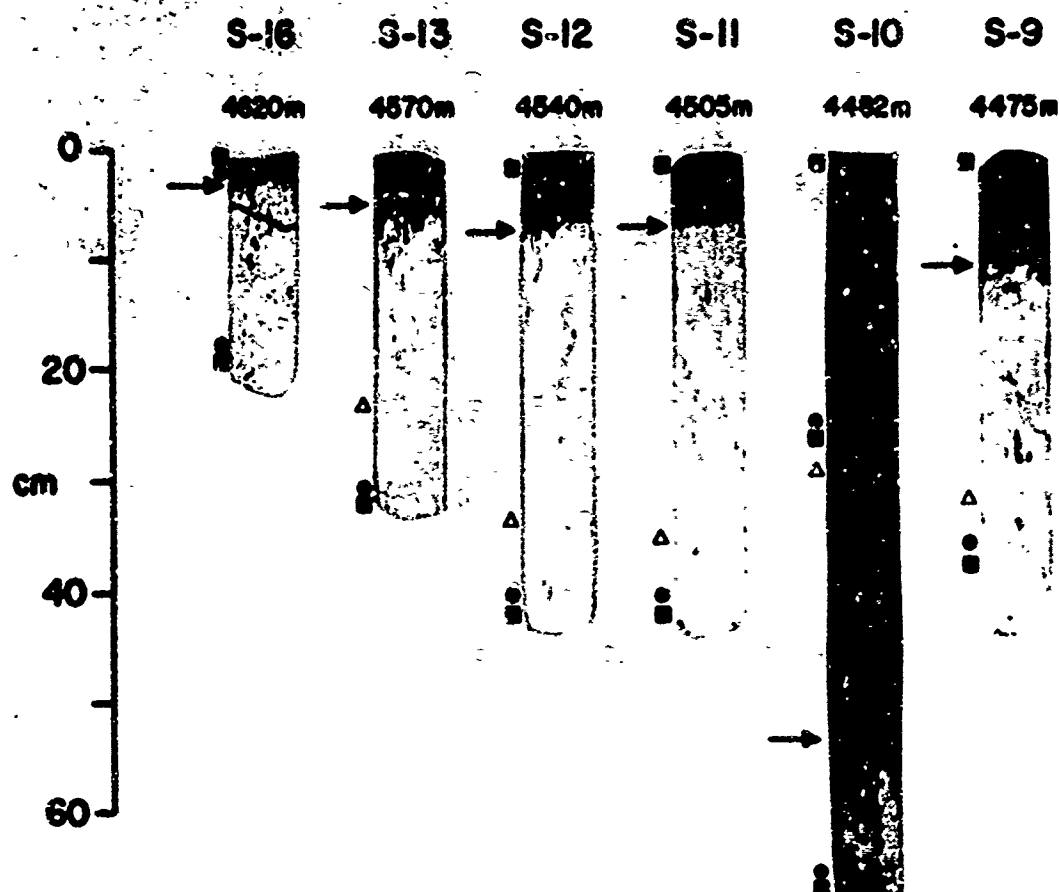
PLATE 5

FREE-FALL CORES: PROFILE II

S-16	S-13	S-12	S-11	S-10	S-9
4620m	4570m	4540m	4505m	4482m	4475m

Samples Taken

△ Radiolaria
● Foraminifera
△ Physical properties

→ Holocene - M. Tertiary
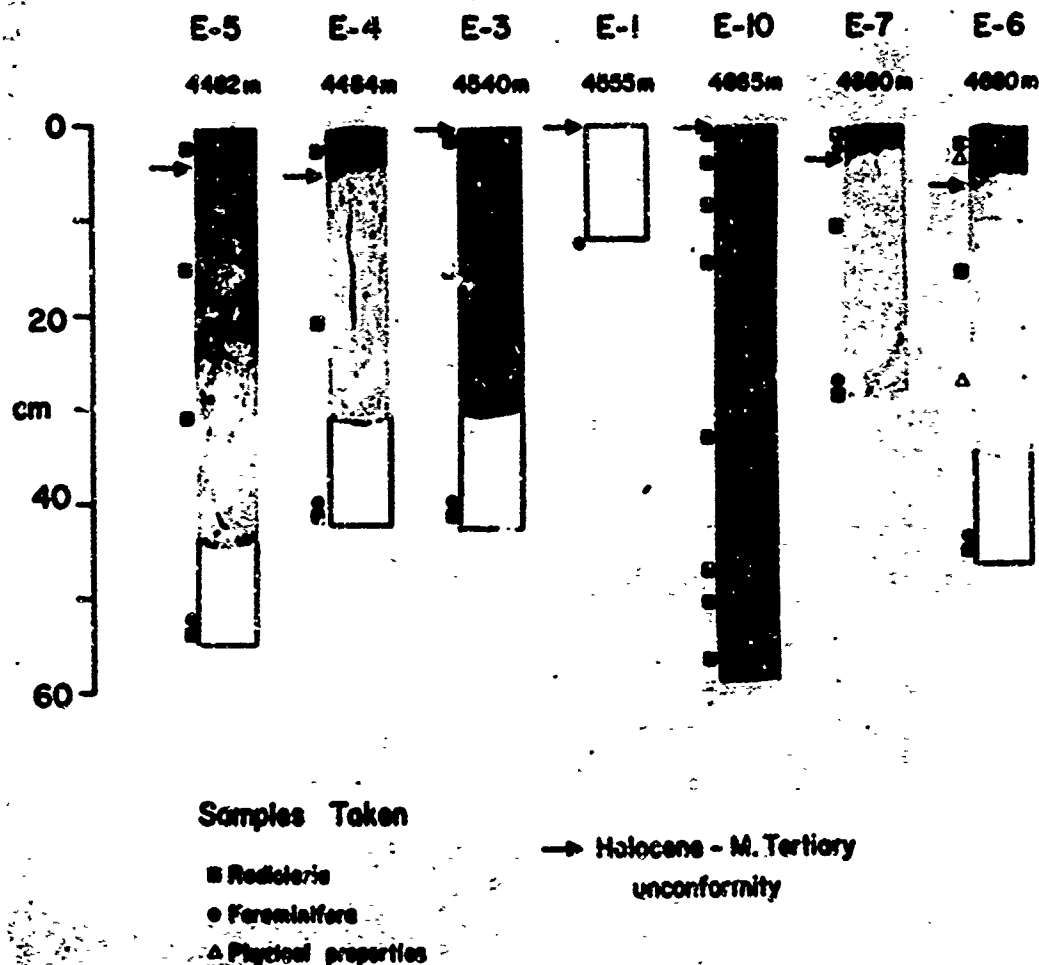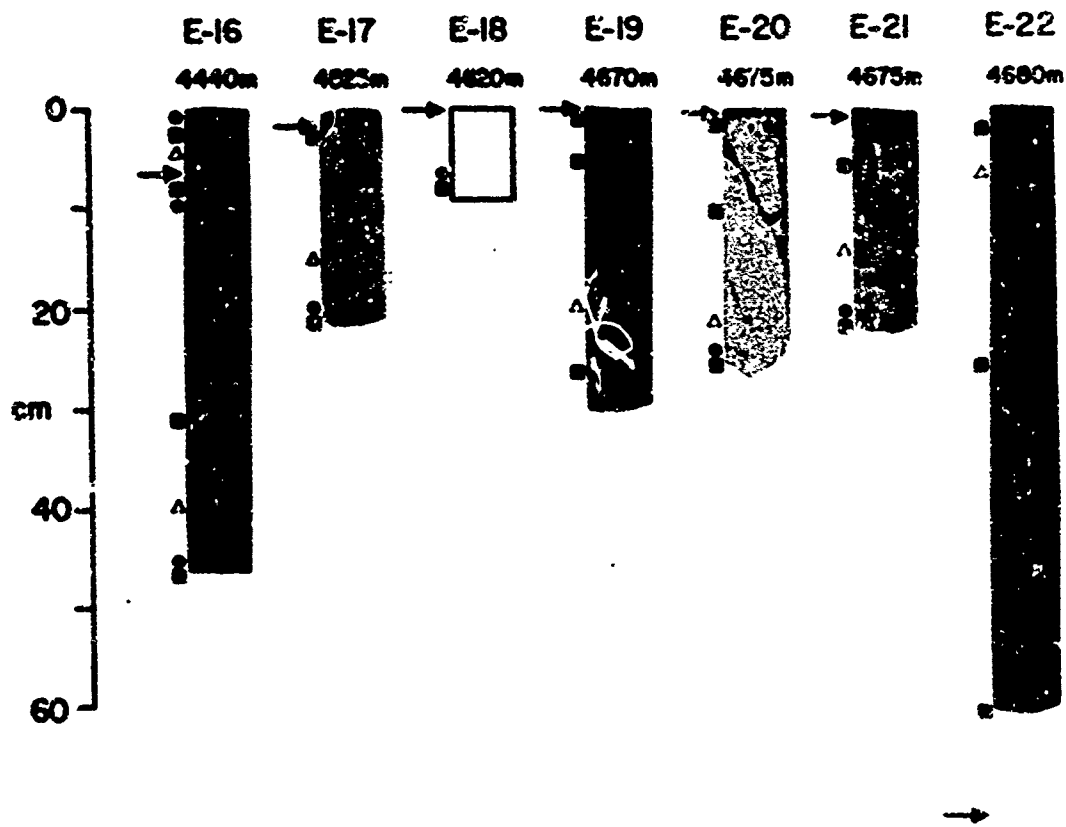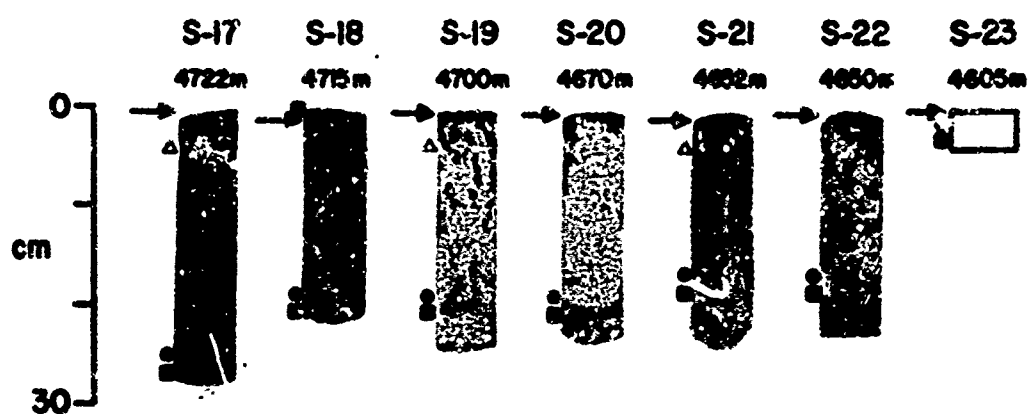unconformity

PLATE 6

FREE-FALL CORES: PROFILE III

E-5   E-4   E-3   E-1   E-10   E-7   E-6
4482m   4484m   4540m   4555m   4665m   4660m   4680m

Samples Taken

■ Radiolaria
● Foraminifera
△ Physical properties

→ Holocene - M. Tertiary
   unconformity

PLATE 7

FREE-FALL CORES: PROFILE IV

Samples Taken

■ Radiolaria

● Foraminifera

△ Physical properties
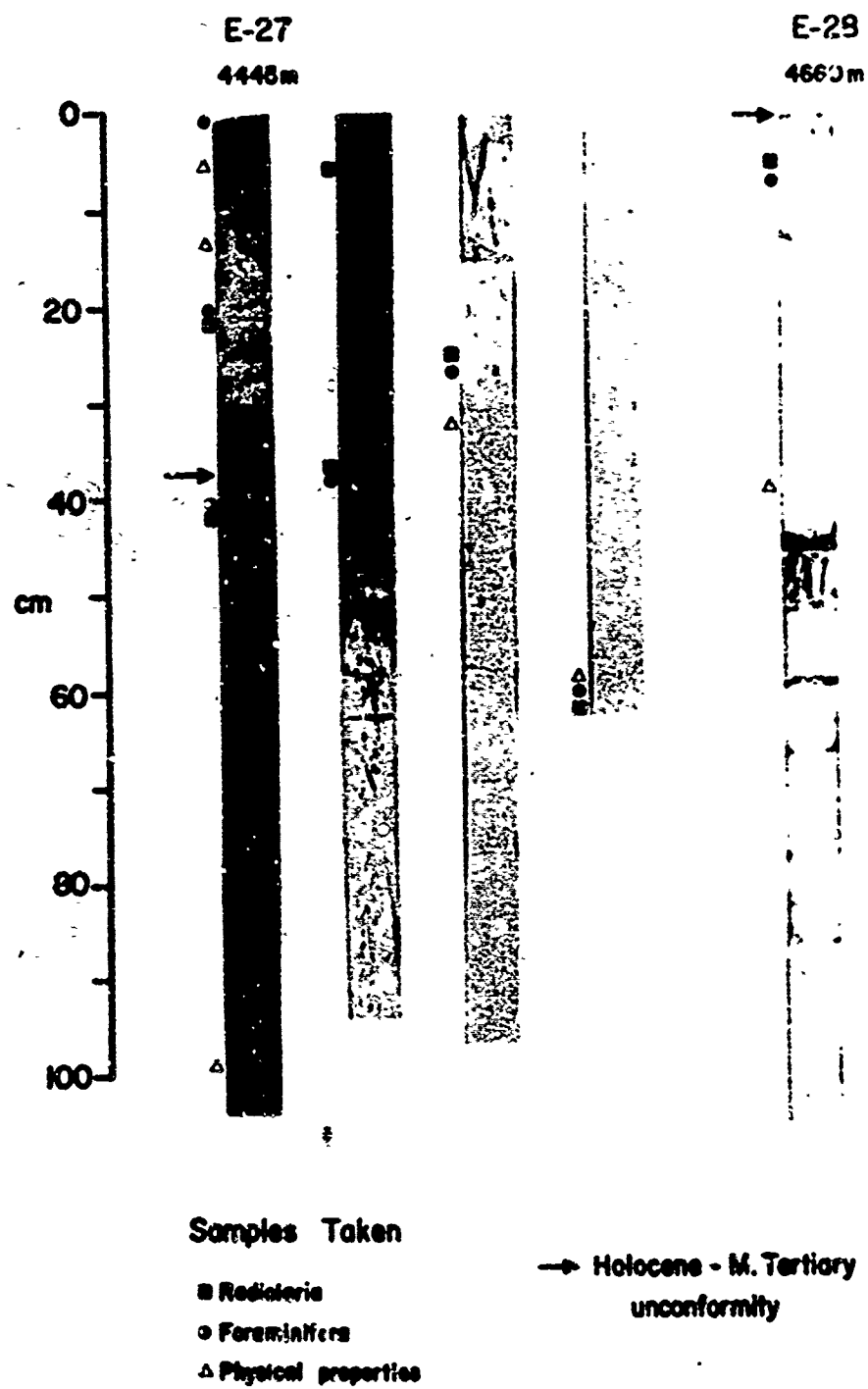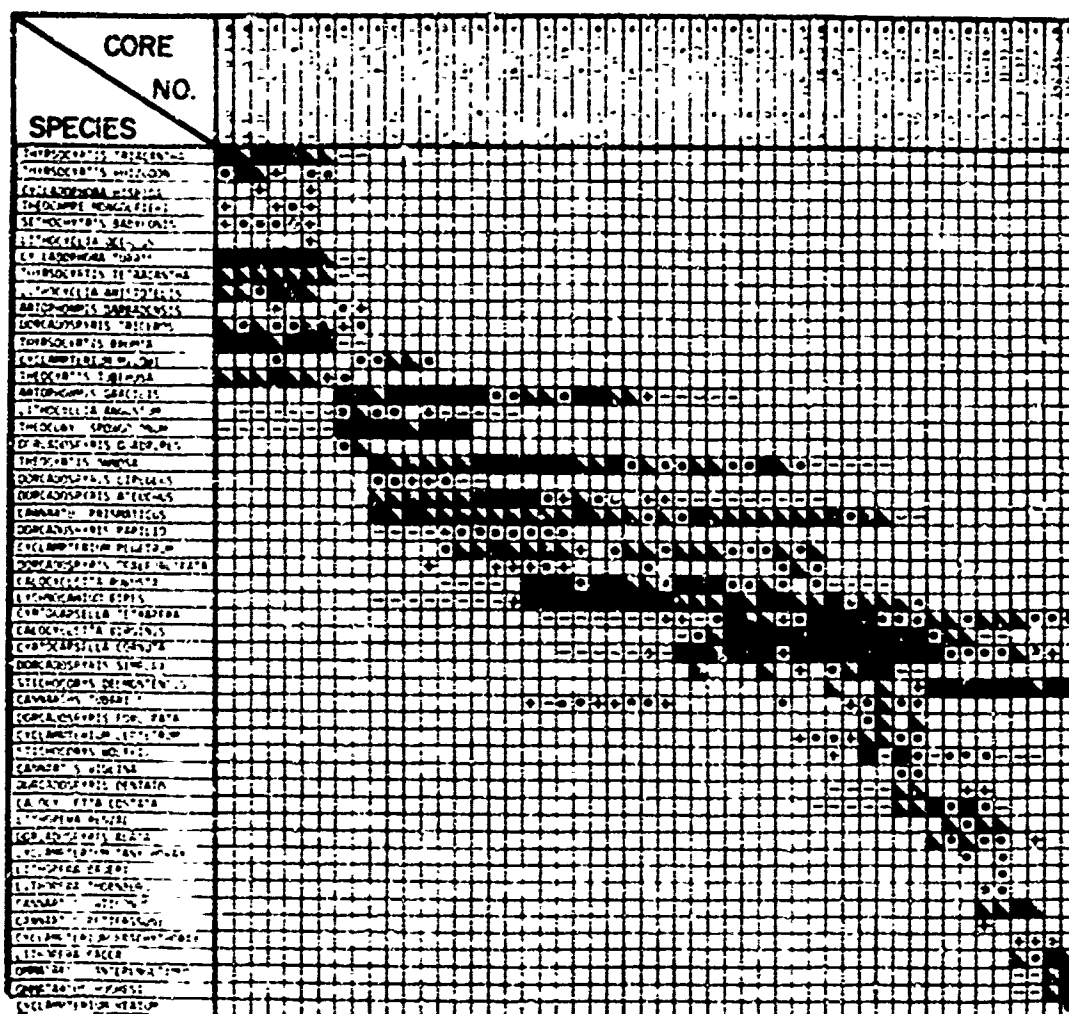
→ Holocene - M. Tertiary
unconformity

PLATE 8

FREE-FALL CORES: PROFILE V

Samples Taken

■ Radiolaria

● Foraminifera

△ Physical properties

→ Holocene - M. Tertiary
unconformity

PLATE 9

PISTON CORES

Samples Taken

- Radiolaria
- Foraminifera
- Physical properties

→ Holocene - M. Tertiary
    unconformity

PLATE 10

PLATE 11

COMMON
FEW
RARE
PRESENT
ABSENT

APPENDIX I

BOTTOM PHOTOGRAPHS

FIGURE A-1

Bottom photograph from camera run C, showing large circular

mounds of sediment 50 to 100 cm in width and several tens of

cm in height.   The mounds were probably formed by a burrowing

organism.

FIGURE A-2

Bottom photograph from camera run C, showing what may be an

outcropping of igneous material. Alternatively, the dark

material may be a manganese oxide coating which formed on

the erosion surface which overlies the Tertiary sediments.

FIGURE A-3

Bottom photograph from camera run D. The organism in the upper
left corner is probably a holothurian (see Fell, 1967, Fig. 19-3).
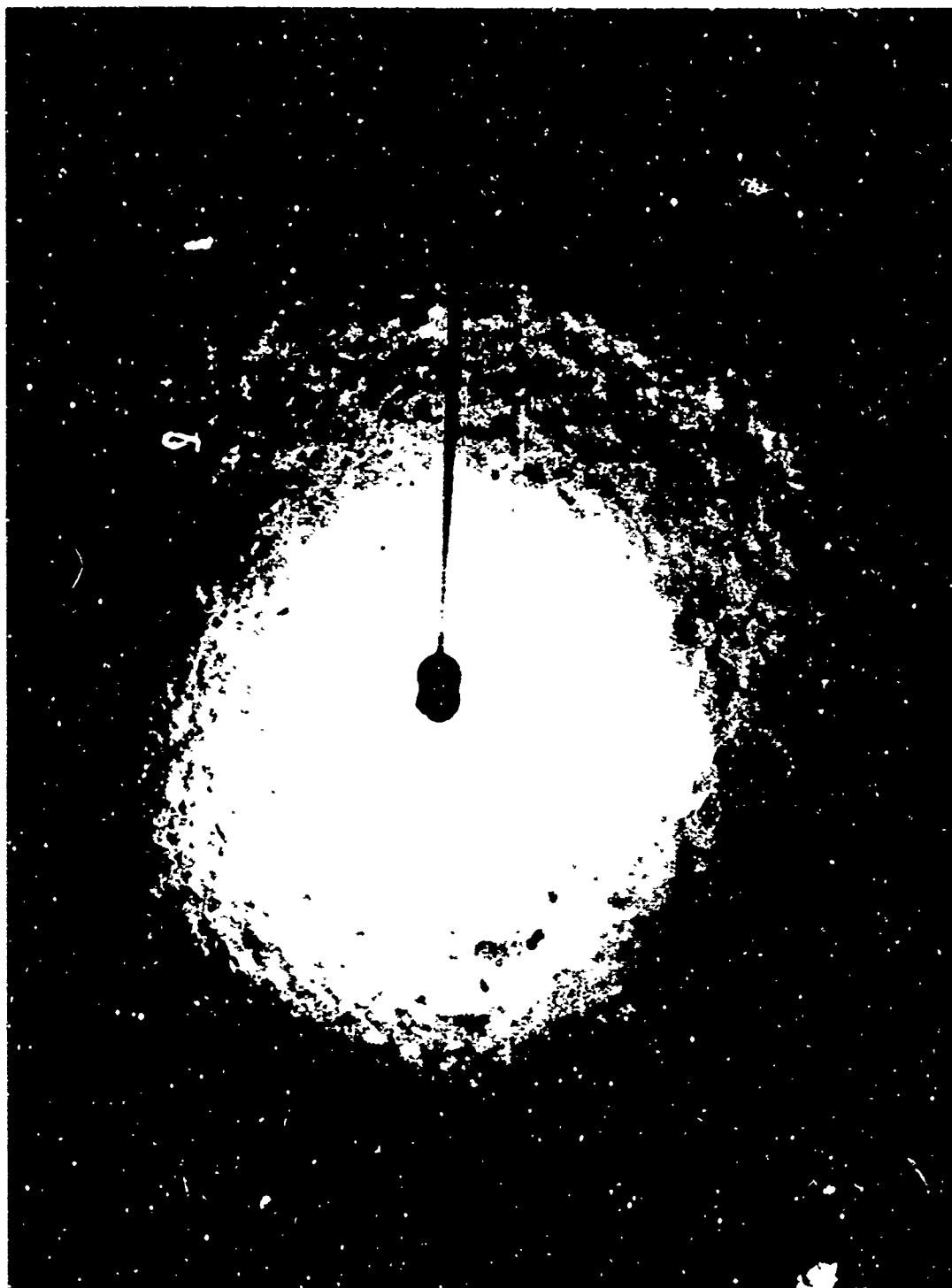
FIGURE A-4

Bottom photograph from camera run K, showing several typec of

structures created by the activity of benthic organisms. The

sea floor is covered with small pits and craters which are

barely visible in this photograph. Near the right edge of the

photograph there is a somewhat larger crater, with a single

straight furrow extending outward from it. A structure

indicative of horizontal burrowing by a relatively large

organism is present near the top of the picture. Width of

the field of view is approximately 3 meters.
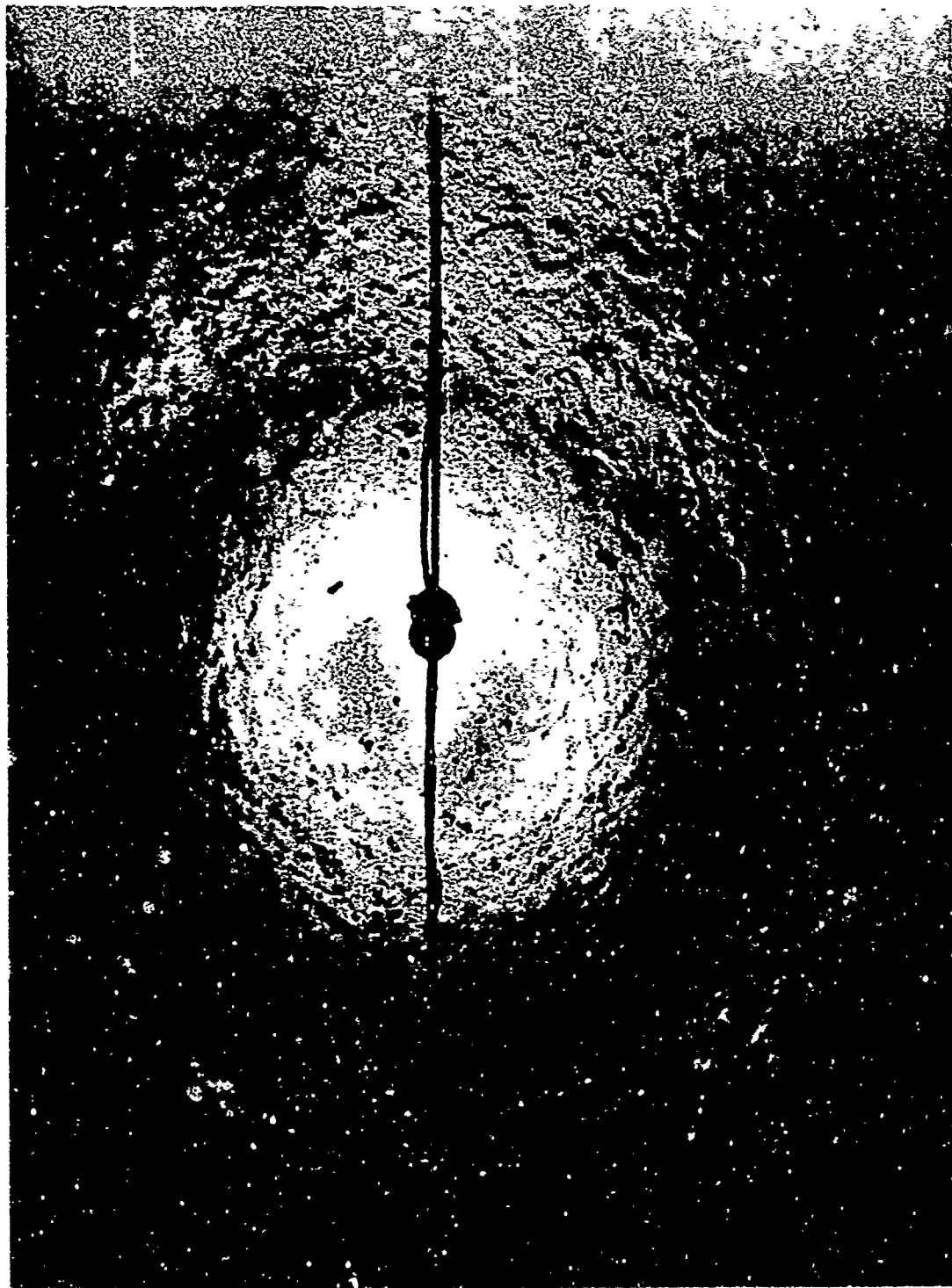
FIGURE A-5

Bottom photograph from camera run K, showing many small craters,

pits, and meandering narrow grooves. Some of the grooves may

have been formed by organisms such as those illustrated by

Ewing and Davis (1967, Figs. 24-40 through 24-44).
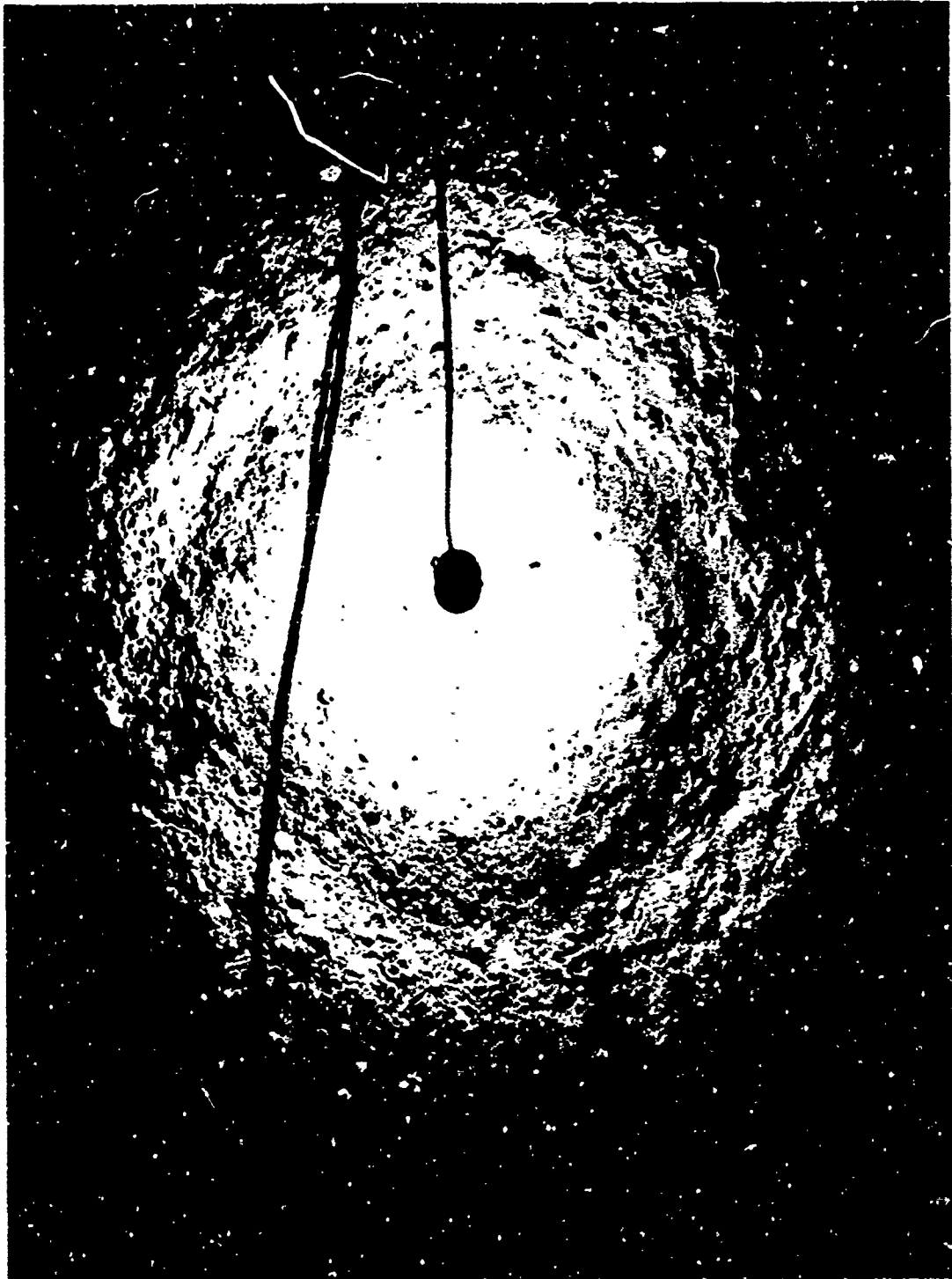
FIGURE A-6

Bottom photograph from camera run K. The meandering path of a
burrowing organism can be seen in the upper-right corner of the
photograph. The circular cloud of fine-grained sediment
beneath the strobe light was put into suspension when the light
struck bottom just before the picture was taken. Width of the
field of view is approximately 3 meters.
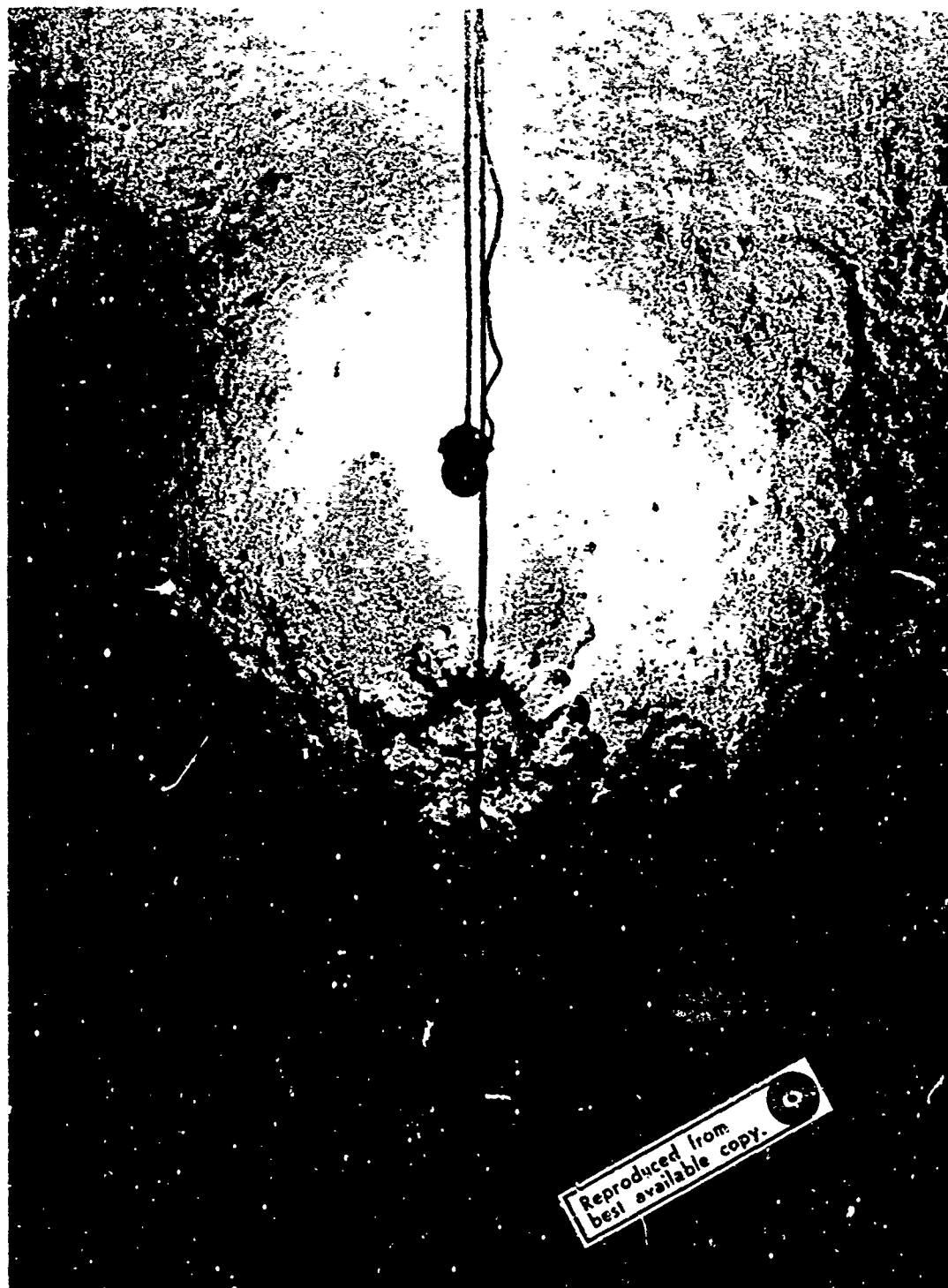
FIGURE A-7

Bottom photograph from camera run K, showing several features
indicative of benthic activity. Pits and craters of variable
size cover the bottom. Below and to the left of the strobe
light is a set of narrow grooves radiating from a central lump
(see Ewing and Davis, 1967, Figs. 24-53 through 24-61). A
faecal structure appears near the left edge of the photograph.
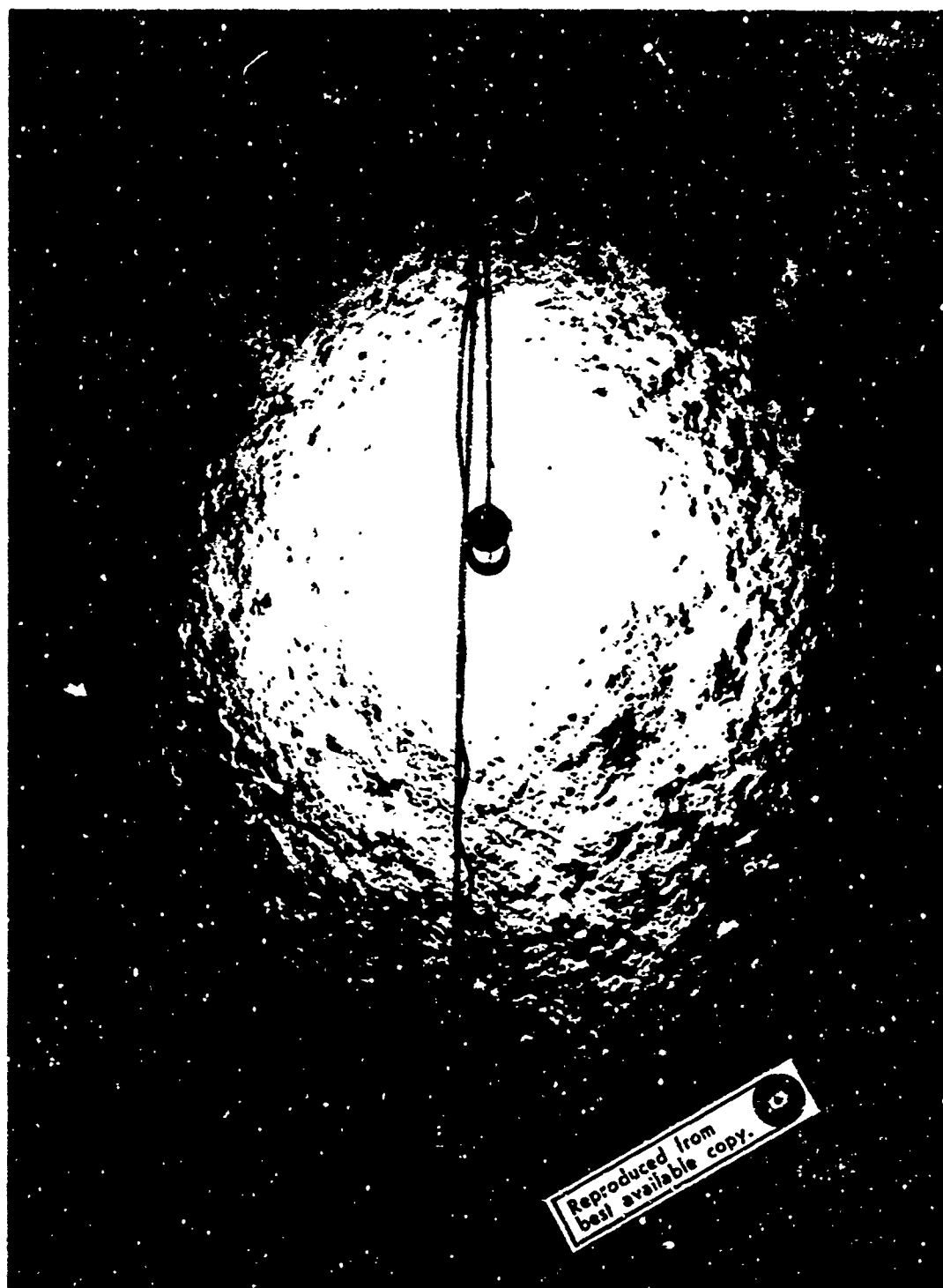
FIGURE A-8

. ttom photograph from camera run K. The dark, irregular fragments
may be igneous in origin, or may be manganese oxide coatings.
Between the fragments are numerous small pits and meandering
trails, indicative of benthic activity.
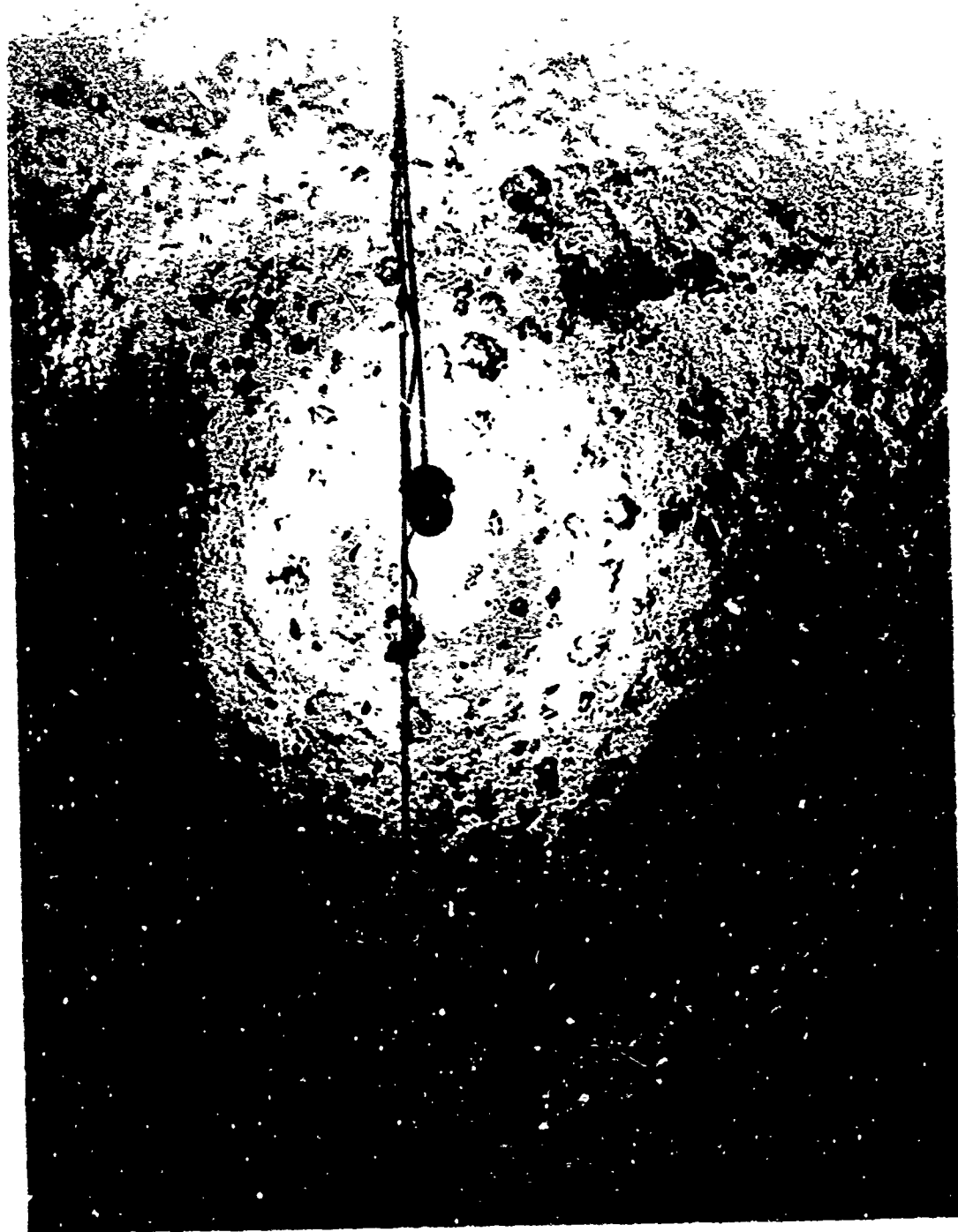
FIGURE A-9

Bottom photograph from camera run M. Two sets of radiating
grooves around a central lump can be seen to the right of the
strobe light. Near the top of the photograph is a meandering
ridge, perhaps formed by an organism of the type illustrated
by Ewing and Davis (1967, Figs. 24-3 and 24-4). Width of the
field of view is approximately 3 meters.
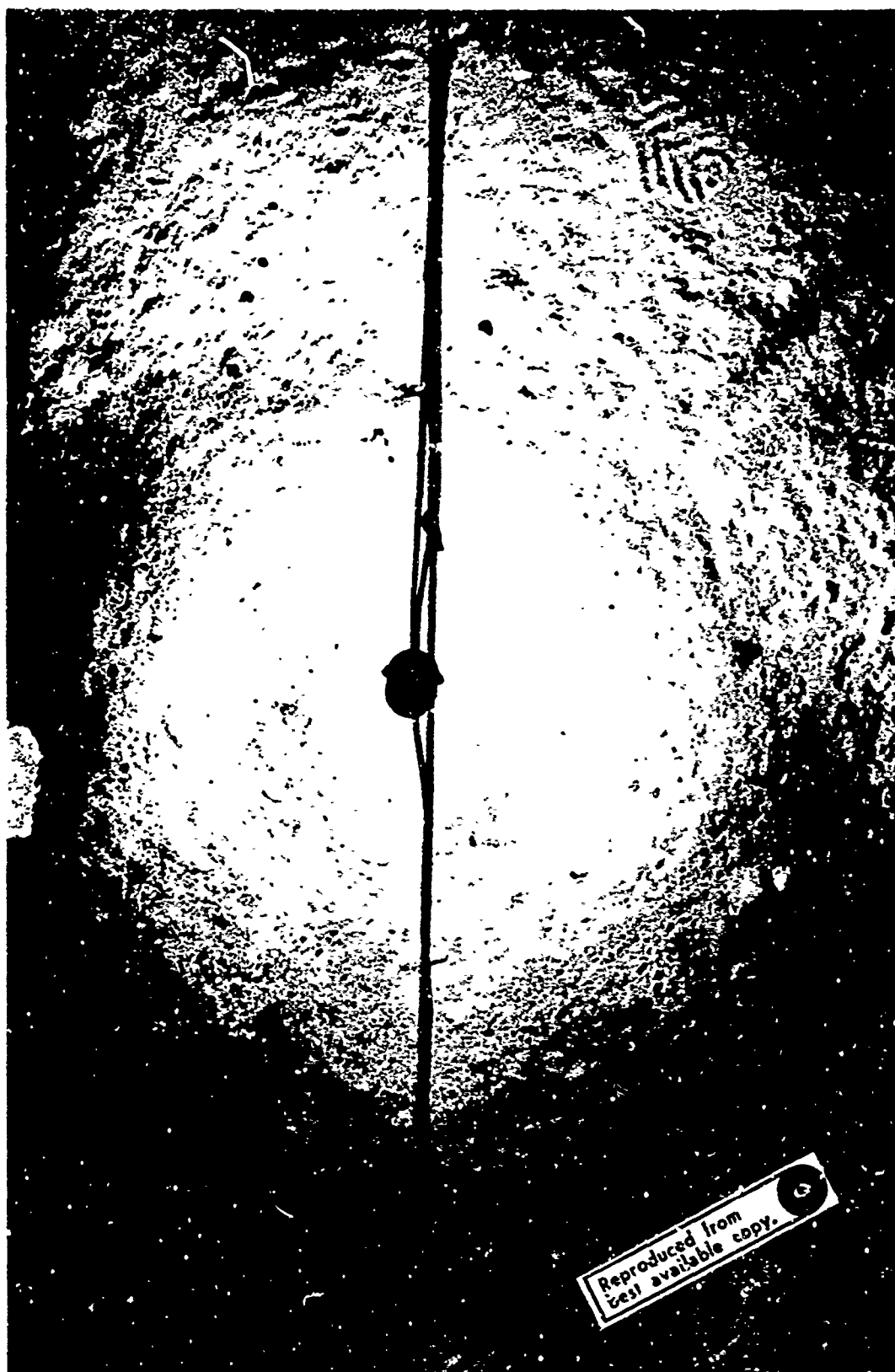
APPENDIX II

CURRENT METER DATA

TABLE 6a

Listing of data obtained by bottom current meters. Instrument #5
recorded current direction only. Speeds indicated are in cm/sec.

DAY	TIME	#2 Direction	#2 Speed	#3 Direction	#3 Speed	#4 Direction	#4 Speed	#5 Direction
17 OCTOBER	0000	015°	5.6					
		035°	5.4					
		022°	4.9					
		032°	5.4	090°	4.2			
		045°	4.7	090°	5.2			
		050°	4.7	100°	4.8	040°	4.8	
	0600	049°	5.4	100°	7.0	058°	4.5	105°
		042°	6.8	096°	7.4	057°	4.8	100°
		048°	8.0	105°	5.5	053°	7.0	079°
		055°	8.0	065°	6.6	055°	7.3	068°
		049°	6.0	072°	8.6	060°	7.4	060°
		035°	6.4	072°	7.4	054°	5.8	050°
	1200	049°	4.3	081°	7.0	044°	4.6	068°
		025°	5.3	095°	3.8	050°	4.8	085°
		040°	5.4	100°	3.4	050°	4.5	075°
		050°	4.9	090°	6.2	052°	5.5	120°
		055°	4.1	090°	6.2	062°	4.8	110°
		070°	3.9	100°	7.0	070°	4.5	110°
	1800	078°	4.5	110°	6.6	080°	4.2	126°
		072°	4.1	104°	6.2	080°	4.2	135°
		059°	4.5	107°	5.8	072°	3.8	135°
		058°	4.7	100°	6.6	058°	3.8	120°
		044°	4.5	084°	5.8	050°	3.8	100°
		033°	4.5	068°	5.2	040°	3.8	095°
18 OCTOBER	0000	018°	4.3	078°	5.5	035°	3.8	105°
		010°	3.1	068°	5.2	025°	4.2	095°
		040°	5.3	071°	5.2	030°	5.2	055°
		038°	6.6	072°	5.8	040°	5.2	049°
		040°	6.8	067°	7.0	035°	6.2	107°
		042°	6.0	072°	7.0	040°	6.6	078°
	0600	046°	4.8	068°	7.0	055°	6.6	072°
		054°	5.3	071°	6.6	058°	6.2	075°
		052°	5.1	080°	6.6	060°	6.2	078°
		049°	4.3	074°	7.0	060°	5.2	080°
		045°	4.1	100°	5.8	054°	4.5	089°
		035°	3.3	080°	3.4	054°	3.8	095°
	1200	026°	2.9	122°	3.9	042°	3.8	098°
		020°	3.1	084°	3.0	040°	3.6	098°
		028°	3.4	095°	3.4	040°	3.4	095°
		036°	4.5	085°	4.8	050°	3.8	112°
		035°	3.7	079°	6.2	060°	4.5	115°
		041°	3.3	120°	4.8	065°	4.5	120°
	1800	059°	3.1	086°	4.2	060°	3.8	135°
		081°	3.1	031°	4.8	060°	3.-	125°
		088°	2.9	095°	5.5	075°	3.0	125°
		082°	2.2	086°	4.8	095°	2.6	125°
		030°	3.4	124°	4.5	080°	2.6	125°
		022°	5.1	095°	5.5	040°	3.8	120°

TABLE 6b

Listing of data obtained by bottom current meters. Instrument #5

recorded current direction only. Speeds indicated are in cm/sec.

DAY	TIME	#2 Direction	Speed	#3 Direction	Speed	#4 Direction	Speed	#5 Direction
	0000	014°	6.4	062°	4.2	030°	5.5	050°
		010°	5.4	065°	4.5	030°	6.2	055°
		025°	6.4	078°	4.8	030°	6.6	050°
		009°	6.0	070°	5.5	035°	6.2	035°
		042°	5.8	073°	7.4	030°	7.0	075°
		032°	5.4	084°	6.2	040°	5.8	090°
	0600	050°	4.1	099°	5.2	050°	5.5	100°
		050°	2.9	096°	5.8	050°	4.8	103°
		050°	3.1	098°	6.6	065°	3.4	115°
		057°	4.7	120°	5.5	070°	3.0	116°
		050°	4.5	111°	5.2	050°	3.8	118°
19 OCTOBER		035°	3.9	105°	5.8	050°	3.8	105°
	1200	013°	4.9	109°	4.2	035°	3.8	095°
		009°	6.8	100°	7.2	020°	4.5	087°
		020°	6.2	030°	0.8	025°	5.2	080°
		023°	4.1	110°	1.7	035°	4.8	075°
		037°	2.1	125°	2.2	043°	3.4	077°
		055°	2.9	110°	2.6	040°	3.4	100°
	1800	030°	2.1	103°	5.2	046°	2.6	125°
		068°	2.9	110°	5.5	043°	2.2	130°
		066°	2.7	116°	6.2	095°	1.7	135°
		059°	2.7	131°	2.2	070°	2.2	130°
		035°	2.2	155°	2.2	050°	1.7	127°
		020°	3.7	101°	3.4	030°	2.5	120°
	0000	010°	4.3	180°	0.8	012°	3.8	095°
		010°	4.3	025°	1.7	008°	3.4	065°
		001°	4.9	055°	1.7	008°	2.4	080°
		001°	4.3	020°	2.2	008°	3.4	058°
		001°	4.9	060°	2.6	010°	3.8	067°
		002°	3.3	075°	2.6	010°	3.8	078°
	0600	008°	3.3	095°	2.2	010°	3.0	105°
		020°	2.4	115°	3.4	028°	2.6	115°
		070°	1.1	111°	4.8	050°	1.7	127°
		075°	1.1	119°	3.6	038°	1.3	128°
		043°	2.1	128°	2.2	060°	1.3	130°
20 OCTOBER		029°	3.1	096°	2.2	050°	1.7	121°
	1200	033°	3.1	095°	3.4	035°	3.0	121°
		015°	3.7	096°	2.6	035°	3.4	116°
		008°	3.9	086°	2.2	025°	2.6	114°
		008°	2.9	086°	3.0	020°	3.4	113°
		355°	2.7	090°	3.0	020°	3.0	100°
		343°	2.1	085°	2.2	010°	3.0	116°
	1800	359°	1.1	055°	3.0	008°	2.2	135°
		000°	0.8	073°	3.0	023°	1.3	140°
		008°	0.8	093°	2.2	030°	1.3	152°
		000°	1.1	100°	2.6	030°	0.8	146°
		355°	1.5	090°	3.4	003°	0.8	149°
		002°	2.4	070°	3.8	000°	1.7	149°

TABLE 6c

Listing of data obtained by bottom current meters.　Instrument #5
recorded current direction only.　Speeds indicated are in cm/sec.

DAY	TIME	#2		#3		#4		#5
		Direction	Speed	Direction	Speed	Direction	Speed	Direction
21 OCTOBER	0000	001°	2.4	070°	4.2	003°	2.6	135°
		001°	3.9	080°	3.4	002°	3.0	114°
		004°	6.0	060°	3.0	002°	4.2	112°
		005°	6.2	040°	3.4	010°	5.8	072°
		005°	4.9	032°	3.4	012°	5.5	064°
		007°	3.1	142°	1.3	020°	4.5	032°
	0600	008°	2.7	130°	1.3	016°	2.6	099°
		010°	2.2	125°	1.3	026°	1.7	130°
		019°	2.4	120°	3.0	030°	2.6	133°
		024°	2.7	128°	3.0	028°	3.0	115°
		016°	3.4	150°	1.3	038°	2.6	104°
		0??	4.3	112°	1.7	025°	2.2	093°
	1200	008°	4.7	096°	1.7	018°	2.6	103°
		010°	4.9	085°	2.2	019°	4.2	082°
		003°	6.2	045°	3.4	017°	4.5	055°
		359°	7.4	033°	3.4	008°	5.8	019°
		000°	5.8	025°	3.0	007°	5.8	010°
		000°	3.7	032°	2.6	007°	3.0	018°
	1800	000°	3.3	060°	2.6	010°	3.0	100°
		000°	2.4	089°	2.2	021°	2.2	122°
		000°	1.5	095°	1.7			135°
		005°	0.8	096°	2.2			141°
		005°	1.3	119°	2.6			150°
		013°	2.7					
22 OCTOBER	0000	009°	4.7					
		004°	5.8					
		004	5.8					
		001°	6.4					
		000°	6.4					
		000°	6.0					
	0600	000°	5.4					
		355°	3.3					
		358°	3.4					

Scientific personnel on R/V THOMAS WASHINGTON during EQUATOW

expedition, October 1969:

C. Ingram, R. Hitchcock, M. D. Benson, H. R. Kaye, R. W. Cooke,

J. T. Donovan, M. Elston, D. E. Boegeman, P. H. Rapp,

C. D. Lowenstein, F. N. Spiess, D. A. Johnson, M. G. Dinkelman,

F. W. Stone, J. Pew.

Not pictured: C. Isaacs, W. B. F. Ryan